THE UNIVERSITY OF MICHIGAN

INDUSTRY PROGRAM OF THE COLLEGE OF ENGINEERING

MEASUREMENTS AND COMPUTER SIMULATION OF INSTANTANEOUS EXHAUST GAS VELOCITIES FROM A SINGLE CYLINDER SPARK-IGNITION ENGINE

Hyo Jong Yun

A dissertation submitted in partial fulfillment
of the requirements for the degree of
Doctor of Philosophy in the
University of Michigan
Department of Mechanical Engineering
1973

August, 1973

IP-853

To my wife Ehi Kyung

ACKNOWLEDGEMENT

I would like to express my sincere appreciation to Professor William Mirsky, Chairman of my doctoral committee, for his guidance and valuable advice throughout my graduate studies. I am also grateful to all other members of my doctoral committee for their valuable suggestions during the course of this work. In particular, thanks are extended to Professor Donald J. Patterson under whose research project the experimental part of this work was originally initiated, to Professor Victor L. Streeter for developing my initial interest in studying transient flow problems and for his guidance on the mathematical simulation techniques, to Professor Charles M. Vest for his active participation and valuable advice.

The financial support of the U. S. Department of Health, Education and Welfare for the initial development of the experimental set-up is gratefully acknowledged. I am also grateful to the Department of Mechanical Engineering and the Rackham School of Graduate Studies of the University of Michigan for their financial aids during my graduate studies.

Particular thanks are due to Dr. Richard Winsor for his hot-wire anemometer measurements. Technical assistance of the staff of the Automotive Laboratory is also gratefully acknowledged. I am grateful to the staff of the Industry Program of the University of Michigan for final preparation and publication of the manuscript. Thanks are also due to Mrs. Kathy Brenniman for her valuable comments while reading three chapters of the original manuscript.

I wish to express my sincere appreciation to my family for their patience and understanding, which have been the constant source of encouragement while this work was completed.

TABLE OF CONTENTS

LIST OF FIGURES

LIST OF FIGURE (CONT'D)

LIST OF FIGURES (CONT'D)

LIST OF FIGURES (CONT'D)

LIST OF TABLES

NOMENCLATURE

Symbol	Meaning
A	Dimensionless speed of sound
a	Speed of sound
a	As a subscript, refers to the air in the intake system
B	Cylinder bore
c	As a subscript, refers to the cylinder
C_p	Specific heat at constant pressure
C_v	Specific heat at constant volume
D	Diameter of the exhaust pipe
D_{vp}	Diameter of the exhaust port
E	Internal energy
e	As a subscript, refers to the exhaust gas in the pipe
EC	As a subscript, refers to the cylinder condition when the exhaust valve closes
EO	As a subscript, refers to the cylinder condition when the exhaust valve opens
F	Pipe cross-sectional area
f	Moody friction factor
f	Focal length of the spherical mirror
F_c	Overall cylinder wall area
F_v	Effective valve area
FA	Fuel-air ratio
h	Specific enthalpy
h_c	Cylinder heat transfer coefficient
h_w	Heat transfer coefficient of the pipe flow
H^o	Stagnation enthalpy

Symbol	Meaning
h^o	Specific stagnation enthalpy
K	Refractivity of the gas
k	Ratio of specific heats
L	Length of the exhaust pipe
L_v	Instantaneous valve lift
M	Optical magnification factor
m	Mass
M_r	Mass of the residual gas
$\dot{m}$	Mass flow rate
n	Refractive index of the gas
p	Pressure
q_w	Heat transfer between the pipe and the exhaust gas
R	Gas constant
R	As a subscript, refers to the reference state
r_c	Compression ratio
s	Stroke
T	Temperature
t	Time
t	As a subscript, refers to the exhaust surge tank
t	As a subscript, refers to the valve throat
T_{cw}	Temperature of the inner surface of the cylinder wall
U	Dimensionless velocity
u	Velocity
v	Volume

Symbol	Meaning
v	As a subscript, refers to the exhaust valve
w	Unobscured width of the uniformly bright image of the light source at the knife edge
w	As a subscript, refers to the exhaust pipe wall
X	Dimensionless distance
x	Distance
Z	Dimensionless time
α	Crank angle
ε	Angular deflection of light due to refraction
ρ	Density
ϕ	Effective valve area ratio
τ_w	Pipe wall shear stress

1. INTRODUCTION

1.1 Purpose and Background

A comprehensive understanding of instantaneous flow conditions in the exhaust system of an internal combustion engine is becoming increasingly important since accurate exhaust flow data are required for a better understanding of various devices used in the exhaust system, such as turbochargers, emission control units, and mufflers. For example, it is highly desirable in a supercharged engine to measure accurate mass flow rates into an exhaust turbocharger in order to study its performance in detail. Information on the instantaneous exhaust enthalpy flow are helpful in designing thermal reactors as emission control devices. Effective muffler designs also require accurate instantaneous flow velocity data if flow variations are to be considered in the study of acoustics in the exhaust system.

The flow in the exhaust system is normally highly pulsating due to the pulsed characteristic of the cylinder discharge and the resulting pressure wave action within the exhaust system. Although attempts have been made in the past to obtain experimental data on the pulsating engine exhaust flow by applying conventional flow measuring devices, poor detector response and complicated calibration procedures have prevented the use of such devices in the exhaust flow measurement. More sophisticated techniques have recently been developed in order to overcome these difficulties, but lack of experimental data on exhaust flow still exists.

Analytical studies of exhaust systems have been quite successful in predicting system performance and in providing certain important

design parameters. The wave action in exhaust systems has been analyzed by developing mathemetical models which are based on the theories of gas dynamics. However, the majority of previous simulations of exhaust systems of internal combustion engines have been evaluated from the experimental data obtained from simulated engine systems, such as a pulse generator or a motored engine fed with compressed air. Due to the experimental difficulties mentioned earlier, comparisons between experiments and theories have been made in terms of pressure data, even when a direct comparison of other flow variables, such as flow velocicy or gas temperature, would have been preferred.

The purpose of this study was to develop an experimental technique to measure instantaneous exhaust gas velocities and to develop a mathematical model of a simplified engine exhaust system in order to provide a basic understanding of the nature of exhaust gas flow in an internal combustion engine.

1.2 Literature Review

1.2.1 Velocity Measurements in Pulsating Flows

The applicability of conventional flow measuring devices, such as orifices and Pitot tubes, to the measurement of pulsating flows is quite limited mainly due to their slow responses and to the fact that the inserted probe creates disturbances in the flow field. Numerous attempts have been made, as well summarized by Oppenheim,[24] in order to take into account the effect of flow pulsations on the steady governing equations of the flow meter. However, the disturbances created by the probe are inevitable and could cause a serious change in flow pattern. More direct methods, such as the tracer particle techniques and the

laser Doppler systems, have been developed in the past years to eliminate these difficulties.

Tracer particle techniques have been widely used for visualizing the flow pattern in steady systems. They have also been used to measure fluid particle velocities. Rann[27] introduced small incandescent particles into a flame to measure gas velocities in the flame. The movement of the incandescent particles were recorded by two photomultipliers, a known distance apart. Thompson[32] used the naturally occurring dust particles in a wind tunnel as the tracer. Two parallel light beams, a known distance apart, pass through the test section, and the light-scattering by the tracer particles is recorded by a photomultiplier. With this system, Thompson was able to measure velocities up to 200 m/sec, and the comparison with the Pitot static tube was excellent.

Ohigashi et al.[23] developed a spark discharge method and applied it to the flow velocity measurements in a two-stroke engine. They investigated carefully the effects of several flow variables on the displacement of the path of the discharged ions and concluded that the displacement of the ion path could be uniquely related to the flow velocity. Kaneko et al.[20] used Ohigashi's technique to measure the exhaust gas velocity into a thermal exhaust reactor core.

An optical method based on the Doppler shift in the monochromatic light scattered from particles in the moving fluid has been developed recently. Foreman et al.[12] among the first investigators, applied this technique to measure velocities up to 14.4 m/sec in an air blower system with a He-Ne gas laser as a light source. Since his work, numerous publications have been made with particular interest

on the pulsating flow velocity measurement. Lanz et al.[22] used 0.73μ latex spheres as the scattering material to measure bidirectional pulsating flow velocities. A comprehensive description of the laser-Doppler system can be found in the paper by Huffaker.[17] Schwar and Weinberg[28] suggest a velocity measurement technique which combines the Doppler principle and the schlieren method to widen the rate of applicability.

The schlieren optical system in the fields of aerodynamics and combustion studies is one of the most widely used optical techniques for flow visualization. This technique, when equipped with a streak camera or any other time-resolving mechanism, is capable of detecting the velocity of a flow field which causes changes in the refractive index. The velocity of shock waves or detonation waves is usually measured by this technique. The theory of the schlieren principle is classic and well described in a textbook by Weinberg[33] and in the paper by Holder and North.[15]

The schlieren technique, however, has rarely been applied to the measurement of flow velocities despite its potential as a flow velocity meter. Daniel and Wentworth[10] applied the schlieren system to the exhaust pipe of a single cylinder engine in order to measure the exhaust gas flow. By observing the location of vortices created by wedge obstructions, they were able to detect the flow reversal in the exhaust pipe. However, the absolute magnitudes of flow velocity were not determined.

Bowman[6] used a schlieren-streak system to measure air velocities up to Mach number 13 in a hypersonic gun tunnel. Small

density variations in the tunnel were detected by the schlieren system and photographed with a streak camera scanning at right-angles to the flow direction. The inclination of the streaks provided a continuous record of flow velocity.

1.2.2 Unsteady Flow Analyses of Exhaust Systems

The gas flow in the exhaust system of an internal combustion engine can be modeled approximately using one-dimensional, unsteady, compressible flow theories. Most of the simulation studies are based on this theory, and the method of characteristics has been used to solve the governing hyperbolic type of partial differential equations.

Jenny[19] was one of the early investigators who applied the one-dimensional, unsteady flow theory to simulate the exhaust pipe flow from an internal combustion engine. He studied the influence of compression and rarefaction waves of large amplitude on the scavenging and utilization of exhaust energy. Benson and Woods[2] studies the wave action in a supercharged two stroke engine model. They used an exhaust pulse generator to simulate the actual engine and investigated effects of several boundary conditions on the wave phenomena. Wright and Gill[36] showed the errors in the timing of pressure waves in the exhaust system of a two-stroke engine when an isentropic flow model was applied in their simulation. Goyal et al.[13] included heat transfer and friction in their simulation work of the intake and exhaust system of a single cylinder engine. They also studied the effects of bell-mouth versus plain pipe termination of the exhaust pipe and the effects of a finite surge tank. Various boundary conditions at the cylinder and of the exhaust pipe were studied by Daneshyar.[9]

Mathematical modeling of the exhaust valve motion is one of the most important parts of the exhaust simulation. Cole and Mills[8] extended the simple theory of incompressible flow for a sudden enlargement model in order to describe the flow phenomena through the poppet exhaust valve. They studied the flow through valves of different geometry at the low pressure ratio across the valve. They also carried out tests on one exhaust valve over a wide range of pressure ratios and valve lifts. Kastner et al.[21] used an isentropic flow model for the valve flow and carried out both steady and unsteady flow tests on inlet valves of different geometry. The results of their steady-flow tests were presented in the form of discharge coefficients. Woods and Khan[35] performed a series of experiments to determine the effective valve area based on the constant pressure model introduced by Jenny.[19] They found that within a certain limit of valve lift the pressure ratio across the valve had little effect on the effective valve area.

The thermodynamic analysis of the cylinder charging and discharging processes is another important part of the exhaust simulation. Horlock and Woods[16] presented a comprehensive analysis of the gas exchange processes which occur in internal combustion engines. They cautioned that certain assumptions regarding the mixing of gases had to be made in the case where a simultaneous charging and discharging took place in a container, while separate charging and discharging processes might be analyzed by a lumped system with reasonable confidence.

1.3 Scope of Investigation

The objectives of this thesis were to accomplish the following

tasks:

1. Develop the schlieren-streak optical system for instantaneous measurements of exhaust gas velocities
2. Develop the theoretical analysis of a simplified exhaust system of a single cylinder spark ignition-engine and a computer simulation based on the analysis
3. Compare measured experimental data with the computer simulation results.

The schlieren-streak optical system is described in Chapter II. This chapter includes a description of the principle of the schlieren system, the optical components, the test section, the timing synchronization and its instrumentation, and a general experimental procedure. This chapter also includes the interpretation of schlieren velocity data and the comparison between the schlieren method and the hot-wire anemometer for velocity measurement. In Chapter III, other experimental apparatus for the measurements of pressure, temperature, and several engine variables are described.

The theoretical analysis and the general structure of the computer simulation program is included in Chapter IV. The boundary conditions are described in detail, and the solution technique for the governing equations is presented. In Chapter V, comparisons between the simulation results and the experimental data are presented. Effects of several engine variables on the exhaust flow are discussed. Some important factors that affect the simulation results are also included in this chapter.

II. SCHLIEREN-STREAK SYSTEM FOR GAS VELOCITY MEASUREMENT

2.1 General

Optical methods, in addition to the almost instantaneous response of their detecting system, have a principal advantage over other methods for investigating fluid flow because they do not require the insertion of detecting probes which inevitably disturb the flow field. There are several optical methods currently being used for flow velocity measurements, notably the tracer particle technique and the laser Doppler system. Basically the same principle is employed in these techniques. Small tracer particles are introduced into the main stream and the movement of these particles are recorded by detecting the light-scattering caused by the particles. The only difference between these two techniques is the method of relating the phenomenon of light-scattering to the particle movement. The tracer particle technique measures the velocity of particles by observing the time lag between two light sensors, a known distance apart, which are triggered by the light-scattering, while the laser Doppler system computes the particle velocity from the Doppler frequency shift in monochomatic light scattered by the particles. Quite successful velocity measurement have been achieved by both of these methods.(12, 17, 22, 27, 32)

However, the application of these techniques to the exhaust flow velocity measurement is somewhat limited by the following reasons: (1) much care must be taken in selecting the tracer particle size in order to minimize the inertia effect which is important in examining the highly pulsatile exhaust flow, (2) the laser Doppler system requires complicated electronic equipment to analyze the light

frequency shift.

This chapter describes an optical method for velocity measurement in which a schlieren-streak system is used to measure the velocity of local density variations generated in the exhaust system as a result of turbulence and combustion in an internal combustion engine. The method does not require the introduction of foreign particles or the use of complicated electronic circuitry, and the true fluid velocity may be calculated directly.

2.2 Schlieren Principle and Local Density Variations as the Tracer

2.2.1 The Schlieren Principle

The schlieren system, among other similar optical methods for investigating the gas flow, detects gradients of the refractive index. For gases, the refractive index n is related to gas density ρ by Gladstone and Dale's law:

$$n - 1 = K\rho \qquad (2.1)$$

where K is the refractivity of the gas. For a given gas and light source, Equation (2.1) states that the refractive index field of the gas is uniquely determined by the density field. Therefore, any flow phenomenon that creates density gradients can be visualized effectively by the schlieren system within its sensitivity limit. Shock or detonation waves are typical examples in which the schlieren system is used as an indispensable tool for flow investigations.

Figure 1 shows one of the simplest types of schlieren systems. A collimated light beam passes through the test section and is brought

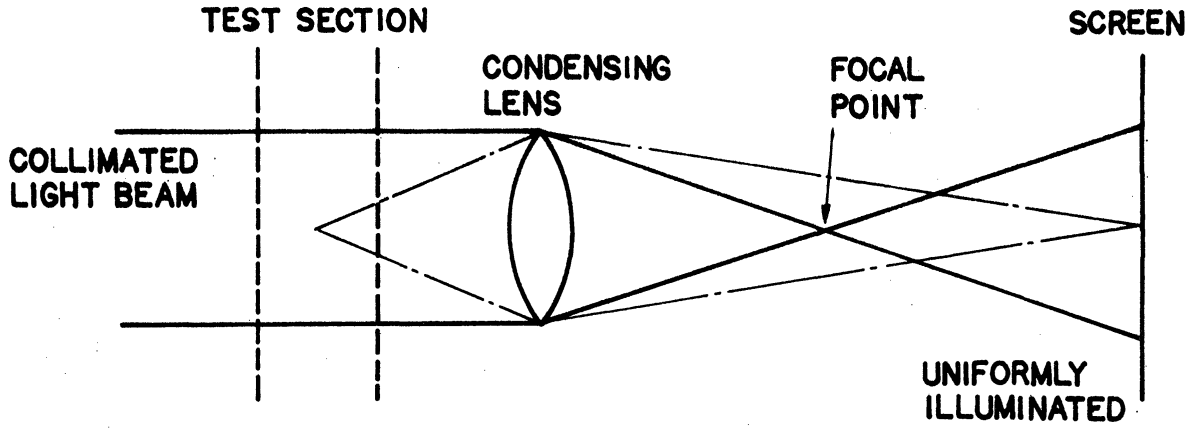

a) NO FLOW OR HOMOGENEOUS FLOW IN TEST SECTION

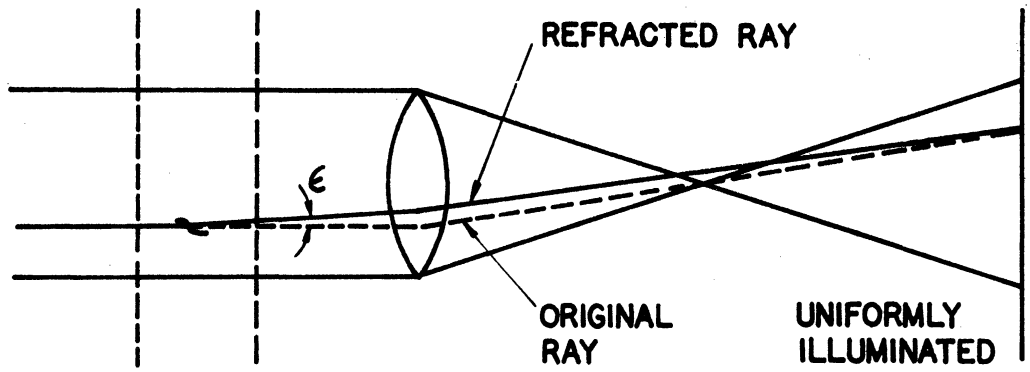

b) INTRODUCTION OF INHOMOGENETIES IN TEST SECTION

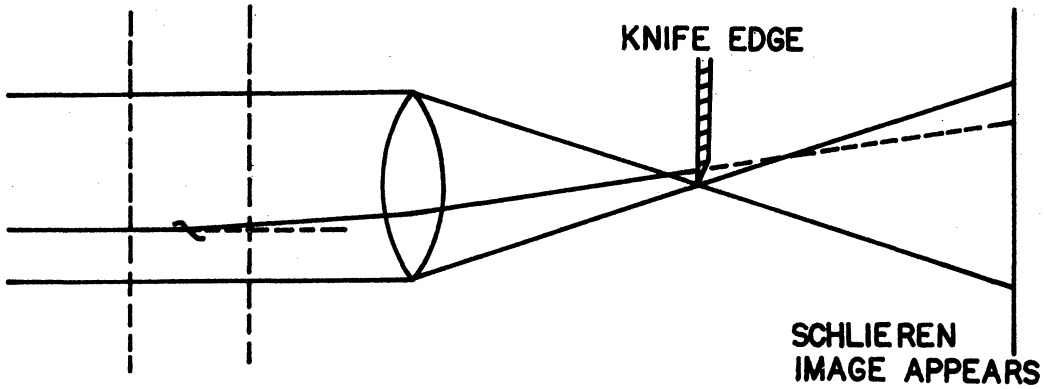

c) INTRODUCTION OF KNIFE EDGE

Figure 1. Schlieren Principle

to a focus by the condensing lens and then projected on the screen. With no flow or homogeneous flow in the test section, as shown in Figure 1a, an image of uniform light intensity appears on the screen. If the flow in the test section contains inhomogeneities which cause local density gradients normal to the light direction, then the incident light will be refracted according to Snell's law of refraction as indicated in Figure 1b. The refracted light beam is still imaged at the same point on the screen, but no longer passes through the same original focal point. The overall image on the screen will still be the same as that in case (a) unless there exist shadowgraph effects. In Figure 1c, the effect of the knife edge is illustrated. By introducing a knife edge at the focal point, the refracted light is cut off by the knife edge and the image on the screen is no longer uniform but shows a certain image caused by the inhomogeneities. Thus, a schlieren picture discloses the instantaneous density gradient field of the flow under investigation. The orientation of the knife edge must be adjusted so that the density gradient is normal to the plane of the knife edge. A comprehensive description of the schlieren system can be found in Weinberg.(33)

The sensitivity of a schlieren system depends upon the optical dimensions of its components and the quality of the film on which the schlieren image is recorded. From Weinberg,(33) the sensitivity is given by

$$\frac{\Delta I}{I} = \frac{\varepsilon f}{w} \qquad (2.2)$$

where $\Delta I/I$ is the proportional change in light intensity due to

cut-off by the knife edge, ε the angular deflection due to refractive index gradient, f the focal length of the schlieren condensing lens or mirror, and w the unobscured width of the uniformly bright image of the light source at the knife edge. Therefore, for a given film and light source, the sensitivity of a schlieren system can be increased in proportion to the focal length of the condensing mirror.

2.2.2 Local Density Variations as the Tracer

The gas flow in an internal combustion engine is usually extremely turbulent due to complex motions of mechanical components and to the chemical processes occuring inside the engine cylinder. The degree of flow turbulence is affected by such factors as the reciprocating motion of the piston, the induction and expansion processes through the valves, and the complicated flow passages within the manifolds. In a firing engine, combustion processes also contribute significantly to the flow turbulence. Due to this flow turbulence, the gas flow in an engine is not homogeneous but contains large numbers of small local eddies which are carried along with the main gas stream. These local eddies possess density gradients across themselves and thus are detectable with an optical flow-visualization technique if the optical system has sufficient sensitivity. The schlieren system, described in Section 2.2.1, has been frequently used to visualize turbulent flows in the past[15] because of its high sensitivity and relatively simple optical set-up.

Since the movements of these local eddies, or local density variations in general, can be traced, it becomes possible to measure

the flow velocities with which local density variations are assumed to travel. Some of the advantages in using the density variations as the velocity tracer are: (1) the tracer is generated naturally and there is no need to introduce any foreign tracer particles as required in most of tracer particle techniques. Also, because of their natural occurrence, the tracers have exactly the same flow history as that of the main stream. (2) The density of the tracer is comparable to that of the main stream, which is a basic requirement for foreign particles used as velocity tracers. This requirement is particularly important in pulsating flow measurements where the mass inertia force cannot be neglected.

The detectability of these local density variations by a schlieren system depends upon the rate of dissipation of density gradients in the flow field. Due to heat and momentum dissipation, the gas flow will eventually become homogeneous and no longer contain distinctive density gradients to be detected by the schlieren system. However, as proved by schlieren pictures photographed during the exhaust period of an engine in Section 2.5, there still exist detectable local density variations at the end of the exhaust stroke.

2.3 Description of the Schlieren-Streak Optical System

In Section 2.2.1 a simple schlieren system was shown to describe the schlieren principle. If movements of the local density variations are to be recorded, additional means must be employed in the basic schlieren system in order to obtain a time-resolved image on the film.

Figure 2 shows the scanning technique used in this study. In this system, a slit and a rotating mirror are installed between the knife edge and the film plane. As the light passes through the slit,

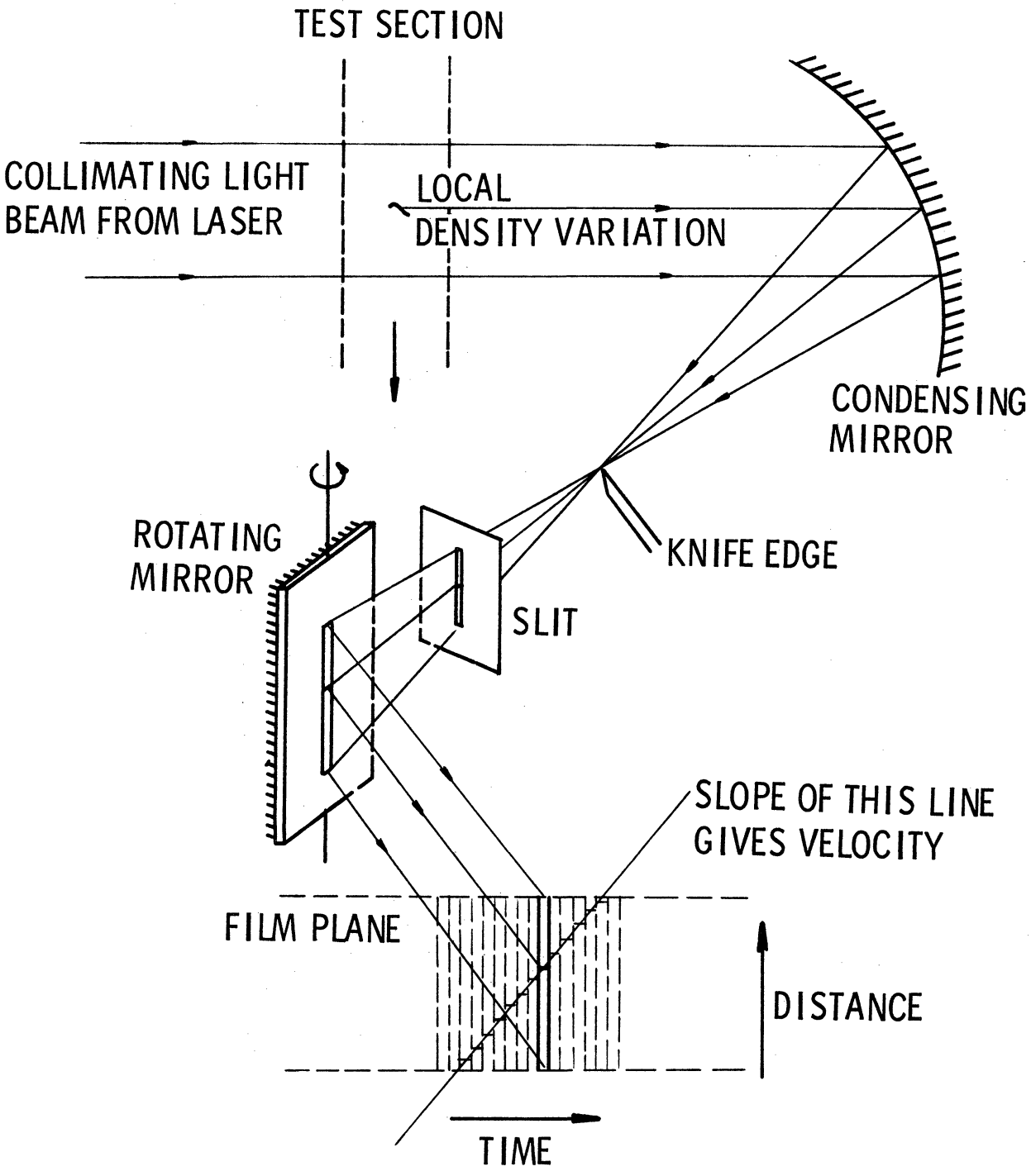

Figure 2. Schlieren-Streak Principle

a narrow slit image is formed. This slit image is then swept across the film by the rotating mirrow. Inclinations of these streaks can be easily adjusted by changing the speed of the rotating mirror. The velocity of the local density variations is then obtained directly by measuring the slopes of these streaks. The instantaneous velocity obtained by this method is not a local value but is averaged over the optical path within the test section. However, in the case where velocity variations along the optical path are not severe, this method will provide accurate instantaneous velocity data.

Figure 3 shows a schematic of the schlieren-streak system employed in this study for the measurement of instantaneous exhaust gas velocities. Figure 4 shows an overall picture of the experimental set-up including the engine and the instrumentation stand.

The test section was located approximately halfway between the engine and the exhaust surge tank. Figure 5 shows a close-up of the test section. Two General Electric Type 101 fused quartz windows, 1 1/2 in. diameter and 1/4 in. thick, were mounted in the window plates. The function of these window plates was to avoid unnecessary exposure of the windows to the exhaust gas flow. When schlieren pictures were not being taken, the window plates were pushed all the way up to avoid exposure to the exhaust gas, so that the quartz windows remain relatively clean. Tapped holes were available on this test section for mounting other flow instruments as needed.

A He-Ne gas laser, 3 mw Spectra-Physics Model 122, was used as a light source. In order to produce an enlarged collimated light beam, a Spectra-Physics Model 331 collimating lens system was connected to the laser unit. This lens system had an effective focal

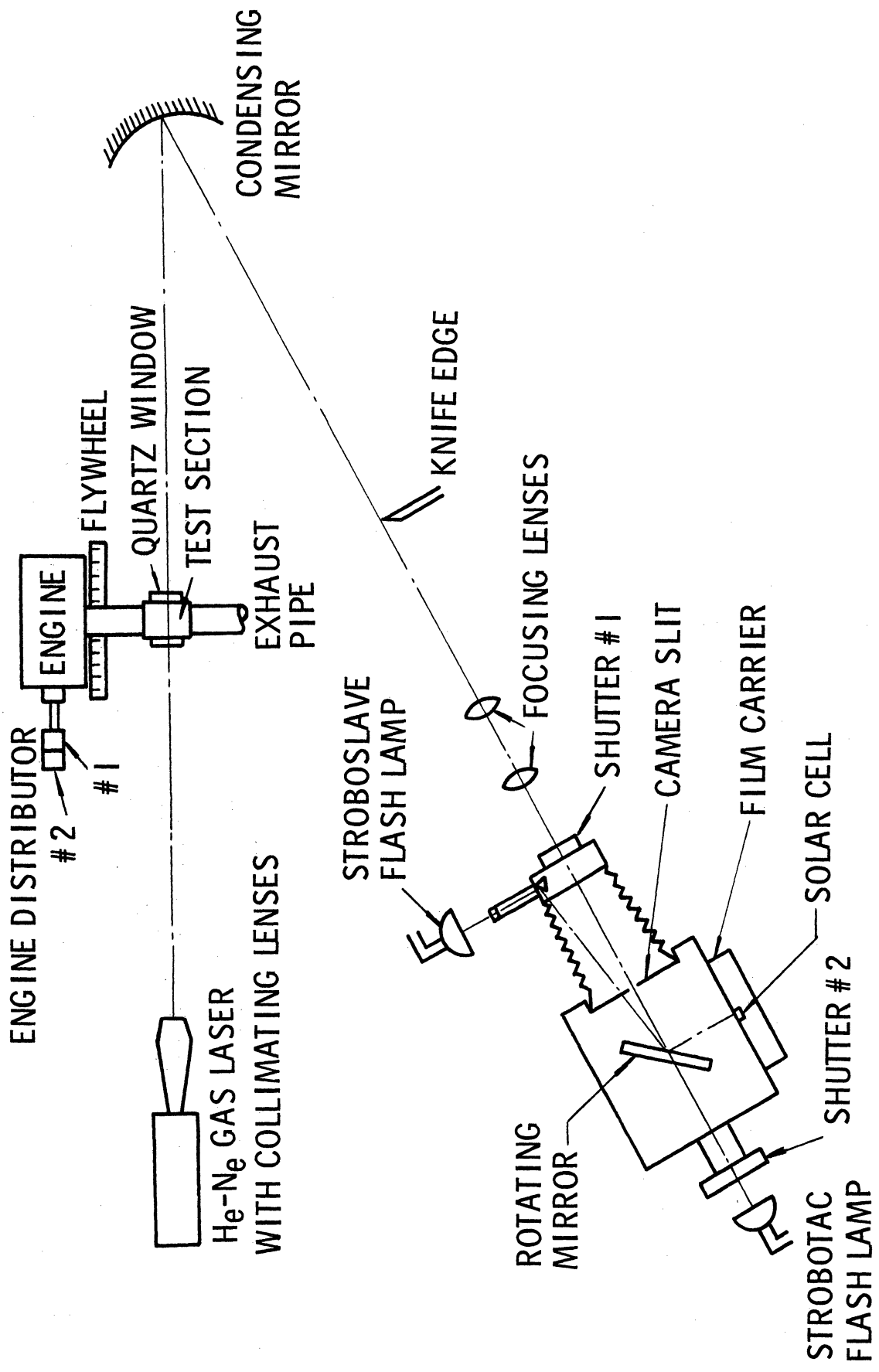

Figure 3. Schematic of Schlieren-Streak System and Its Accessories

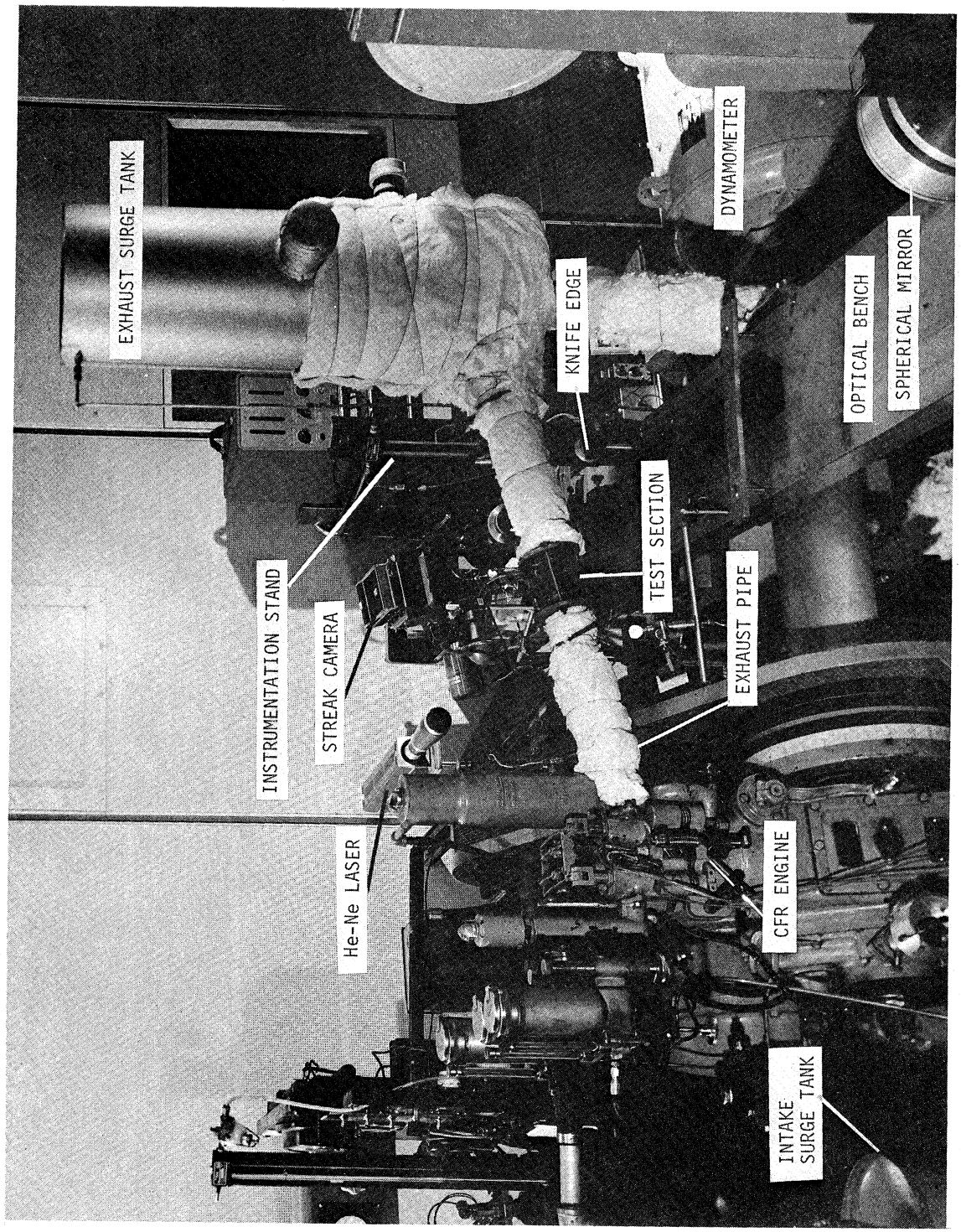

Figure 4. Overall View of Experimental Set-Up.

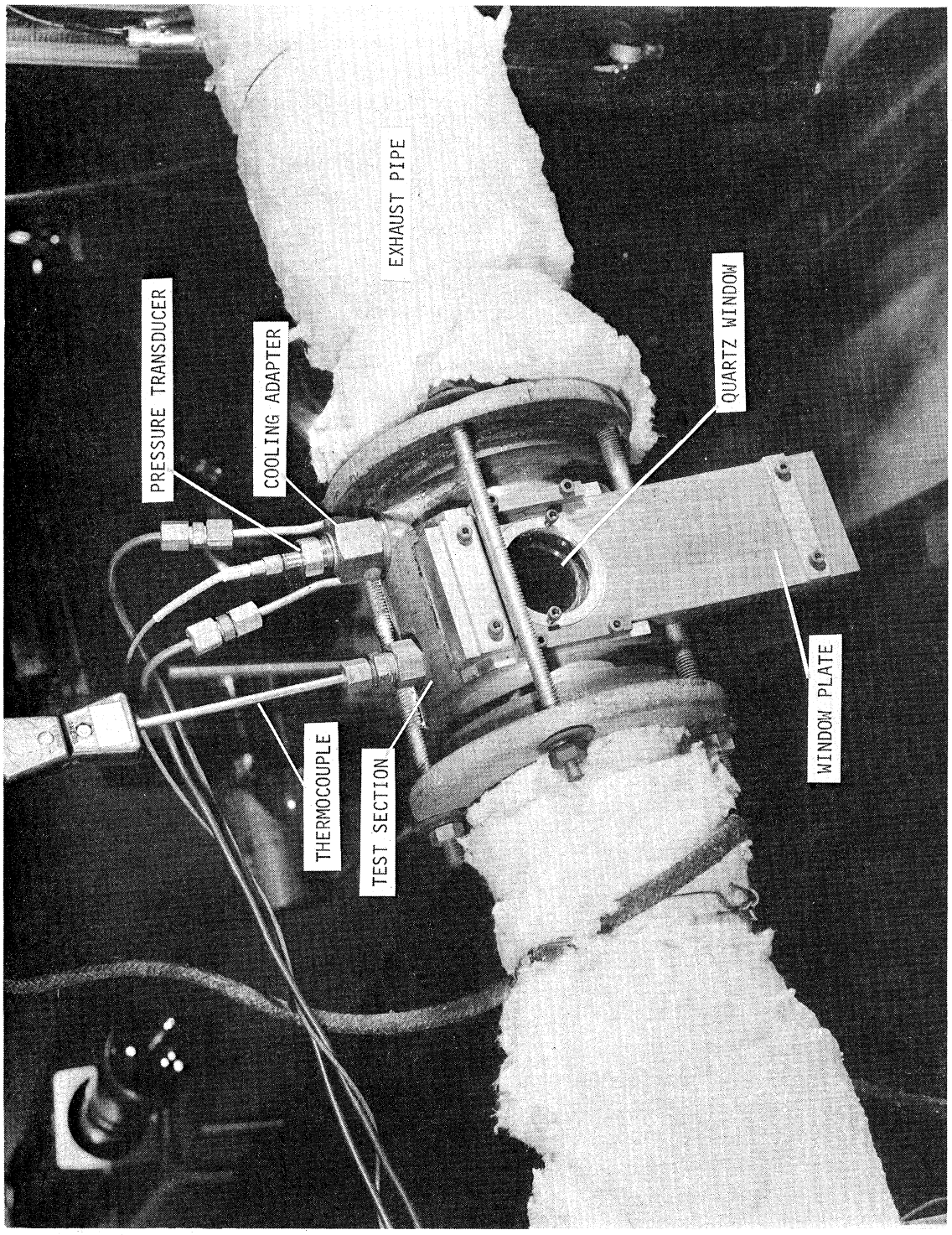

Figure 5. Test Section.

length of 182 mm and produced a collimated beam of approximately 1 in. diameter. This laser optical unit provided a continuous stable light beam and simplified the optical arrangement considerably.

The schlieren condensing mirror used in this system was a spherical mirror of 5 3/4 in. diameter with a focal length of 48 in. This mirror was mounted on a Keuffel & Esser Model 71-5020 optical stand. Two small lenses of short focal lengths were used to focus the schlieren image on the film plane. A commercially available spectrographic slit, mounted in an adjustable housing, was used as the knife edge. Both angular orientation and linear movement of the knife edge could be adjusted with micrometer precision on this unit.

The streak-camera used in this study was designed and built at the Automotive Laboratory of the University of Michigan for the specific purpose of photographing transient events. Figure 6 shows the streak camera in detail. A flat mirror, 3 in. wide and 4 in. long, was mounted on a shaft which was connected to a DC shunt motor, Jones Motrola Model 8200-B52R. A general Radio Type 1701-AK Variac Speed Control was used to vary the motor speed. A constant-voltage transformer was used to minimize voltage variations in the power input to the Variac Speed Control. The mirror sweep rate was recorded on the film using a General Radio Type 1538-A Strobotac. Two commercial camera shutters were mounted on the front and rear ends of the camera. These shutters were operated by two 12-volt DC solenoids. The slit was mounted on a plate and installed inside the camera. The slit position could be adjusted in a direction normal to the light beam. A Polaroid film

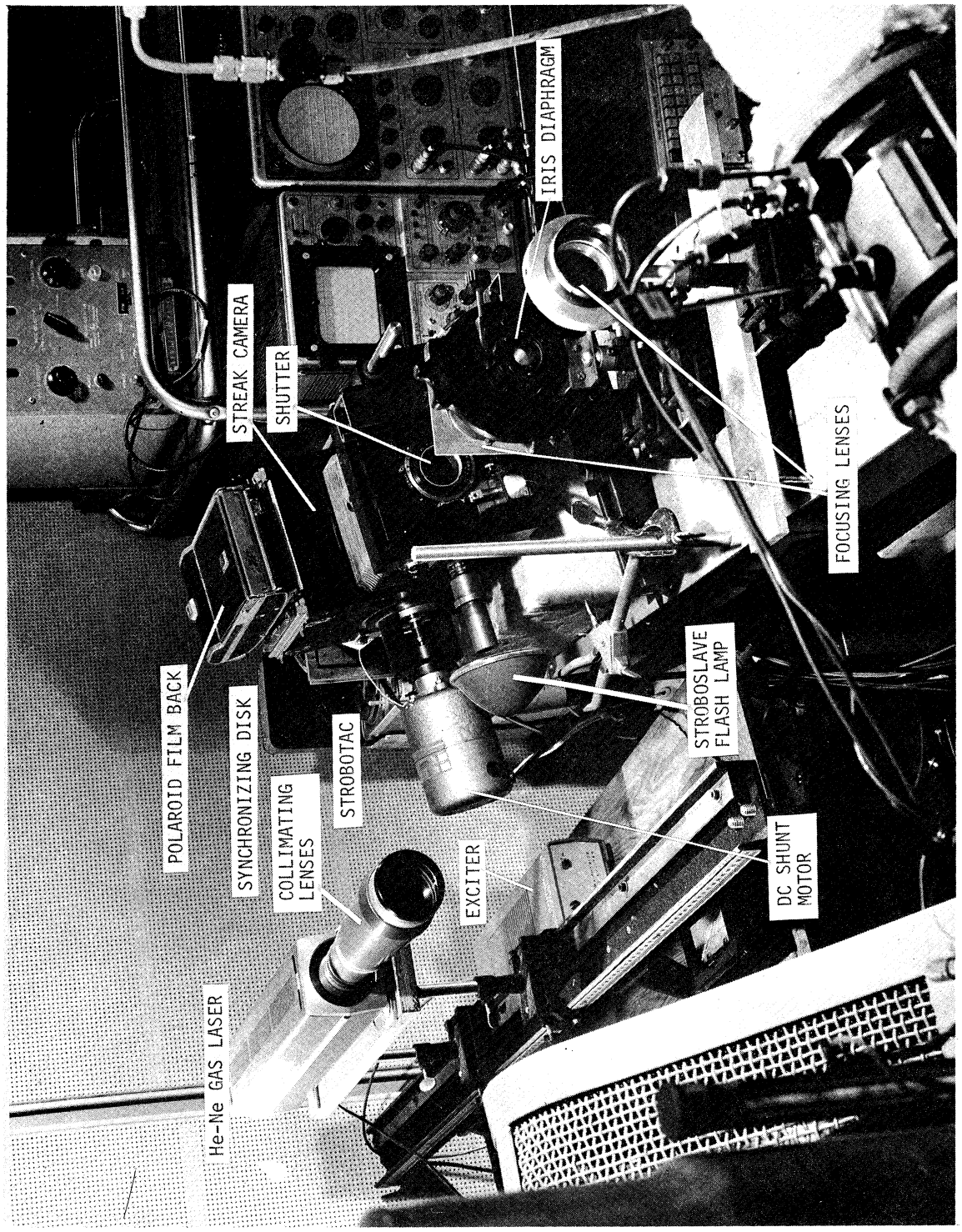

Figure 6. Streak Camera Unit and He-Ne Gas Laser.

back for type 47 film was used for recording the schlieren-streak images. An additonal feature of this camera was a small slit-mirror combination attached to the camera. This unit was used to place a flash mark on the film in order to identify an exact engine flywheel angular position.

Other components which are shown in Figure 3 will be described in Section 2.4. All the optical components, except the streak camera and the spherical mirror, were mounted on Cenco Model 85802 hinged-carriages which rested on the precision ground sliding surface of Cenco Model 85801 optical benches. This precision mounting system provided easy optical adjustments during test runs. These optical benches rested on a heavy steel channel in order to isolate the optical system from ground vibrations. Much of the ground vibration was eliminated by this system. However, for a firing engine at full load, some ground vibration produced slight distortions of the schlieren images.

The sensitivity of the schlieren system described above may be estimated approximately from Equation (2.2). The minimum value of $\Delta I/I$ for visible schlieren images to appear on the film is estimated at 10%. The size of the aperture in the collimating lens system is 22μ. This source projects an image size of .006 in. on the knife edge. This value is computed from the source size multiplied by the ratio of focal length of the schlieren mirror to that of the collimating lens system. The unobscured width w is estimated as half the size of the source image on the knife edge. For f=48 in., Equation (2.2) gives the minimum detectable angular deflection, ε_{min}.

$$\varepsilon_{min} = \frac{w}{f}\left(\frac{\Delta I}{I}\right)_{min} = \frac{.006/2}{48}(.1) \simeq 6 \times 10^{-6} \text{ rad.} \qquad (2.3)$$

2.4 Timing Synchronization and Instrumentation

In order to photograph the exhaust flow at any desired instant in an engine cycle, the streak camera had to be synchronized with the engine. To be more specific, while the camera shutter remained fully open, the rotating mirror had to be properly oriented to reflect the schlieren slit image onto the film, exactly when the engine was at a predetermined crank angle position. Figure 7 shows the control circuit that was used for the timing synchronization. Figure 8 illustrates the sequence of timing events that occurred when a single schlieren picture was being photographed.

Timing events in the engine, in the rotating mirror, and in the camera shutters were all observed at the same instant at which the camera shutters were triggered by both switch S1 and the Bentley sensor. However, the shutters had a certain time delay before they were fully open. This delay necessitated corresponding delays in both the rotating mirror and the engine. Therefore, the major goal of timing synchronization and its instrumentation was to achieve these necessary time delays in the mirror and the engine.

Figure 9 illustrates the delay mechanism employed to control the mirror delay. A circular disk, which was called a synchronizing disk, was mounted on the rotating mirror shaft. This disk could be rotated freely about its axis by loosening a set screw. A small metal piece was attached to the disk, as shown in Figure 9a, and generated a triggering pulse in a Bentley magnetic sensor whenever it passed the sensor. This pulse triggered the transistor Q, which in turn triggered solenoids R1 and R2, when S1 was closed by the engine. Thus, a correct

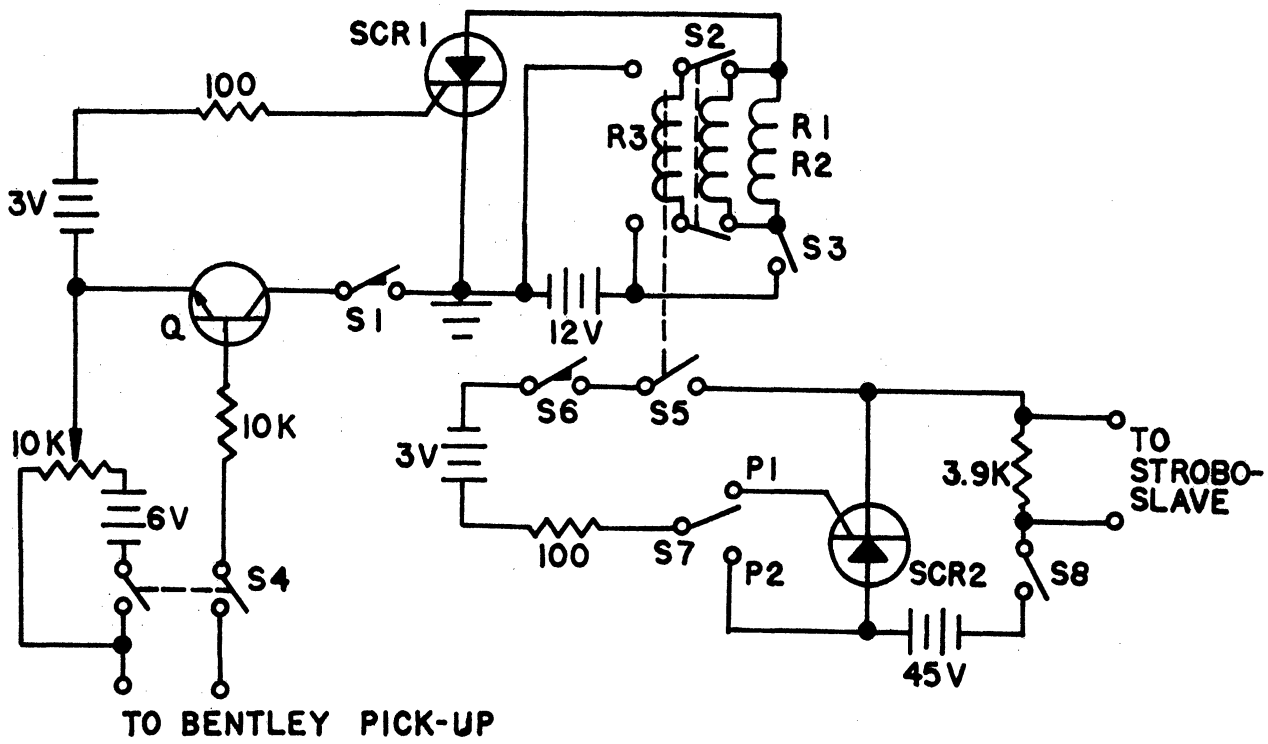

S1 ; Engine Distributor Switch #1
S2, S4 ; Manual DPDT Switch
S3, S8 ; Manual on-off Switch
S5 ; Relay Switch Operated by R3
S6 ; Engine Distributor Switch #2
S7 ; Manual SPDT Switch
R1 ; DC Solenoid for Camera Shutter #1
R2 ; DC Solenoid for Camera Shutter #2
R3 ; DC Relay Coil for S5
P1 ; Position of S7 for Single Flash
P2 ; Position of S7 for Multiple Flash

Figure 7. Control Circuit for Timing Synchronization

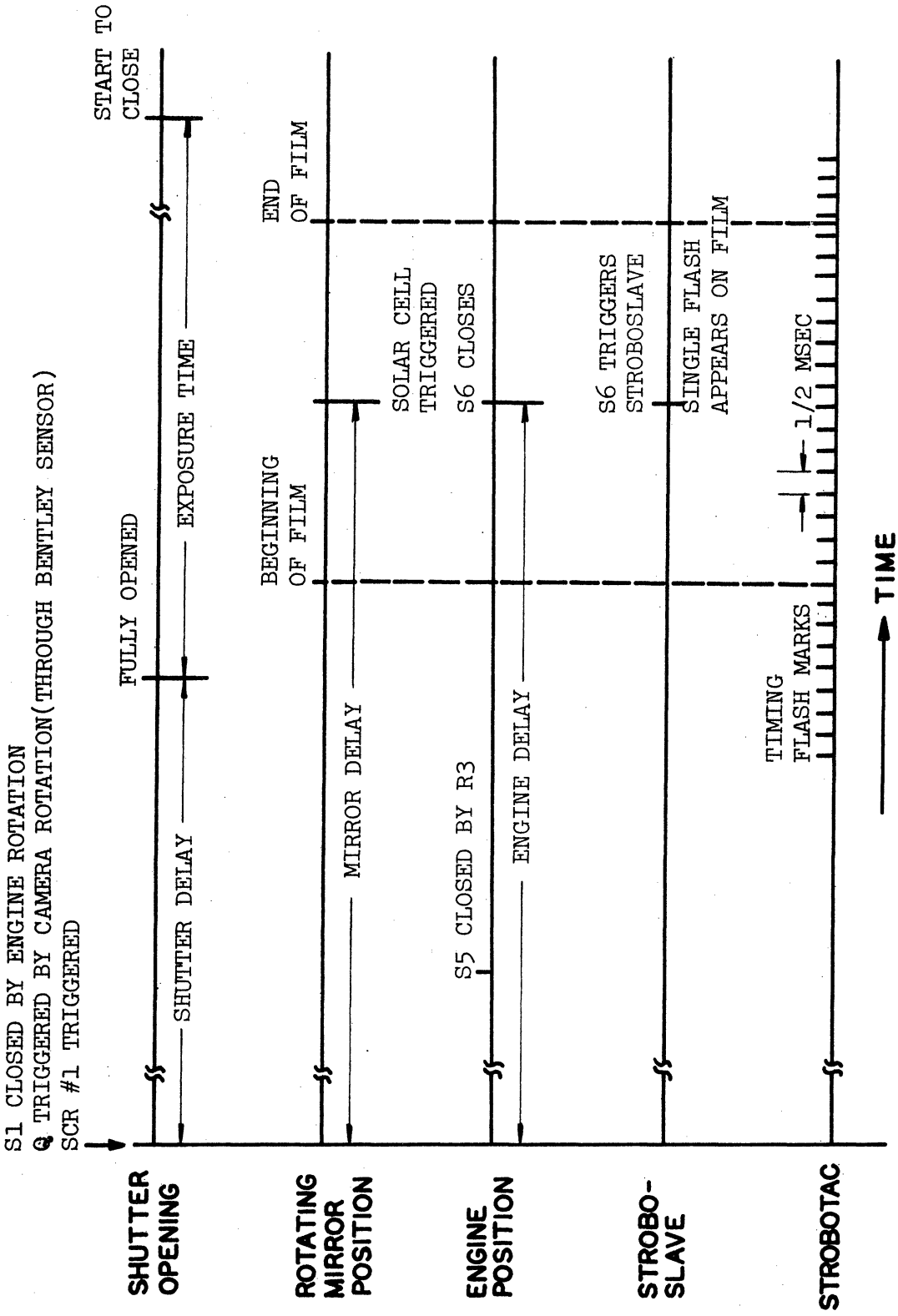

Figure 8. Timing Sequence of Engine and camera

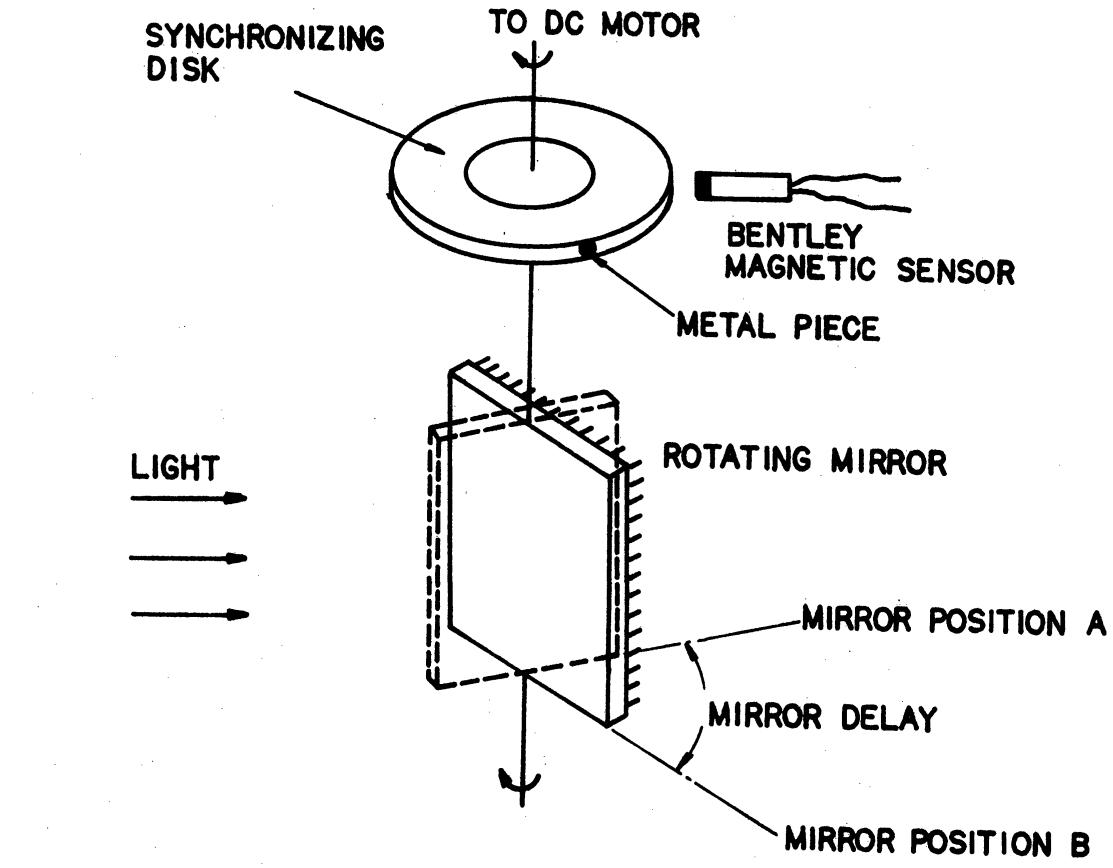

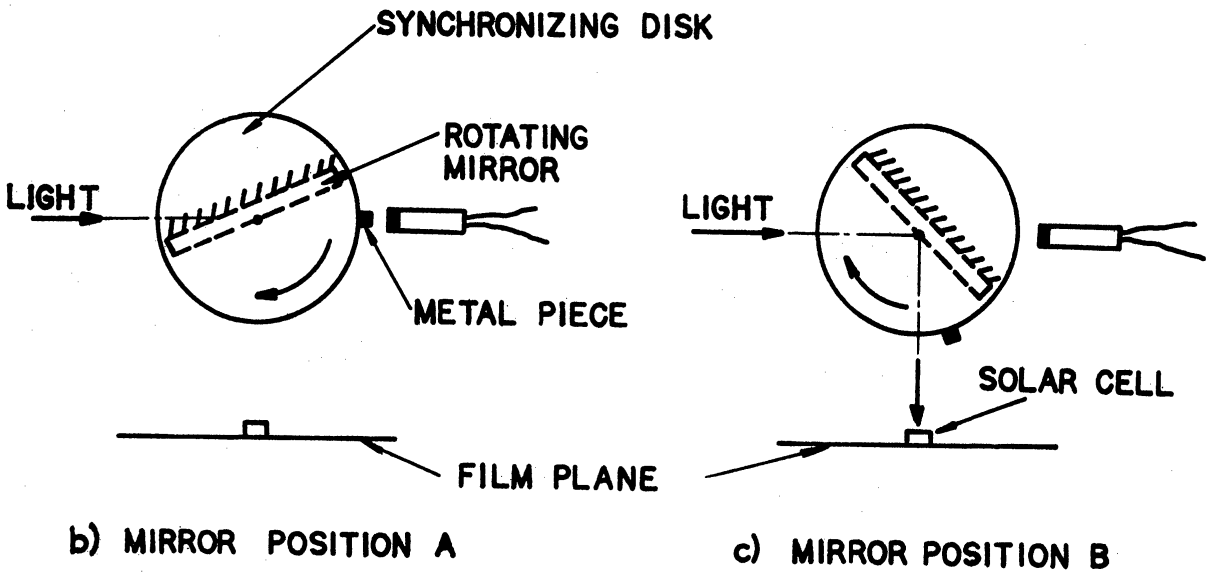

Figure 9. Mirror Delay Mechanism

mirror delay could be obtained by adjusting the relative angular position between the metal piece and the mirror, once a desired rotating speed of the mirror was determined.

Figure 10 shows the engine delay mechanism. It is a mechanical delay system similar to the mirror delay mechanism. Distributor #1 was mounted directly on the distributor shaft of the engine. Distributor #2 was mounted on the case of distributor #1. The distributor shaft was connected to the engine crankshaft by a 2 to 1 gear reduction system. Distributor #1 served as switch S1, and distributor #2 as switch S6. Switch S1 triggered the shutter when Q was closed, while switch S6 triggered a General Radio, Type 1539-A stroboslave and generated a single flash mark on the film. This flash mark was used to identify schlieren pictures in terms of engine crank angle. Therefore, a desired engine delay could be obtained by adjusting the relative angular position between S1 and S6.

Both the engine and mirror delays had to be equal and slightly greater than the shutter delay in order for the single flash mark to appear on the film. The shutter exposure time was set to avoid double exposures. Although the selection of a proper shutter exposure time depended upon the speed of the rotating mirror, an exposure time of 1/10 sec. was used for most of data runs. The sweeping rate of the rotating mirror was adjusted to provide satisfactory slopes of schlieren streaks on the film. Figure 11 shows the instrumentation used for the timing synchronization.

The procedure for photographing schlieren pictures is summerized as follows:

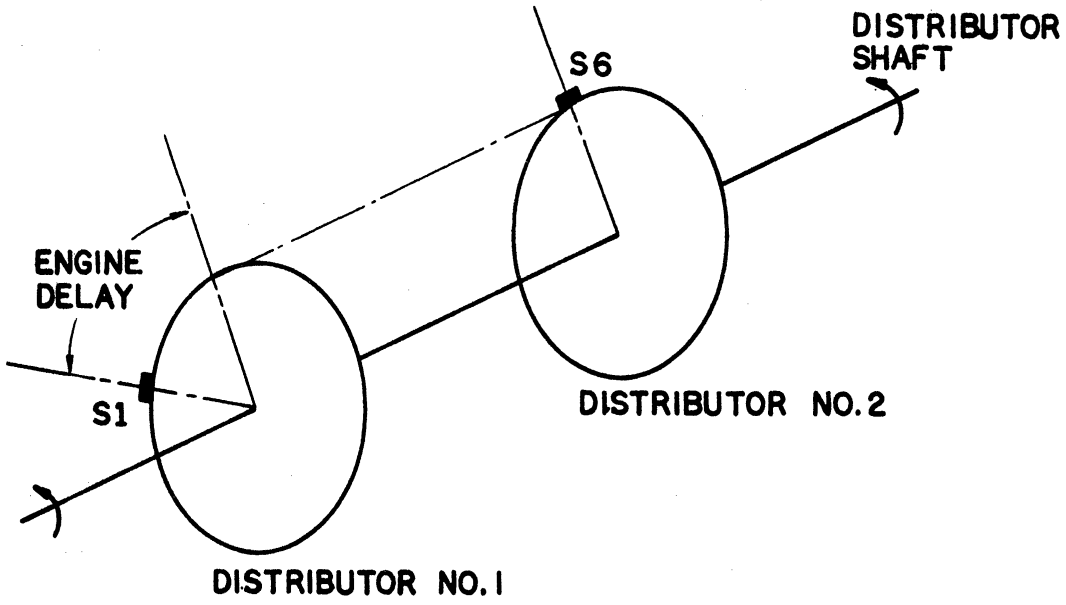

Figure 10. Engine Delay Mechanism

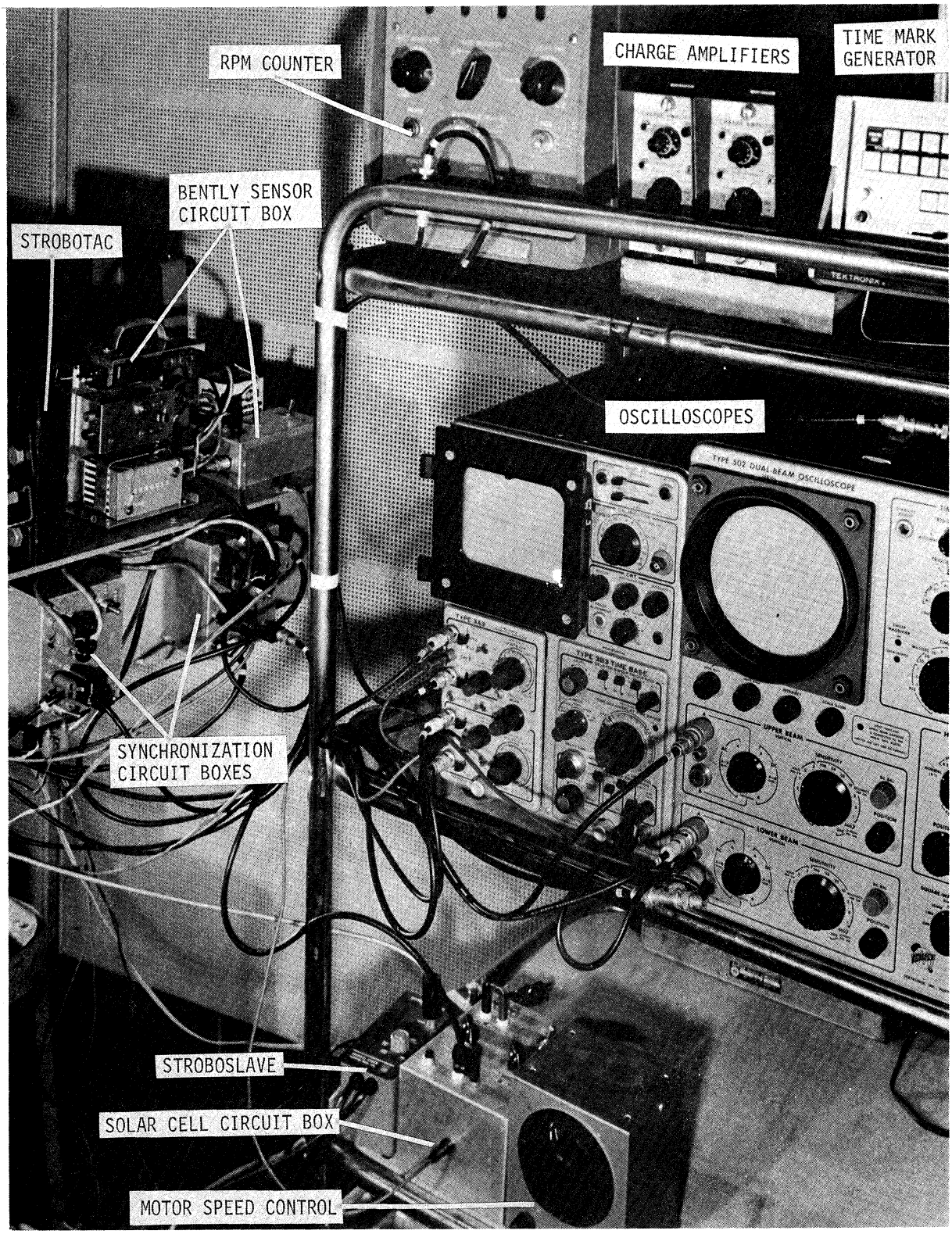

Figure 11. Instrumentation for Timing Synchronization and Other Flow Measurements.

a) Determine a proper speed of the rotating mirror that would give reasonable slopes of schlieren streaks on the film. The gas velocity to be measured may be roughly estimated.

b) Select a shutter exposure time such that a complete, single trace of schlieren streaks appear over the full length of the film.

c) Based on the rotating mirror speed just obtained from step a), adjust the mirror delay until it becomes slightly longer than the shutter delay. For a shutter delay of 33 msec. and a shutter exposure time of .1 sec., a mirror delay of 40 msec. was used in this study. Adjustment of the mirror delay can be made by observing the delay of the solar cell signal on a oscilloscope which is triggered by Q. (See Figures 7 and 9)

d) With a desired engine RPM, adjust the engine delay until it becomes equal to the mirror delay. (See Figures 7 and 10)

   (1) Short transistor Q manually.

   (2) Close Switch S5 by activating relay R3 manually.

   (3) Turn switch S7 to position P2

   (4) While adjusting the position of distributor point S6, observe the delay of the input pulse to the Stroboslave on a oscilloscope which is triggered by S1.

e) Select the engine crank angle at which a schlieren picture is to be taken.

   (1) The switch combinations are the same as described in step d).

   (2) Adjust the position of the distributor switch S1 while

observing the crank angle on the engine flywheel at which the Stroboslave flash mark appears.

f) Recheck the optical alignment.

g) The engine and the camera are now properly synchronized. Rearrange the switch combination as follows:

(1) Close switches S4 and S8.

(2) Connect relay coil R3 in parallel with solenoid R1 by S2.

(3) Turn switch S7 to position P1.

h) Remove the film slide and close switch S3.

i) The photographing sequence will be automatically followed as soon as S1 and Q are closed at the same time.

2.5 Analysis of Schlieren-Streak Velocity Data

All the velocity data presented in this study were measured at a test section location 21 in. downstream from the exhaust valve. This distance includes an effective pipe length of 3 in. for the exhaust flow passage within the engine exhaust port.

Figure 12 shows a typical schlieren-streak photograph recorded on Polaroid Type 47 film. The bright single flash mark indicates the engine crank angle at which the picture was photographed. The timing marks, each 1/2 msec apart, are used to compute the sweeping rate. From the streak principle described in Figure 2, the slope of a schlieren streak at any instant gives the instantaneous gas velocity at that particular instant. Thus, the instantaneous exhaust gas velocity u in ft/sec at crank angle α may be computed as follows:

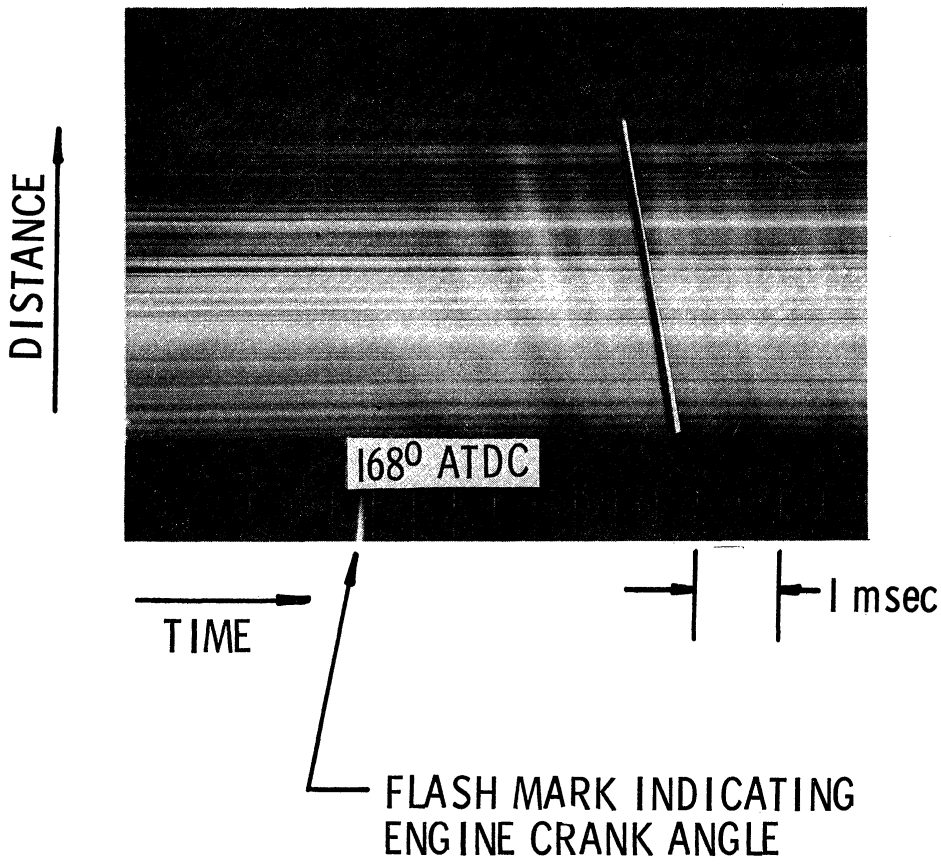

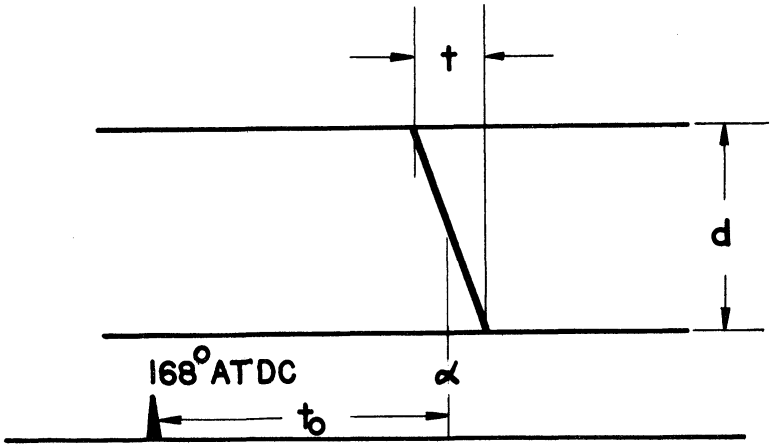

Figure 12. Computation of Gas Velocity from Schlieren-Streak Picture

$$u = \frac{1000}{12} \frac{d}{t} \frac{1}{M} , \qquad (2.4)$$

where M is the optical magnification factor between the test section and the film plane, d the distance in in., and t the time in msec. For the schlieren system used in this study, M was measured at 2.625. The crank angle may be computed from the engine speed and the time distance t_o:

$$\alpha = 168^\circ + \frac{360}{(60)\ (1000)} t_o \times RPM , \qquad (2.5)$$

where α is measured in degree ATDC, t_o in msec, and RPM is the engine speed in revolution per minute.

Figure 13 illustrates how the velocity profile was drawn as a function of crank angle. These pictures were taken with a motored engine at 1000 RPM. The timing marks are 1/2 msec apart. Figure 13a shows the beginning of exhaust gas flow at near the bottom dead center. The exhaust gas flows from the pipe to the engine cylinder during the early portion of the exhaust stroke, due to the low pressure in the cylinder at the time of exhaust valve opening. Figure 13b shows the flow reversal occuring at near the top dead center, just before the exhaust valve closes. The valve closing action creates a low pressure in the upstream portion of the pipe and causes this flow reversal.

Figure 14 shows a series of schlieren pictures photographed over the entire exhaust stroke of a motored engine at 1000 RPM. The instantaneous velocity profile obtained from these data is shown in Figure 15. The exhaust valve opens at 146° ATDC and closes at

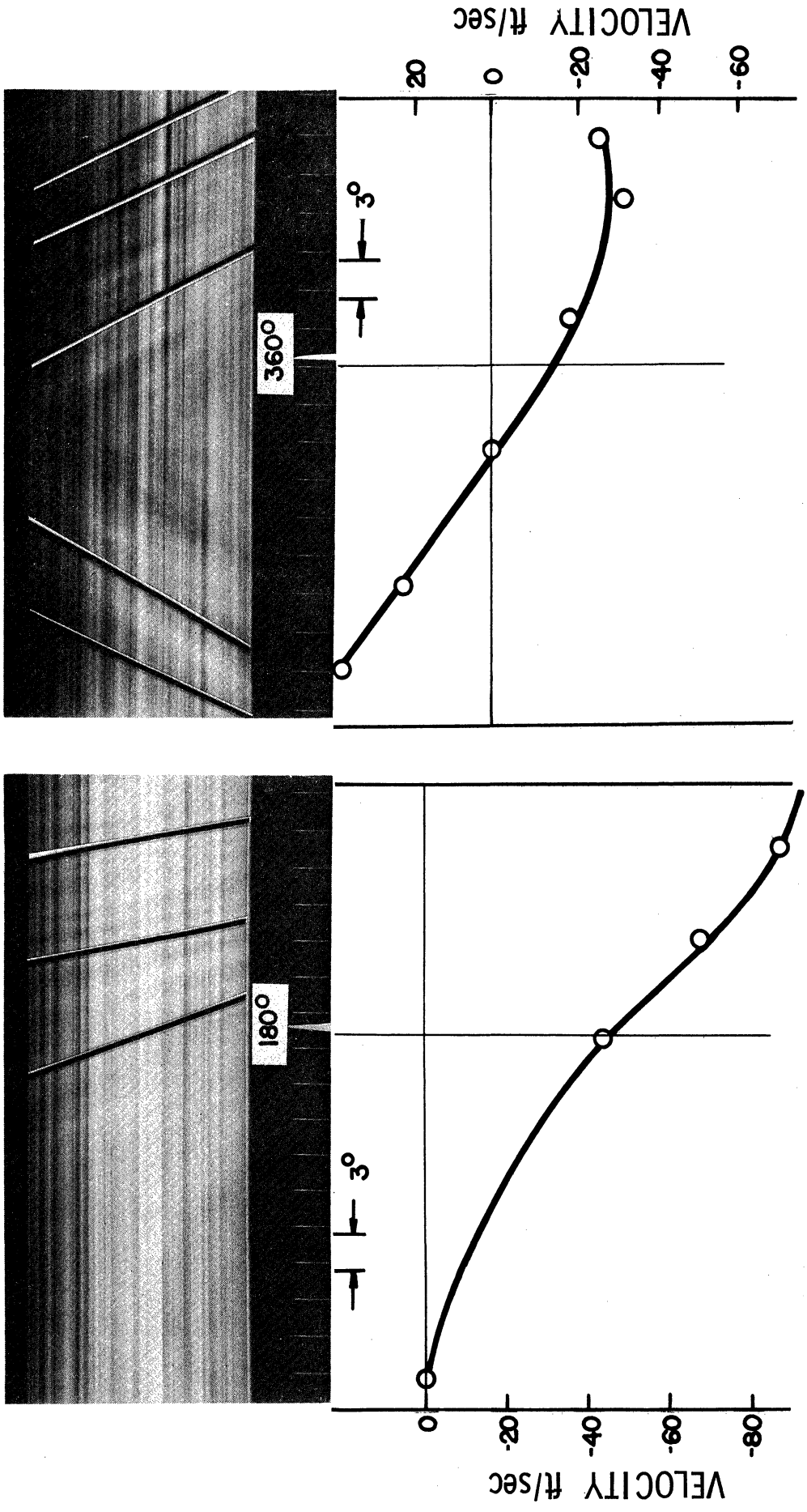

Figure 13. Plotting of Velocity Profile from Schlieren-Streak Picture

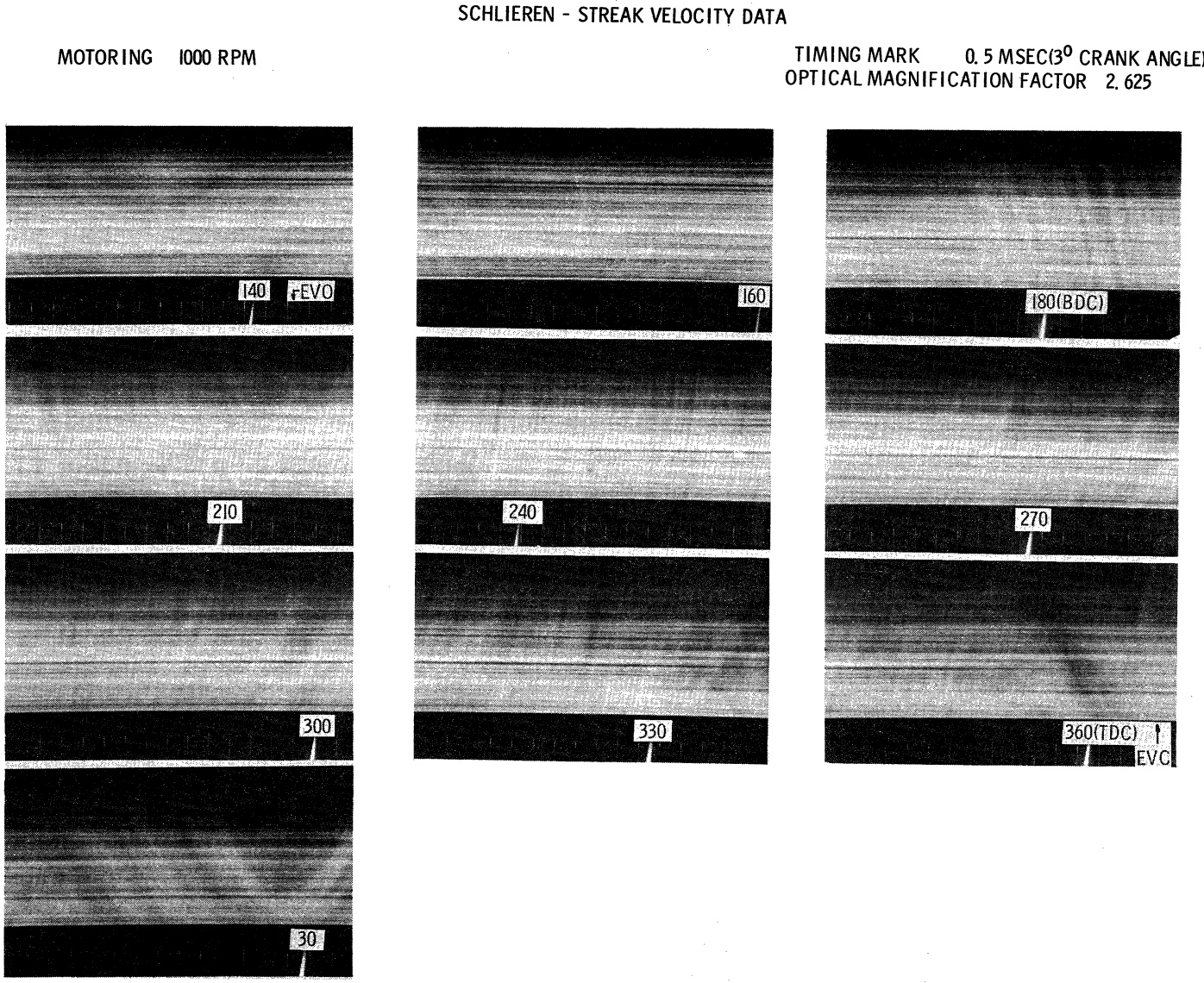

Figure 14. Schlieren-Streak Velocity Data in a Motored Engine.

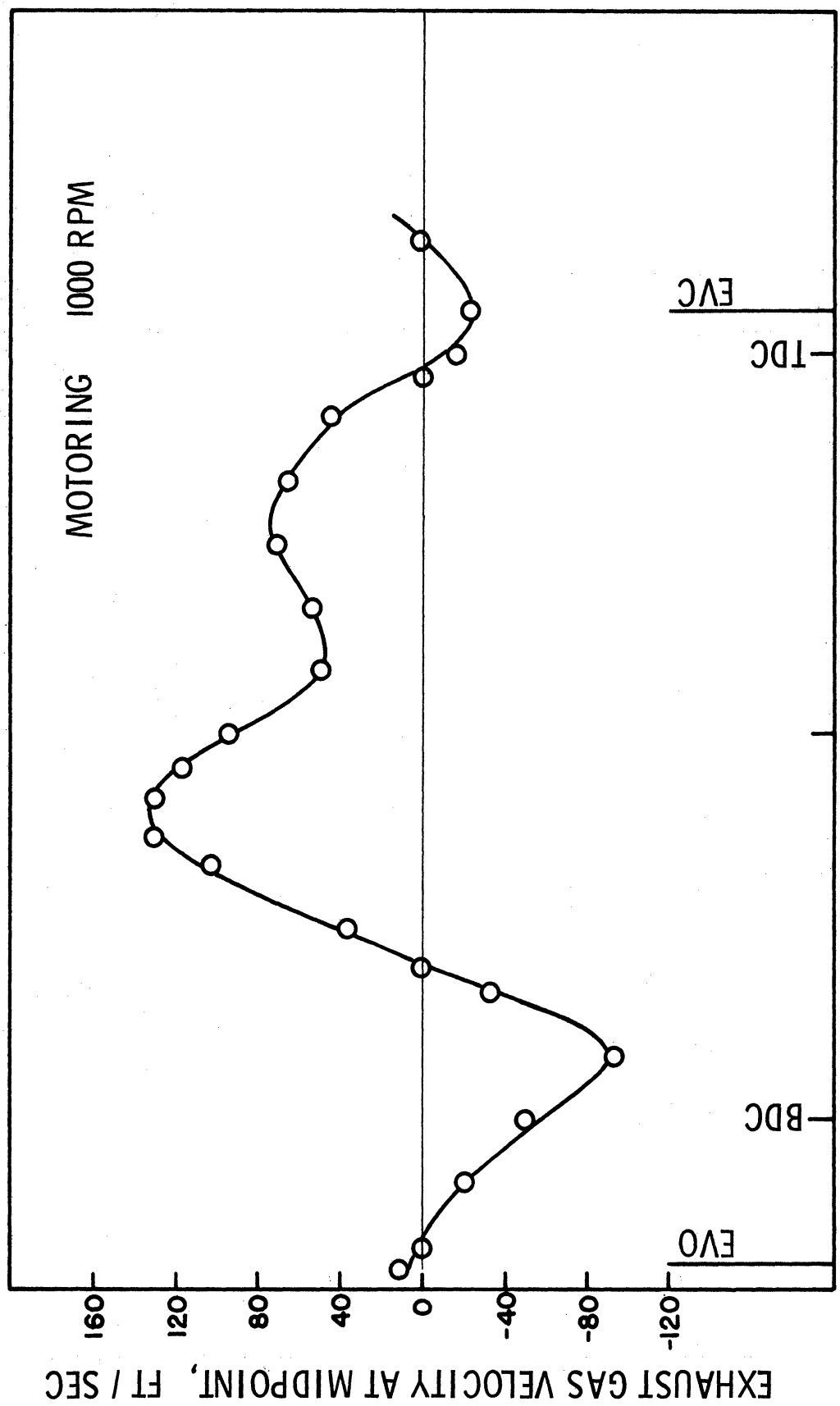

Figure 15. Instantaneous Exhaust Velocity Computed from Figure 14

10° ATDC. Very slow fluctuations of flow are vaguely visible at the start of the exhaust stroke. These slow fluctuations are caused by the residual pressure waves from the previous cycle. The absence of streaks during the early part of the exhaust stroke can be explained as follows: During the closed valve period of the previous cycle, the local density variations continuously lose their strength as density fronts due to heat and momentum dissipation and becomes less and less detectable by the schlieren system. At the beginning of an exhaust stroke, the exhaust gas in the pipe no longer contains strong local density variations and behaves like a homogeneous gas flow.

At 170° ATDC, intense streaks with negative slopes begin to appear. This time lag, between the valve opening and the appearance of the streaks, is necessary for the velocity front to travel from the valve to the test section. The cause of the reverse flow was explained in the discussion of Figure 13. The exhaust gas flow reverses its direction and becomes a normal flow (flow from the cylinder to the pipe) at 216° ATDC. This flow reversal is primarily due to the piston motion. As the piston starts to move toward the top dead center it compresses the gas in the cylinder while the exhaust gas flows into the cylinder. The cylinder pressure increases rapidly and finally becomes greater than the exhaust pressure. This positive pressure differences across the valve causes a change in flow direction. The first velocity peak appears at 246° ATDC. After this peak the gas in the cylinder expands rapidly in a manner similar to the blow-down in a firing engine. The second velocity peak occurring at 322° ATDC is affected not only by the piston motion but also the pressure wave actions in the exhaust

pipe.

At about 355° ATDC, the second flow reversal occurs. This flow reversal is caused by the valve closing action which tends to create a low pressure near the valve. After the valve closes, the exhaust gas merely fluctuates back and forth by wave actions in the pipe. The flow fluctuation diminishes rapidly as the amplitude of the pressure wave in the exhaust pipe decreases due to the damping effect of the pipe wall friction and the energy loss resulting from imperfect wave reflections at both ends of the pipe.

Figure 16 and 17 shows the schlieren velocity data for a firing engine at 1000 RPM. The reduced quality of the schlieren-streak image was caused by ground vibrations. A firing engine generated much greater vibrations than a motored engine, and some of the vibrations were detected by the sensitive schlieren optical system, despite the use of a vibration-isolated bench. However, slopes of streak images could be determined with reasonable accuracy and flow reversals could be located precisely without any difficulties.

Schlieren-streak pictures in Figures 14 and 16 were taken with the slit positioned at the centerline of the exhaust pipe. This implies that exhaust velocities were computed from the motion of the local density variations traveling along the centerline of the pipe. If there exist any velocity variations along a radial direction of the pipe, the local density variations near the wall might travel with a velocity different from the velocity at the centerline. The possibility of velocity variations along the radial direction was examined by comparing schlieren-streak data measured at two different slit positions,

SCHLIEREN - STREAK VELOCITY DATA

ENGINE SPEED 1000 RPM
IGNITION TIMING 13° BTDC
LOAD Part Load

TIMING MARK 0.5 MSEC(3° CRANK ANGLE)
OPTICAL MAGNIFICATION FACTOR 2.625

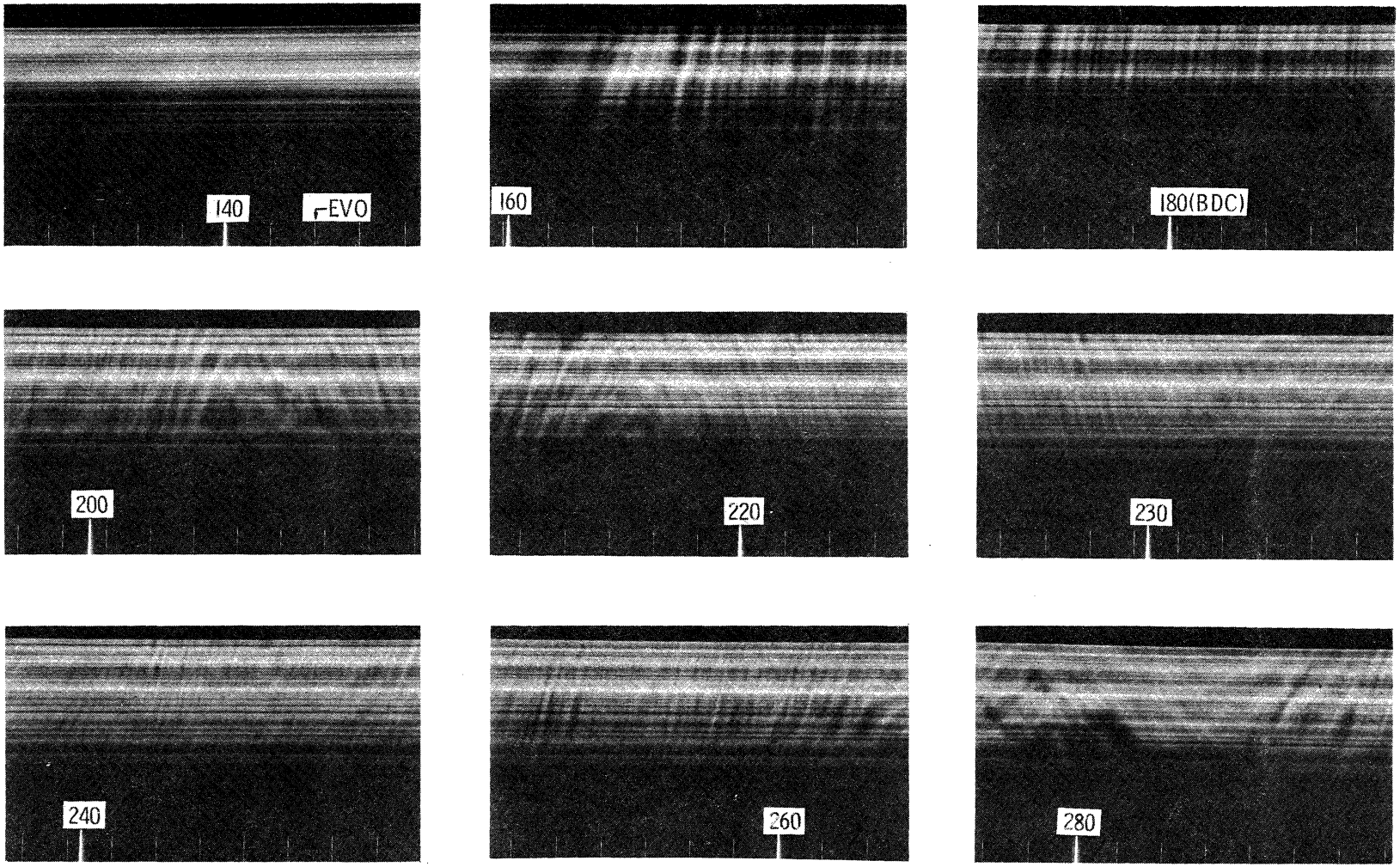

Figure 16. Schlieren-Streak Velocity Data in a Firing Engine.

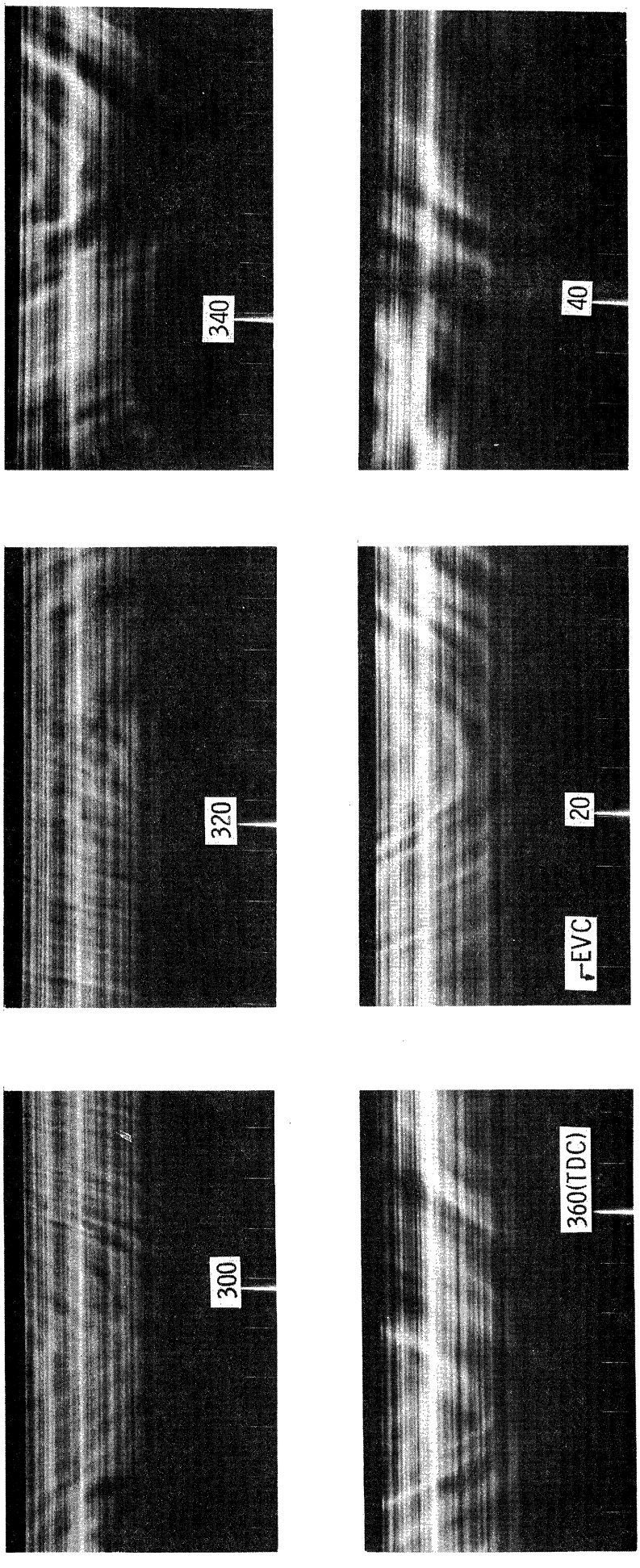

Figure 16 (Continued). Schlieren-Streak Velocity Data in a Firing Engine.

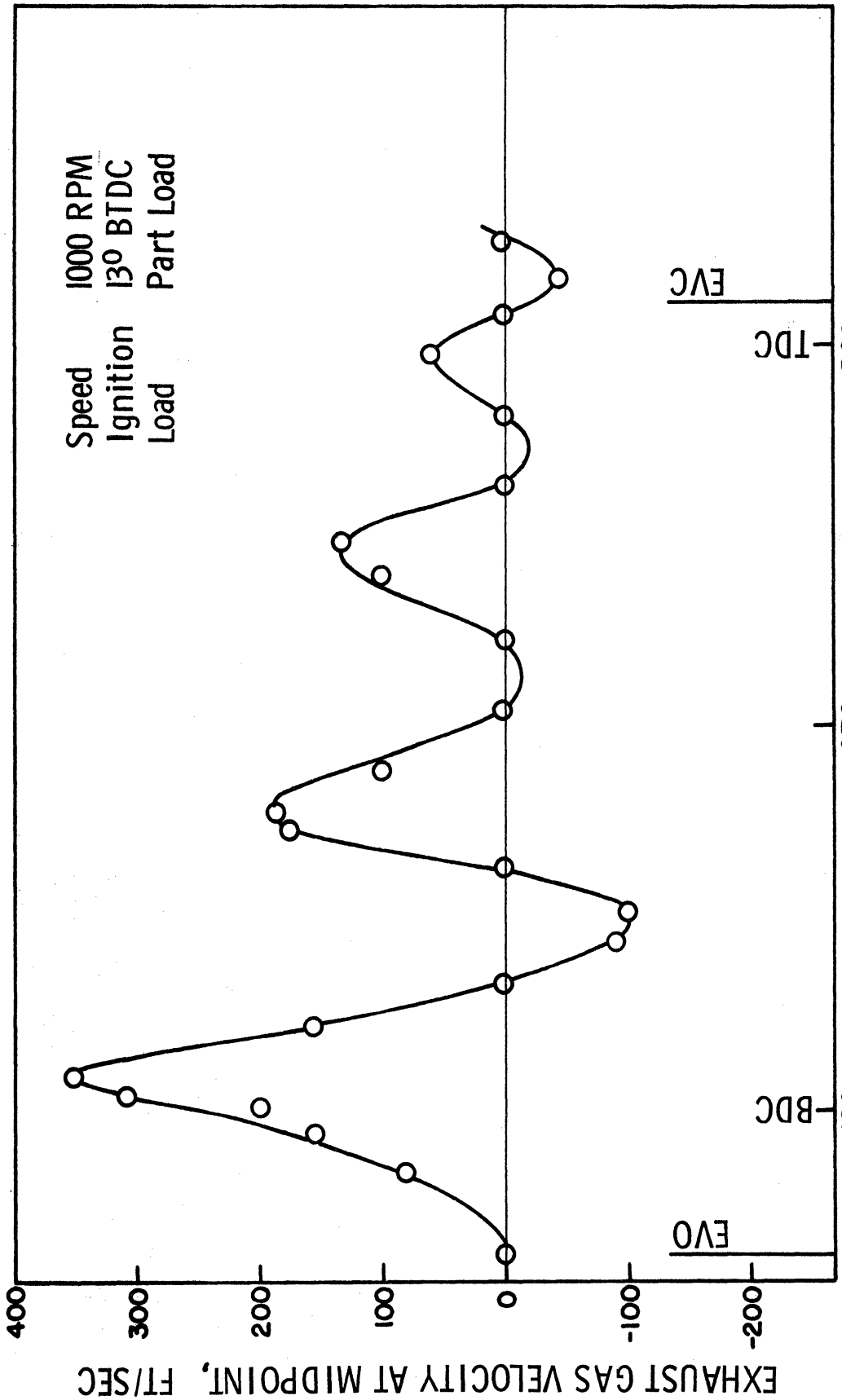

Figure 17. Instantaneous Exhaust Velocity Computed from Figure 16

one at the centerline and the other at 1/4 in. above the centerline. As shown in Figure 18, there appear no distinguishable velocity variations along the radial direction, at least within the radial distance of 1/4 in. from the centerline.

The effect of complex motions of cylinder components on the local density variations was also examined by a somewhat indirect manner. By feeding compressed air through a stationary engine, a flow velocity, comparable to that obtainable in a motored engine, could be obtained in the test section. The schlieren-streak picture taken with this system revealed that no visible trace of local density variations appeared on the film. This result implies that the complex motions of the piston and the valve plays an important role in generating the local density variations.

2.6 Comparison with Hot-Wire Anemometer

The performance of the schlieren-streak system as a flow velocity meter was checked with a constant temperature hot-wire anemometer. The anemometer used for this purpose was built by Winsor[34] for his measurements of mixture motion in a spark-ignition engine. A detailed description of the wire calibration and the instrumentation procedure are given by Winsor. A platinum wire of .0002 in. diameter was used to insure a sufficient frequency response of the anemometer. The hot-wire probe was inserted into the test section where the schlieren-streak velocity data were obtained. The hot-wire velocity data were taken at two different wire temperatures in order to compute the flow velocity from the wire output voltage. Figure 19 shows the velocity data measured at a wire temperature of 818° F. Each picture contains

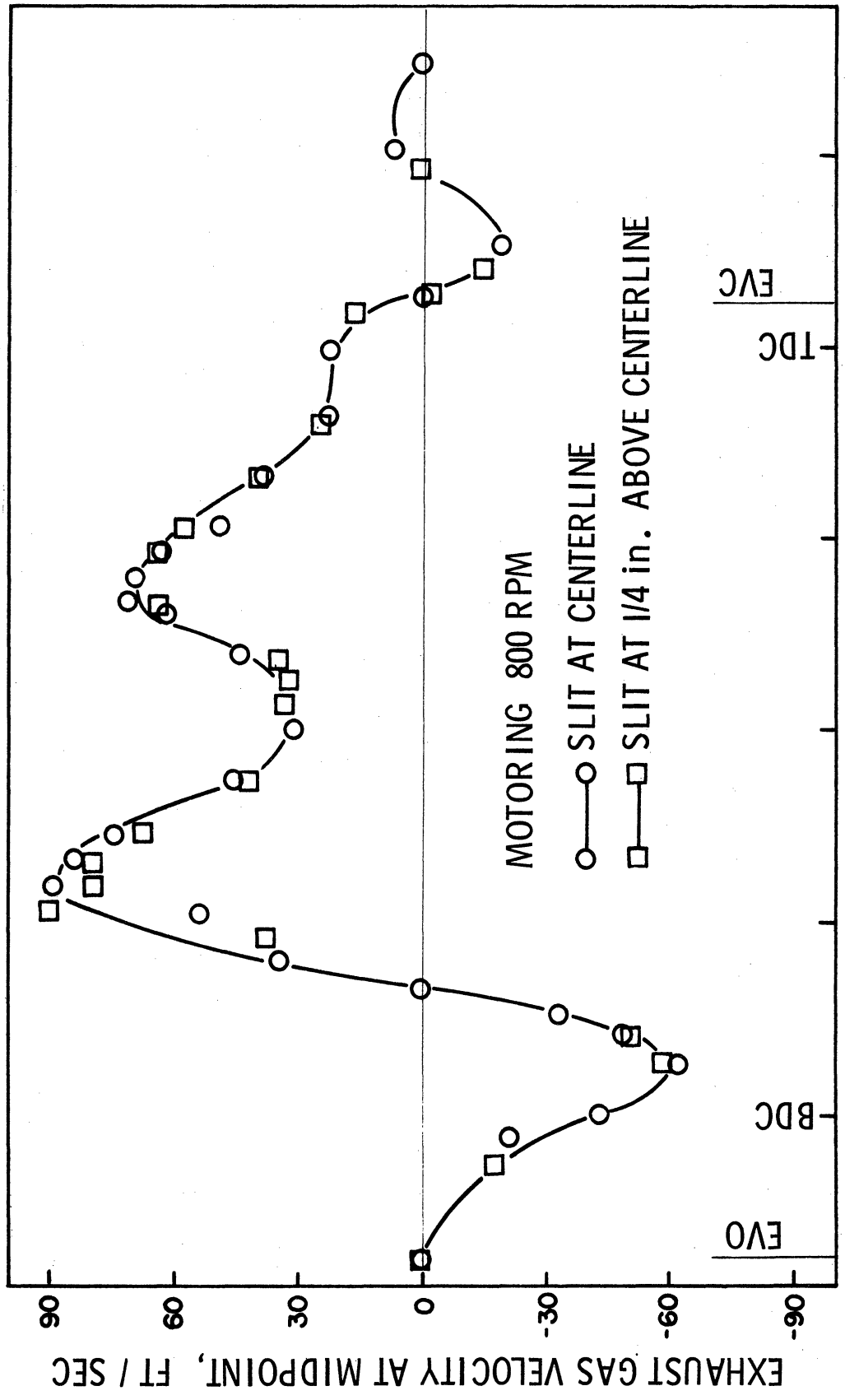

Figure 18. Effect of Slit Position on the Schlieren-Streak Velocity Data

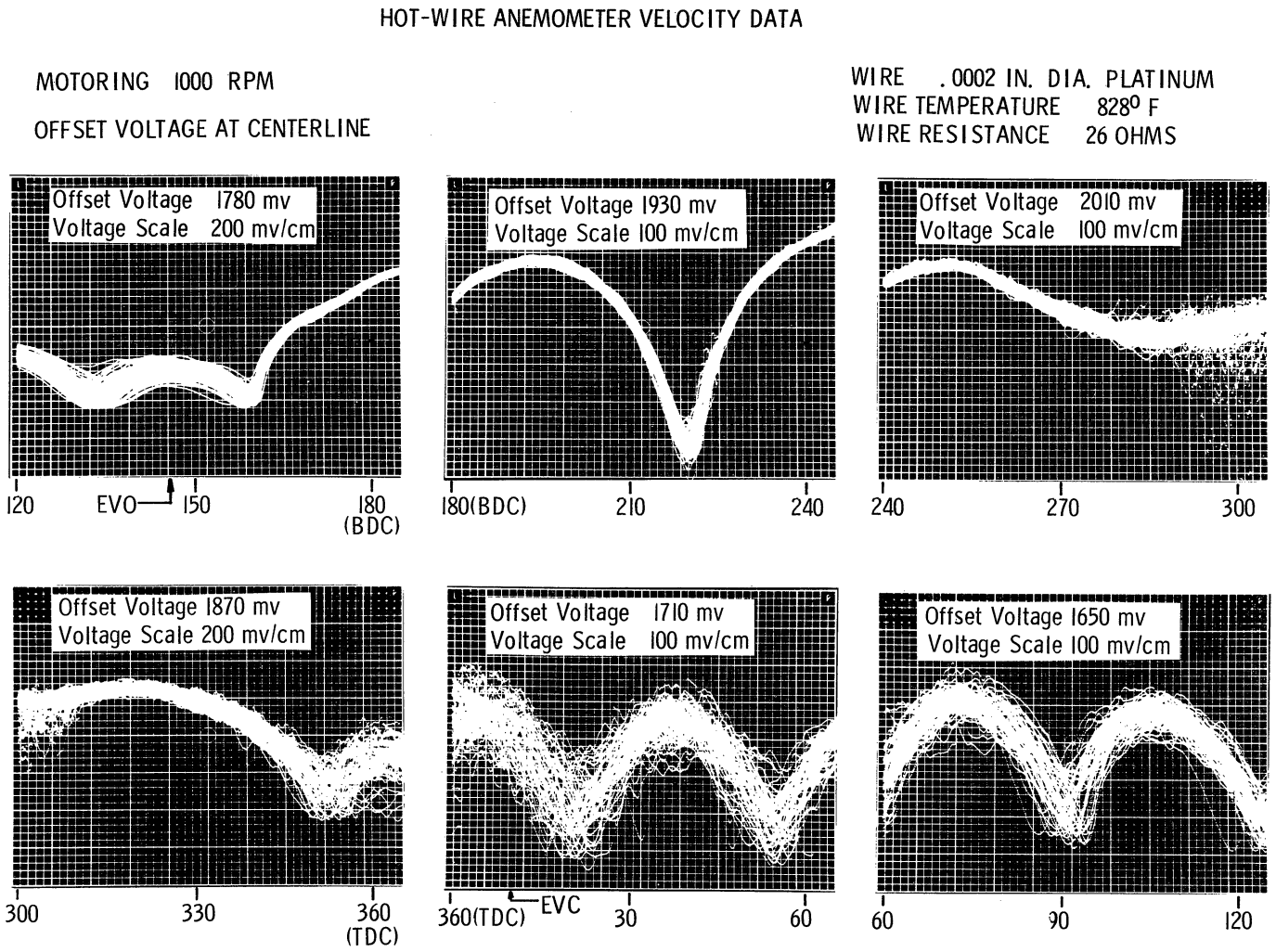

Figure 19. Exhaust Velocity Traces from Hot-Wire Anemometer.

50 traces of the wire output signal. Since a hot-wire anemometer does not respond to the direction of flow, the nodal points in these pictures represent the instant of zero velocity at which flow reversals occur. Figure 20 shows the comparison of velocity data measured by the schlieren-streak system and the hot-wire anemometer in a motored engine at 800 RPM. The agreement between these two methods indicates that the schlieren-streaks represent the flow velocity, and demonstrates the capability of the schlieren-streak system as a flow velocity meter.

Another important conclusion may be drawn from the above comparison. The hot-wire anemometer measures a local flow velocity while the schlieren-streak system measures an average flow velocity over the optical path within the test section. Hence, good agreement between two methods suggests that the velocity profile at any instant is relatively flat over the cross-sectional area of the pipe except the boundary layer as expected in highly turbulent flow. This result is in agreement with the conclusion drawn in Section 2.5 that there was no effect of slit position on the velocity data. The result also suggests that the boundary layer on the window surface does not have any appreciable effect on the schlieren-streak velocity data. This implies that the streaks recorded on the film are caused mainly by the local density variations traveling in the central region of the main stream where the velocity profile is relatively flat.

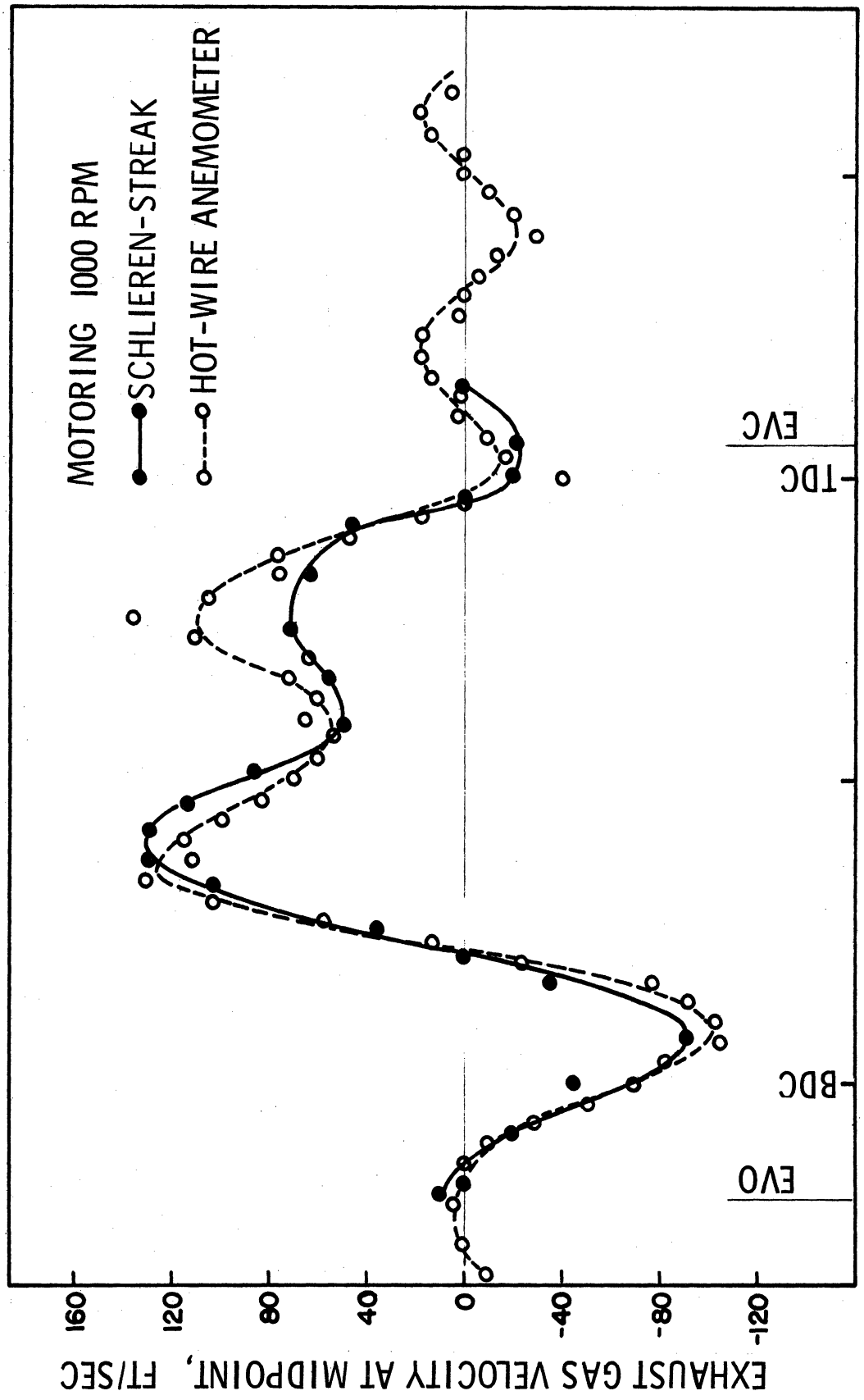

Figure 20. Comparison of Exhaust Velocity Data Measured by Schlieren-Streak System and Hot-Wire Anemometer

III. CFR SINGLE CYLINDER ENGINE AND AUXILIARY EXPERIMENTAL APPARATUS

3.1 CFR Single-Cylinder Engine and Its Exhaust System

The engine used in this study was a CFR single cylinder, four-stroke, spark-ignition engine with variable compression ratio. Pertinent dimensions of this engine are listed in Table 1. Figure 21 shows the engine and its instrumentation for various engine measurements. The original engine system, which had been used for the standard fuel testing at a constant engine speed, was slightly modified in order to increase variability of some of the engine parameters. The original motor-generator set was replaced by a General Electric Type TLC-2242 DC electric dynamometer. An electronic engine speed regulator was used to control the engine speed within an accuracy of 2 RPM variations. A throttling valve was installed in the intake system. A distributor shaft, separate from the ignition breaker, was connected to the crankshaft through a two to one worm gear ratio. On this distributor shaft, two commercial distributor points were mounted as described in Section 2.4 for the timing synchronization.

An intake surge tank with a volume approximately 100 times larger than the engine displacement was used to minimize flow pulsations in the intake. The fuel was gravity-fed through the standard CFR engine carbureter system. Commercial lead-sterile gasoline was used to provide sufficient photographing time without cleaning the window at the test section. The resistance type spark plug was used to eliminate electronic noise which had caused difficulties in triggering the Strobolave flash unit.

TABLE I

CFR ENGINE PARAMETERS

Bore	3.25 in.
Stroke	4.50 in.
Displacement	37.33 $in.^3$
Connecting Rod	10 in.
Compression Ratio	6.18 : 1
Exhaust Valve Port Diameter	1.25 in.
Maximum Exhaust Valve Lift	0.2207 in.
Intake Valve Opens	10° ATDC
Intake Valve Closes	34° ATDC
Exhaust Valve Opens	146° ATDC
Exhaust Valve Closes	10° ATDC
Exhaust Pipe Diameter	1 5/8 in.
Exhaust Pipe Length	36 in.
Exhaust Surge Tank Volume	4070 $in.^3$
Intake Surge Tank Volume	4070 $in.^3$

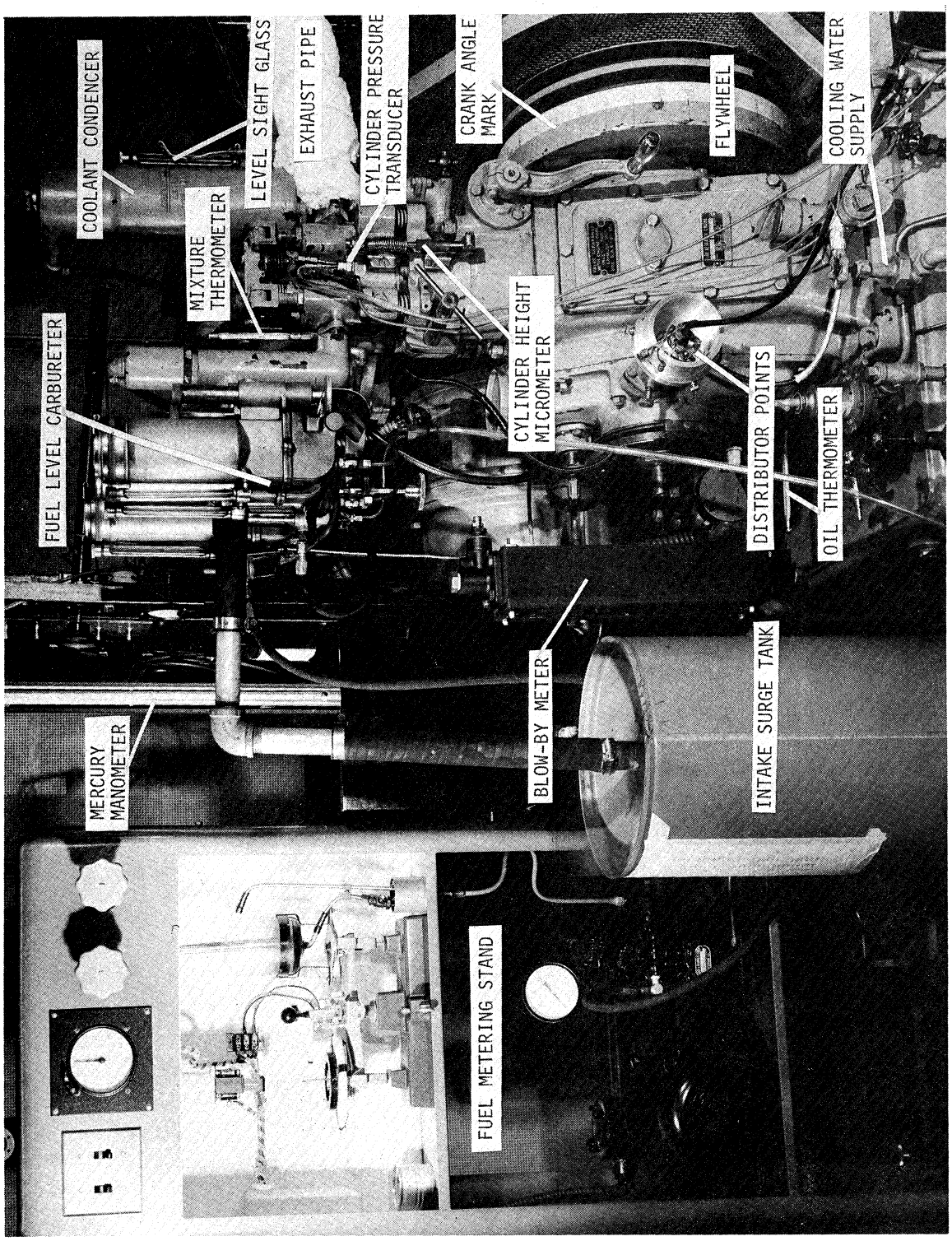

Figure 21. CFR Engine and Its Instrumentation.

The exhaust system consisted of a straight pipe and a surge tank. The pipe ended at the surge tank with a flare-ending. The volume of the exhaust surge tank was the same as that of the intake surge tank. The exhaust gas was vented to the atmosphere through the laboratory extraction system. The exhaust pipe and the bottom half of the exhaust surge tank were insulated from the room atmosphere in order to prevent any convection air currents from disturbing the schlieren optical images, as shown in Figure 4.

3.2 Measurements of Pressure and Temperature

Several measurements of pressure and temperature were required to provide input data for the simulation program and to evaluate the program performance. These experimental parameters are listed as follows:

a) Instantaneous cylinder pressure

b) Instantaneous exhaust pressure

c) Exhaust surge tank pressure

d) Intake manifold vacuum

e) Average exhaust gas temperature

f) Average exhaust surge tank temperature

g) Exhaust pipe wall temperatures

For the cylinder pressure measurement, a Kistler 601A quartz pressure transducer was used with a Kistler Model 503 charge amplifier. A cooling adapter was used to cool the transducer. Since piezoelectric type transducers respond only to the change of pressure, a base line pressure must be determined in order to read the pressure trace in terms of absolute magnitude.

In a firing engine, the base line was determined by the exhaust surge tank pressure as shown in Figure 22a. In a motored engine, however, the cylinder pressure was fairly close to the exhaust pressure throughout the exhaust period, requiring a more accurate method for determination of the base line pressure. A balanced diaphragm built by General Motors Research Laboratories, was used for this purpose. Its details are shown in Figure 23. This unit is basically a mechanical switch that is activated by a predetermined differential pressure across the diaphragm. One side of the diaphragm was exposed to the cylinder and the other side to a reference chamber with a known pressure. Therefore, by locating the instant at which the diaphragm was activated, the absolute cylinder pressure at that instant could be determined. Figure 22b illustrates how a base line could be drawn on a cylinder pressure trace for a motored engine. The reference chamber was maintained near atmospheric pressure. The contact on the balanced diaphragm indicator remained closed most of the time during an engine cycle because of high cylinder pressure. Just before the exhaust valve opened, the cylinder pressure dropped below the reference pressure and opened the contact at point A. This contact was connected to a simple on-off electric circuit and thus provided an electric pulse indicating the instant of on or off position of the contact. With a diaphragm of .003 in. thick, the differential pressure that activated the diaphragm indicator was measured statically at 0.386 psi. By adjusting the reference pressure, the position of point A could be easily adjusted. At point B, the cylinder pressure increased and the contact was closed until point C was reached at which the contact was once again opened. For most of the cylinder pressure data presented in this study, point A was used

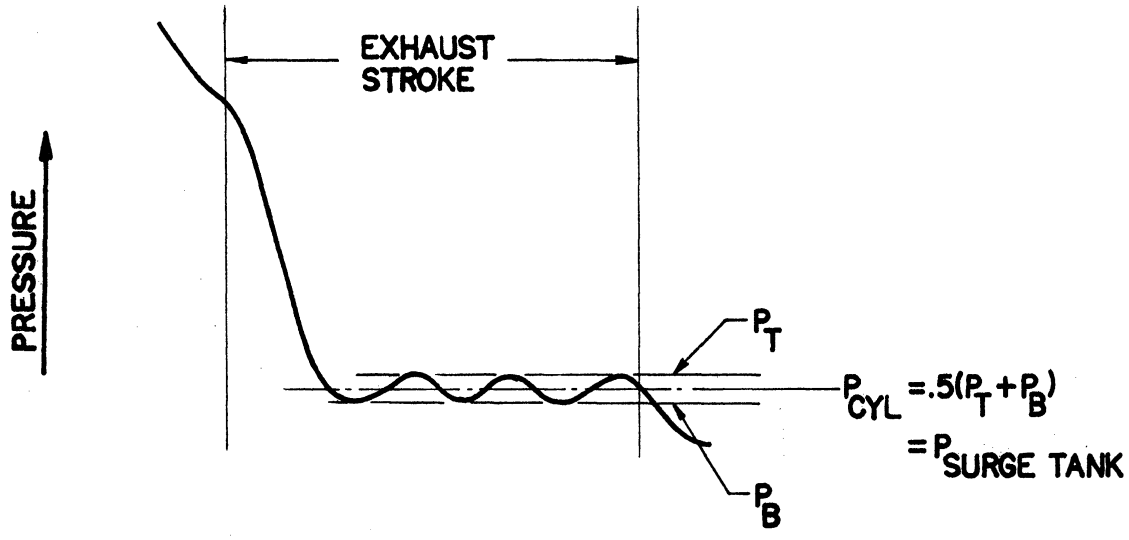

a) FIRING ENGINE

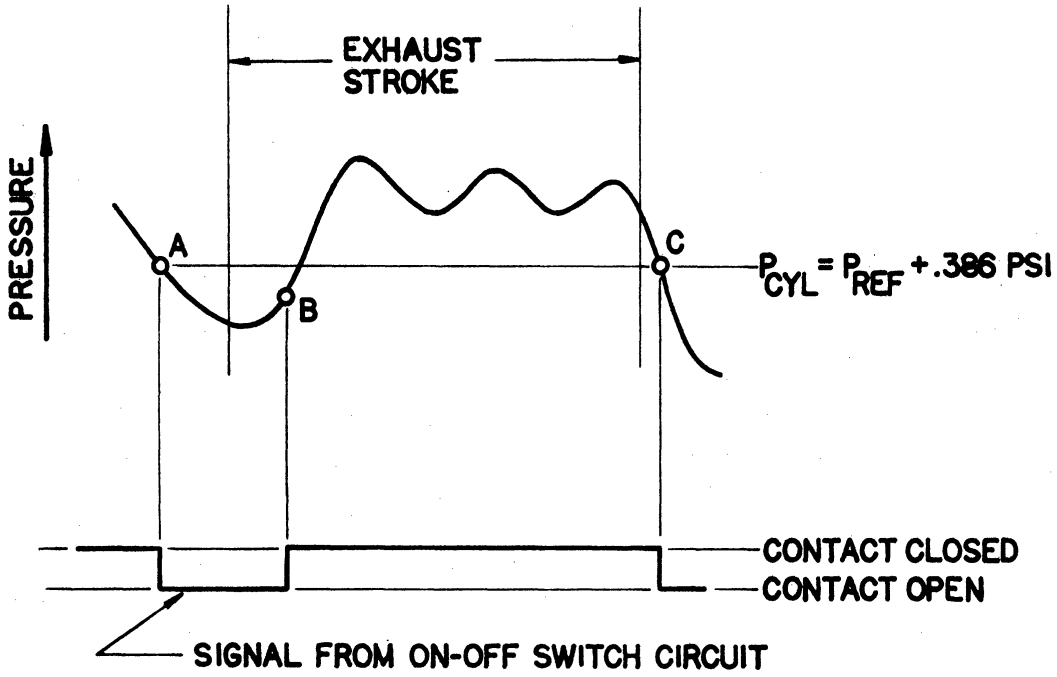

b) MOTORED ENGINE

Figure 22. Determination of Base Line on Cylinder Pressure Traces

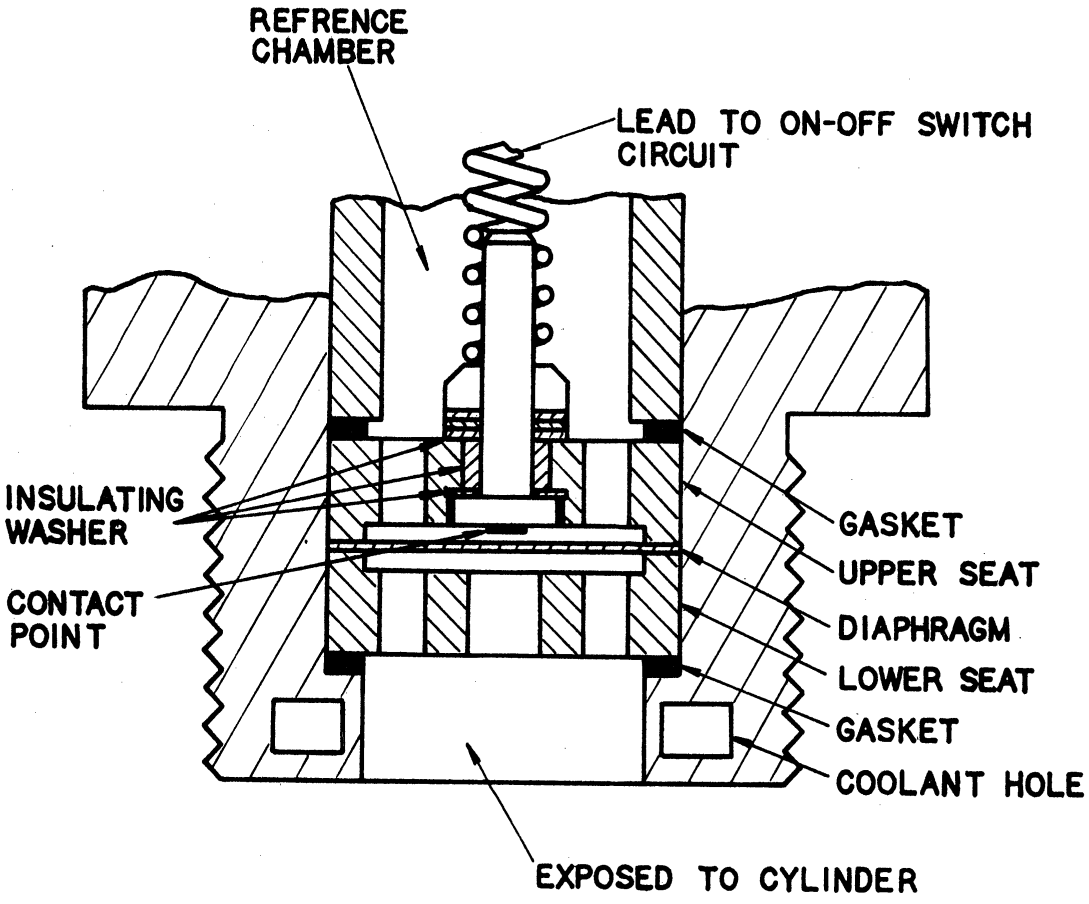

Figure 23. Balanced Diaphragm Indicator

to determine the base line pressure.

The instantaneous exhaust pressure was measured at the test section by a Kistler 701A quartz pressure transducer. The base line for exhaust pressure traces was determined by the exhaust surge tank pressure, which was measured by a water manometer. The exhaust surge tank pressure was always lower than the atmospheric pressure by approximately 1 1/2 in. of water due to the laboratory exhaust extraction system. Typical cylinder and exhaust pressure traces are shown in Figures 24 and 25. These pressure traces were recorded on a Tektronix oscilloscope type 564. The oscilloscope was calibrated by a Tektronix Type 184 time mark generator.

The average exhaust gas temperature was also measured at the test section by a .003 in. platinum - 13% rhodium thermocouple with the copper alloy extension wire. The average exhaust surge tank temperature was measured by a 1/16 in. Chromel-Alumel thermocouple. The exhaust pipe wall temperatures were measured at both ends of the exhaust pipe by an 1/16 in. iron-constantan thermocouple. The wall temperature distribution along the pipe was assumed to be linear.

3.3 Measurements of Other Engine Parameters

In order to furnish the input data for the simulation program, measurements of several other engine parameters were required. The air flow rate into the engine was measured by a 1/2 in. nozzle mounted upstream of the intake surge tank. The pressure drop across the nozzle was measured by a water manometer. The fuel flow rate was measured by a Cenco fuel scale. The fuel-air ratio was adjusted by the fuel level

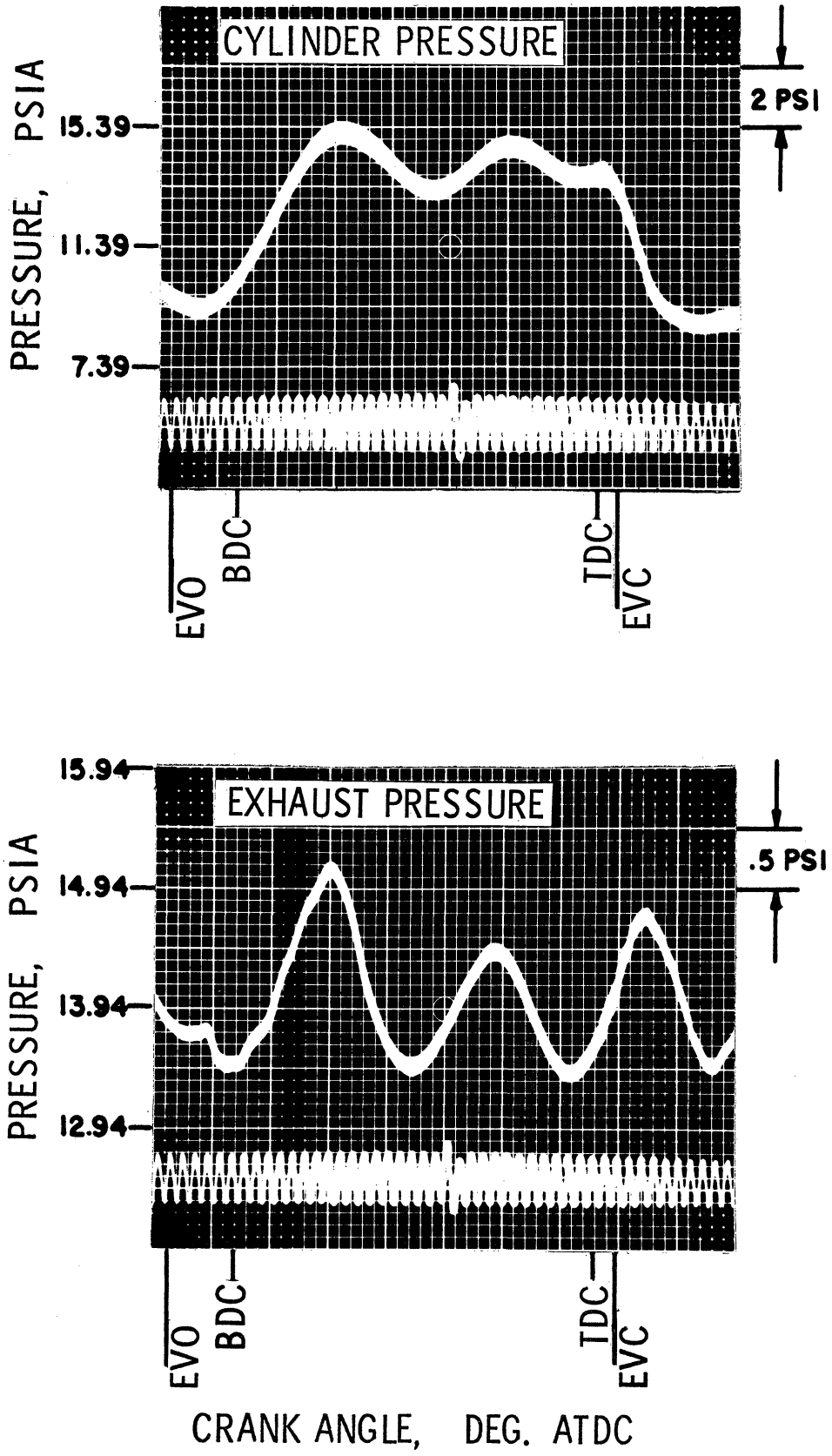

Figure 24. Oscilloscope Records of Pressures in a Motored Engine at 1000 RPM

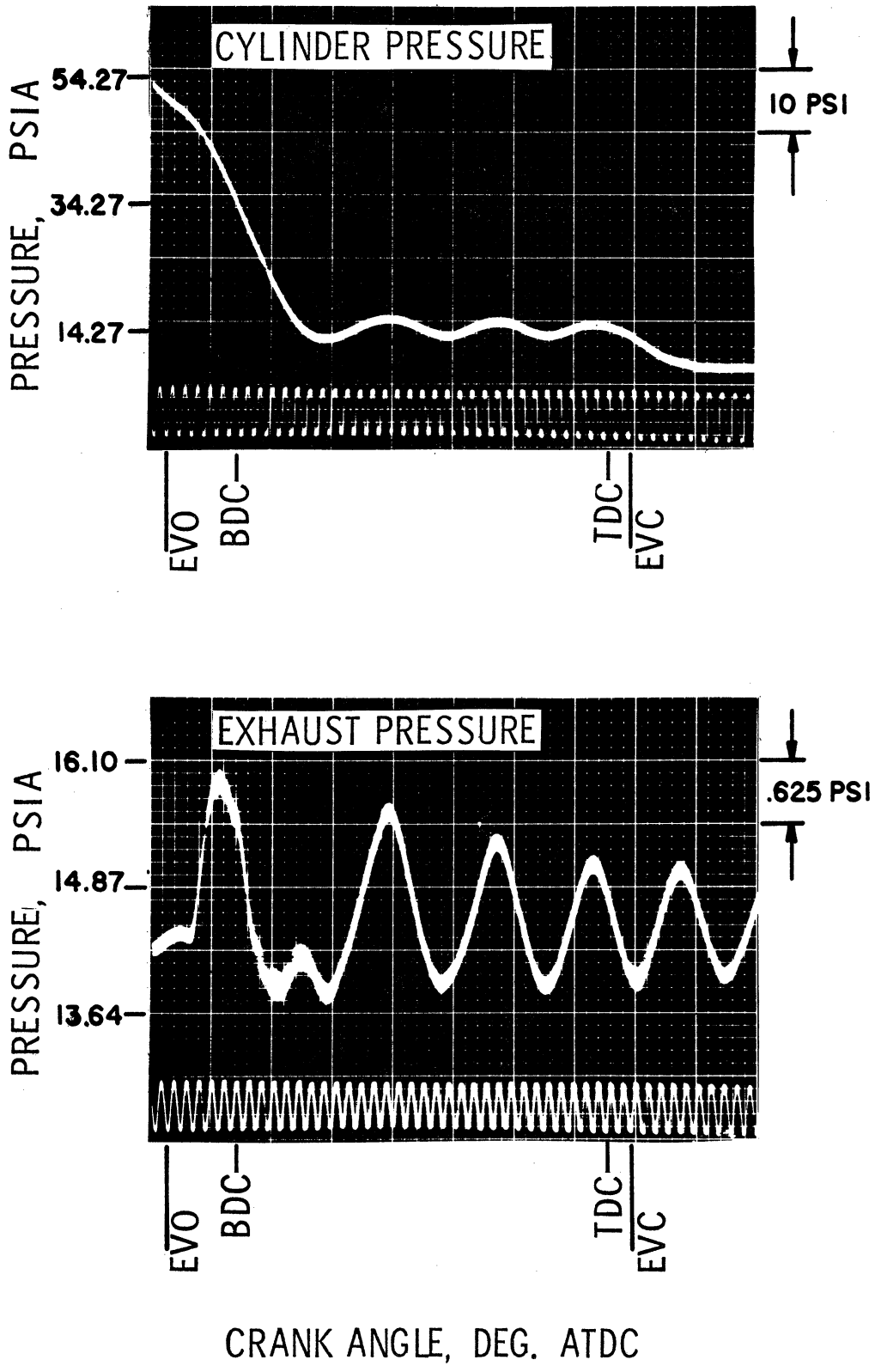

Figure 25. Oscilloscope Records of Pressures in a Fired Engine at 1000 RPM, 13° BTDC Ignition Timing, and Full Load

adjustment knob which was originally equipped with the CFR engine carbureter system. The engine speed was recorded by a Hewlett-Packard Model 521A electronic RPM counter. Figure 21 shows some of the instruments described in this section.

IV. SIMULATION OF AN EXHAUST SYSTEM

4.1 Scope of Simulation

The typical exhaust system of a commercial automobile engine consists of pipe branchings, changes of section, and open, closed, and semiclosed ends of piping. Automobile emission exhaust treatment devices result in more complicated exhaust systems. The simulation of a more complicated exhaust system, although quite possible,[4] was beyond the scope of this study.

The purpose of the computer simulation presented in this investigation is not to analyze exhaustively each component of a commercial exhaust system, but to understand the applicability of basic theories of gas dynamics in a simplified exhaust system of a laboratory engine. One of the advantages of using a simple exhaust system is that one can evaluate the performance of the computer simmulation in a more precise and simple manner because the unknown parameters in the theoretical analysis can be reduced in proportion to the simplicity of the system.

Another complication of the computer simulation arises from the cyclic nature of the internal combustion engine. In order to simulate truly the exhaust system, one must perform a cyclic computation where the initial state matches the final state, which is equivalent to the initial state of the next cycle. For simplicity, however, the cyclic computation is excluded in the present study. A transient solution is obtained during a typical exhaust period by feeding into

the simulation program the experimentally measured initial conditions of the engine and the exhaust system.

The geometry of the exhaust system employed in this study is described schematically in Figure 26. The dimensions of each compoment are given in Section 3.1. The governing equations for the pipe flow will be developed. The cylinder charging and discharging processes and the effect of the surge tank will be described in detail in the section dealing with boundary conditions. The solution technique employing the method of characteristics will be described. A step-by-step description of the computation procedures is also included in this chapter.

General assumptions in the development of the theoretical analysis of the exhaust system are listed as follows:

a. The exhaust gas is a homogeneous mixture of ideal gases.
b. No chemical reaction occurs either in the engine cylinder or in the exhaust system during the exhaust period.
c. Thermal properties such as the specific heat ratio and the gas constant of the exhaust gas remain constant.
d. The effects of heat transfer and friction are computed based on quasi-steady theories.
e. Quasi-steady theories are also applied in the valve flow and the inlet section of the exhaust surge tank.
f. No flow discontinuities in the exhaust system, such as shock waves, are assumed.

Specific assumptions related to each component of the exhaust system are described in the corresponding sections in this chapter.

4.2 Governing Equations for the Exhaust Pipe Flow

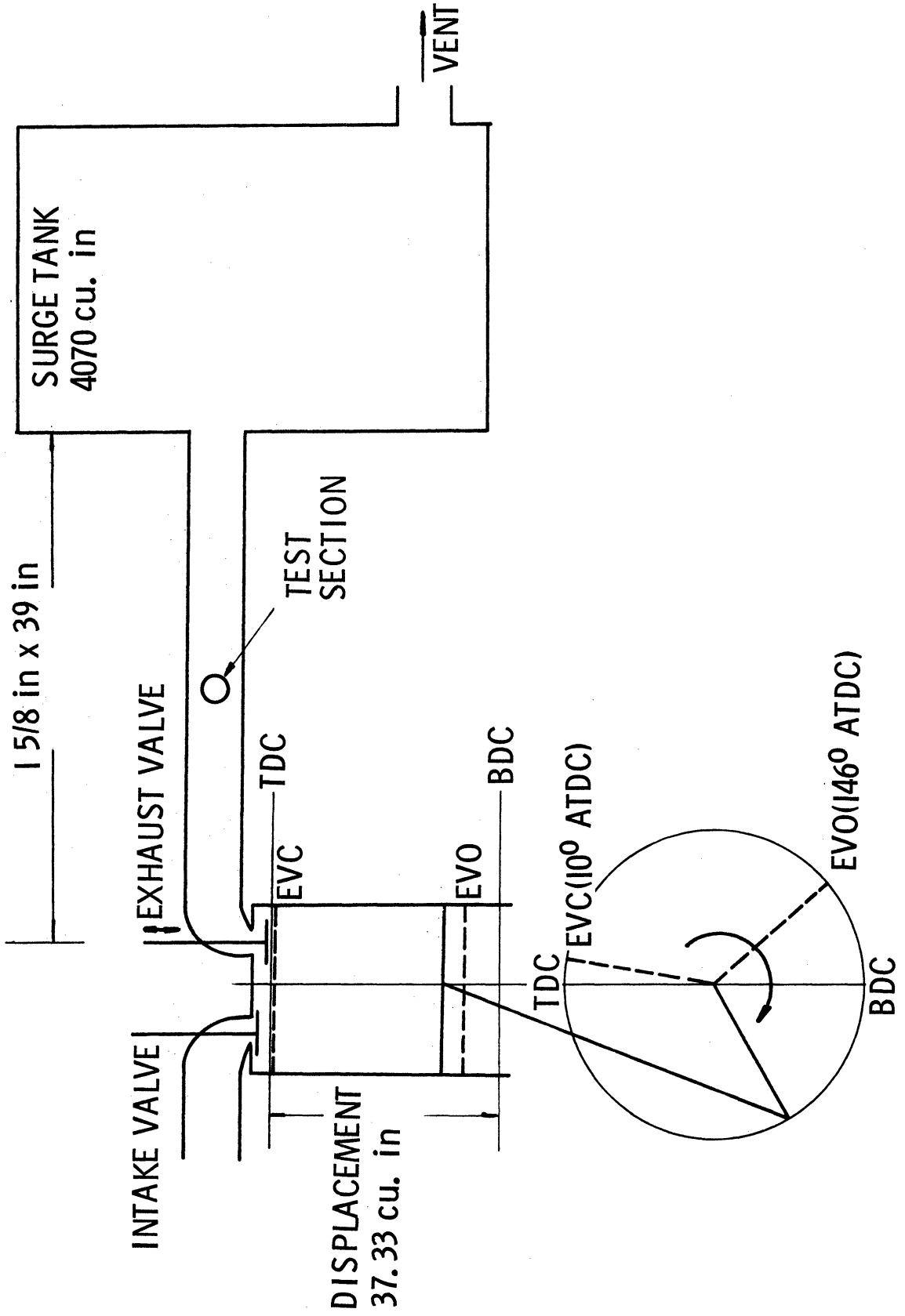

Figure 26. Exhaust System of CFR Single-Cylinder Engine

The theory of one-dimensional unsteady gas flow with heat transfer and friction is developed in this section. The assumption of one-dimensional flow, while not describing transverse velocity variations, provides a simplification which enables one to use the method of characteristics as a solution technique for the governing equations. The conservation laws of mass, momentum, and energy are given in Equations (4.1) to (4.3) for the one-dimensional unsteady gas flow. The derivation of these equations is available in standard text books.[26]

Mass: $$\frac{\partial \rho}{\partial t} + \frac{\partial}{\partial x}(\rho u) = 0 \qquad (4.1)$$

Momentum: $$\frac{\partial u}{\partial t} + u\frac{\partial u}{\partial x} + \frac{1}{\rho}\frac{\partial p}{\partial x} + \frac{1}{\rho}\frac{4}{D}\tau_w = 0 \qquad (4.2)$$

Energy: $$C_v\left(\frac{\partial T}{\partial t} + u\frac{\partial T}{\partial x}\right) + \frac{p}{\rho}\frac{\partial u}{\partial x} - \frac{4}{\rho D}(q_w + \tau_w u) = 0 \qquad (4.3)$$

where τ_w is the wall shear stress, q_w the heat transfer rate per unit area at the pipe wall, and D the pipe diameter. The axial heat conduction is neglected in deriving Equation (4.3).

The equation of state for a mixture of ideal gases is

$$p/\rho = RT \qquad (4.4)$$

and the speed of sound in an ideal gas is given by

$$a^2 = kp/\rho \ . \qquad (4.5)$$

Equation (4.3) is more usefully presented in terms of pressure. Combining Equations (4.3) and (4.4) and using the relationship between the gas constant and the specific heats result in the relation

$$\frac{\partial p}{\partial t} + u\frac{\partial p}{\partial x} - a^2\left(\frac{\partial \rho}{\partial t} + u\frac{\partial \rho}{\partial x}\right) - (k-1)\frac{4}{D}(\tau_w u + q_w) = 0 \ . \qquad (4.6)$$

Equations (4.1), (4.2), (4.5), and (4.6) are the set of governing equations which are used to solve for the dependent variables p, ρ, u, and a.

From the definitions of τ_w and q_w,

$$\tau_w = \rho u^2 f/2 \qquad (4.7)$$

and

$$q_w = h_w(T_w - T) \qquad (4.8)$$

where f is the friction factor, h_w the pipe wall heat transfer coefficient, and T_w the pipe wall temperature.

Very little data are available for the effect of flow pulsation on friction and heat transfer. As the velocity, pressure, and temperature in the pipe vary not only with time but also with distance, values of f and h_w based on steady flow conditions may be different from the true values under pulsating flow. In addition, several rapid flow reversals occur in the pipe during the exhaust period under certain conditions. It is quite certain that these flow reversals affect the boundary layer development, resulting in changes in heat transfer and friction.

Bayley et al.[1] studied the effect of flow pulsation on heat transfer from a flat plate and found that heat transfer increased as a function of a pressure pulsation parameter P defined by $P=\Delta p/\rho u^2$. Heat transfer increased approximately by a factor of $P^{0.23}$ after a certain critical value of P. Below this limit there was no appreciable

effect of pulsation on heat transfer. Bayley suggested this critical value of the pressure pulsation parameter corresponded to the flow conditions at which the flow reversal occurs. Hatta et al.[14] also studied experimentally the effect of oscillating flow on heat transfer by varying the pulsation frequency between 1 to 10 cps and the amplitude up to 80%. Their results showed no appreciable change in heat transfer due to pulsation. The effect of viscous dissipation on heat transfer was studied theoretically by Ishigaki[18] in an oscillating flow system. He found that viscous dissipation had a large effect on heat transfer, particularly in the region of high pulsating frequencies. Increase in heat transfer by a factor of up to 6 was predicted by his theory at a certain extreme combination of Eckert number and Strouhal number.

In the absence of accurate data for unsteady heat transfer, it is common practice to use the quasi-steady heat transfer assumption in which the steady heat transfer coefficient is applied to the instantaneous flow conditions. Goyal et al.[13] used the empirical heat transfer coefficient proposed by McAdam[7] for steady turbulent flow in their simulation of the exhaust system of an internal combustion engine. During the valve closing period, however, they arbitrarily used the Eichelberg coefficient multiplied by a factor of 3. Wright and Gill,[36] in their simulation of the exhaust system of a two-stroke engine, used Reynolds analogy to compute heat transfer from the measured friction factor. Their result showed good agreement between experiment and theory.

In this study the heat transfer was computed from Reynolds analogy[7] for turbulent pipe flow as follows:

$$h_w = \frac{\tau_w C_p / U}{1 + (v_{xj}/U)(N_{pr} - 1)} \quad , \qquad (4.9)$$

where

C_p = Specific heat at constant pressure

U = Mean flow velocity

v_{xj} = Flow velocity at the limit of the laminar sublayer

N_{pr} = Prandtl number.

the term v_{xj}/U in Equation (4.9) is a function of the Reynolds number.[7] The typical Prandtl number of the exhaust gas at a relative fuel-air ratio of 1.3 was estimated at 0.75, and the typical Reynolds number of the exhaust flow was estimated at 10^5. From these values of the Prandtl number and the Reynolds number, the denominator in Equation (4.9) was computed as 0.83.

The increase in heat transfer due to flow pulsation was estimated from the experimental data of Bayley et al.[1] for similar pulsating conditions. This estimation gave approximately a 25% increase in heat transfer over the steady value. Hence, the final form for the heat transfer coefficient that was used in the present simulation program is

$$h_w = (1.25/0.83)(1/2) f \rho u C_p . \qquad (4.10)$$

A constant value was used for the friction factor. From the Moody chart, $f = 0.0045$ was obtained for typical exhaust flow conditions.

4.3 Boundary Conditions

The complexity of the simulation of an exhaust system depends largely upon the boundary conditions. Even in a simple exhaust system, such as used in the present study, the cylinder-discharging process through the exhaust valve must be precisely described in order to obtain an accurate result.

4.3.1 Cylinder-Charging and -Discharging Processes

In the present analysis of the cylinder-charging and -discharging processes, the following assumptions are made in addition to the general assumptions listed in Section 4.1:

a. The gas in the cylinder is treated as a lumped control volume.

b. The boundary work consists of ideal PV work only.

c. The specific stagnation enthalpy of the leaving gas stream is equal to that in the cylinder.

The last assumption is based upon the reasoning explained in the analysis of the cylinder discharging process later in this section.

If one selects a control volume as the volume of the gas occupying the cylinder, the rate form of the first law of thermodynamics can be written as

$$\frac{dE}{dt} = \dot{Q} - \dot{W} + \frac{d}{dt}(H^{\circ}_{in}) - \frac{d}{dt}(H^{\circ}_{out}) \ , \qquad (4.11)$$

where

$\frac{dE}{dt}$ = The rate of change of internal energy within the control volume.

$\dot{Q}$ = The rate of heat transfer to the control volume

$\dot{W}$ = The rate of work done by the moving boundary of the control volume

$\frac{dH^{\circ}_{in}}{dt}$, $\frac{dH^{\circ}_{out}}{dt}$ = The rate of stagnation enthalpy flow into and out of the control volume, respectively.

Expressing the equation of state for the gas in the cylinder in terms of its internal energy and the work term $\dot{W}$ in terms of cylinder pressure and volume,

$$E = p_c v_c/(k-1) \qquad (4.12)$$

$$\dot{W} = p_c \frac{dv_c}{dt} \qquad (4.13)$$

Substituting Equations (4.12) and (4.13) into Equation (4.11) results in

$$\frac{dp_c}{dt} = \frac{1}{v_c}\left[(k-1)\{\frac{d}{dt}(H^{\circ}_{in}-H^{\circ}_{out})+\dot{Q}\} - kp_c \frac{dv_c}{dt} \right] . \qquad (4.14)$$

Since there is no valve overlap, two cases are considered with regard to the flow conditions at the exhaust pipe inlet only.

a) Cylinder Discharging Process

In this case, there is no mass inflow and only the mass outflow through the exhaust valve is considered. A thermodynamic analysis for the discharging process,[16] reveals that the specific stagnation enthalpy of the leaving gas stream is equal to the specific stagnation enthalpy of the gas remaining in the cylinder if there is no heat transfer to the system and no change of specific entropy within the cylinder. The equality is also valid if the heat transfer takes place in

a reversible manner. In the cylinder of an internal combustion engine the heat transfer during the expansion and exhaust strokes can be approximated by a reversible process and a polytropic process is often used in the engine cycle analysis. On this basis of reversible heat transfer, the specific stagnation enthalpy of the leaving gas stream is assumed to be equal to that in the cylinder. Thus,

$$h^{\circ}_{out} = h^{\circ}_{c} = h_{c} \tag{4.15}$$

where h°_{out} is the specific stagnation enthalpy of the leaving gas stream, h°_{c} and h_{c} the specific stagnation enthalpy and the specific enthalpy of the gas remaining in the cylinder, respectively.

The rate of mass change in the cylinder at any instant is computed by using the assumption of quasi-steady flow across the exhaust valve.

$$\frac{dm_{c}}{dt} = -\rho_{e} u_{e} F_{e}. \tag{4.16}$$

Expressing the enthalpy of the gas in the cylinder in terms of the speed of sound and applying Equations (4.15) and (4.16), Equation (4.14) reduces to

$$\frac{dp_{c}}{dt} = \frac{1}{v_{c}} \left[(k-1)\dot{Q} - \rho_{e} u_{e} F_{e} a_{c}^{2} - k p_{c} \frac{dv_{c}}{dt} \right] , \tag{4.17}$$

where F_{e} is the pipe cross-sectional area and the subscript e denotes conditions at the pipe. Since the piston motion can be exactly described from the engine geometry and engine speed as shown in Appendix II, Equation (4.17) represents the equation describing the cylinder-discharging process.

b) Cylinder Charging Process

In this case H°_{out} becomes zero, and only the flow properties in the pipe determine the net stagnation enthalpy flow rate. Thus,

$$H^{\circ}_{in} = m_e(h_e + \frac{u_e^2}{2}) = m_e(\frac{a_e^2}{k-1} + \frac{u_e^2}{2}) \quad . \tag{4.18}$$

Substituting Equation (4.18) into Equation (4.14) gives

$$\frac{dp_c}{dt} = \frac{1}{v_c}[(k-1)\dot{Q} - \rho_e u_e F_e(a_e + \frac{k-1}{2}u_e^2) - kp_c \frac{dv_c}{dt}] \quad . \tag{4.19}$$

The heat transfer term $\dot{Q}$ in Equations (4.17) and (4.19) is computed from

$$\dot{Q} = h_c F_c(T_{cw} - T_c) \tag{4.20}$$

where h_c is the cylinder heat transfer coefficient, F_c the overall cylinder wall area, and T_{cw} the cylinder inner wall temperature. The heat transfer coefficient proposed by Eichelberg[11] is used in this study with an estimated value of the cylinder inner wall temperature. The Eichelberg coefficient is given by

$$h_c = .0564\, U_p^{1/3}(p_c T_c)^{1/2}, \tag{4.21}$$

where h_c is in Btu/hr-ft^2-F and U_p is the average piston speed in ft/sec. From the experimental data obtained by Overbye et al.,[25] the cylinder inner wall temperature is estimated at 400° F.

4.3.2 Valve Flow Equations

The flow pattern through the poppet valve in an internal combustion engine is complex and difficult to analyze by

theoretical means. Most of the previous works on the flow through the poppet valve thus concentrated on the experimental determination of a flow coefficient which was defined by a given ideal flow model. Among recent works on the valve flow, three different models have been widely used. These are the isentropic flow model,[21] the sudden enlargement model,[8] and the constant pressure model.[19] Details of each model can be found in the corresponding reference.

Each model has its own advantages, but the constant pressure model is used in the present study because of the following reasons. First, the flow coefficient in this model has a relatively simple form, particularly in the range of low valve lift. Secondly, the calculation of the mimimum flow area of the valve is not required in this model.

The constant pressure model considers the gas to flow isentropically from the cylinder to a throat; and when the flow at the throat is subsonic, then the static pressure at the throat is assumed to be equal to that in the pipe. As the mass flow increases, the Mach number at the throat increases and eventually reaches unity at the sonic threshold. The sonic threshold is the limiting condition where the pipe pressure is equal to the throat pressure. Beyond this sonic threshold, there is no assumption of constant pressure; and the unity Mach number will replace the constant pressure condition. When the flow reverses its direction, the constant pressure condition applies between the throat and the cylinder while the isentropic flow is assumed between the pipe and the throat.

Woods and Kahn[35] performed a series of experiments on a

poppet valve to determine the effective valve area, which is equivalent to the valve discharge coefficient, based on the constant pressure model. They devised a simple empirical equation which relates the effective valve area to the valve lift as follows:

$$\frac{F_v}{(\pi D_{vp}^2/4)} = 2.6 \frac{L_v}{D_{vp}} \qquad (4.22)$$

where

F_v = Effective valve area, $in.^2$

L_v = Instantaneous valve lift, in.

D_{vp} = Diameter of the exhaust port, in.

Equation (4.22), according to Woods and Kahn, is applicable to the poppet exhaust valve for the dimensionless valve lift L_v/D_{vp} up to approximately 0.2 in both normal and reverse flow. Beyond this limit, the pressure ratio across the valve begins to affect the effective valve area.

Considering the similarities in configuration between the valve used by Woods and Kahn and the one employed in the present study, it was decided to use Equation (4.22) for the computation of the valve flow. The maximum dimensionless valve lift measured for the exhaust valve of the CFR engine was 0.177.

The effective valve area ratio ϕ is defined as the ratio of the effective valve area to the cross-sectional area of the exhaust pipe. Thus,

$$\phi \equiv \frac{F_v}{(\pi D^2/4)}$$

where D is the diameter of the exhaust pipe. Therefore, from

Equation (4.22), the effective valve area ratio becomes

$$\phi = 2.6\frac{L_{vp}}{D_{vp}}\left(\frac{D_{vp}}{D}\right)^2 \qquad (4.23)$$

The valve equations which relate the flow properties between the cylinder and the exhaust pipe are derived in Appendix III. Only the final results, depending on the flow conditions at the valve throat, are listed here.

Closed valve: $u_e = 0$ (4.24a)

Sonic flow: $u_e/a_c = -W_1 + \sqrt{W_1^2 + 2/(k-1)}$ (4.24b)

Subsonic flow: $u_e/a_c = -W_2 + \sqrt{W_2^2 + 2/(k-1)}$ (4.24c)

Reverse flow:

$$u_e/a_e = -\left[\frac{[2/(k-1)][1 - (p_c/p_e)^{(k-1)/k}}{[(1/\phi^2)(p_c/p_e)^{-2/k} - 1]}\right]^{1/2} \qquad (4.24d)$$

where W_1 and W_2 are functions of p_e/p_c and are defined in Appendix III.

4.3.3 Flow Into and Out of the Exhaust Surge Tank

Flow into and out of the exhaust surge tank may be analyzed in a manner similar to that used for the cylinder-charging and -discharging processes. The analysis, however, is much simpler since the tank volume remains constant and there is no valve motion to be considered. Since the volume of the surge tank is almost 100 times larger than the cylinder displacement, it is reasonable to assume that the gas temperature in

the surge tank remains virtually constant. Goyal et al.[13] used the constant temperature assumption to compute the pressure change within the surge tank. The analysis presented here is similar to the one developed by Goyal et al.

From the equation of state for the gas in the surge tank and the conservation of mass within the surge tank, one abtains

$$P_t v_t = m_t R T_t \tag{4.25}$$

and

$$\frac{dm_t}{dt} = \dot{m}_e - \dot{m}_{vent} \tag{4.26}$$

where $\dot{m}_e$ is the mass flow into the tank from the exhaust pipe and $\dot{m}_{vent}$ is the mass flow out of the surge tank to the vent system of the laboratory. The subscript t denotes the conditions at the surge tank. The energy equation is not required in the analysis because the temperature is assumed to be constant. By differentiating Equation (4.25) and from Equation (4.26),

$$\frac{dp_t}{dt} = (RT_t/v_t)(\rho_e u_e F_e - \dot{m}_{vent}) \ . \tag{4.27}$$

Since the volume of the surge tank is large compared with the cylinder displacement, $\dot{m}_{vent}$ may be assumed to be constant and equal to the average mass flow into the engine system. Therefore,

$$\frac{dp_t}{dt} = (RT_t/v_t)[\rho_e u_e F_e - \dot{m}_a(1+FA)] \tag{4.28}$$

where $\dot{m}_a$ is the air flow rate into the engine measured at the intake system of the engine and FA is the fuel-air ratio.

For the relation in flow properties between the exhaust pipe and the surge tank, two flow conditions are analyzed. First, for normal flow, a constant pressure between the pipe end and the surge tank is assumed. For reverse flow, an isentropic flow is assumed for the flow from the surge tank into the pipe. Thus one obtains

Normal flow : $$p_e = p_t \tag{4.29a}$$

Reverse flow:

$$u_e/a_t = - [\{2/(k-1)\}\{1 - (p_e/p_t)^{(k-1)/k}\}]^{1/2} \tag{4.29b}$$

4.4 Transient Solutions by the Method of Characteristics

Equations (4.1), (4.2), and (4.6) in Section 4.2 form a system of hyperbolic partial differential equations of the first order. Due to the nonlinearities occurring in the above equations, an exact analytical solution for these equations is not known. Among several numerical procedures currently available for the solution to these equations, the method of characteristics has been extensively used in the field of gas dynamics. Since the method of characteristics requires relatively little computer storage, the method is economically quite suitable for the analysis of short duration transients such as the exhaust flow in internal combustion engine.

The method of characteristics converts the partial differential equations into a set of ordinary differential equations, which are

then integrated numerically. Although a rigorous mathematical approach [29] can be applied to perform this conversion process, a simple method described by Benson et al.[3] is used in this study.

From Equations (4.1), (4.2), (4.6) and Appendix I, a set of ordinaly differential equations are obtained as follows:

$$\frac{dp}{dt} + \rho a\frac{du}{dt} - (k-1)\frac{4}{D}(\tau_w u + q_w) + \frac{4a}{D}\tau_w = 0 \qquad (4.30)$$

along the C^+ wave characteristics of

$$\frac{dx}{dt} = u + a \ , \qquad (4.31)$$

while

$$\frac{dp}{dt} - \rho a\frac{du}{dt} - (k-1)\ (\tau_w u + q_w) - \frac{4a}{D}\tau_w = 0 \qquad (4.32)$$

along the C^- wave characteristics of

$$\frac{dx}{dt} = u - a \ , \qquad (4.33)$$

and

$$\frac{dp}{dt} - a^2\frac{d\rho}{dt} - (k-1)\frac{4}{D}(\tau_w u + q_w) = 0 \qquad (4.34)$$

along the C^p path-line characteristics of

$$\frac{dx}{dt} = u. \qquad (4.35)$$

Equations (4.30), (4.32) and (4.34) are the compatibility relations

which describe variations in dependent variables along respective characteristic lines. Equations (4.30) can only be applied when Equation (4.31) is satisfied. Likewise, Equations (4.32) and (4.34) are valid only when Equations (4.33) and (4.35) are satisfied, respectively. It must be emphasized that, according to the derivation, every solution of the original partial differential equations satisfies this set of total differential equations and the converse is also true.

Before proceeding further with the numerical procedure, it is useful in the computer program to convert the equations into dimensionless forms. By introducing a reference state, the nondimensionalized terms are defined as

$$P = \frac{p}{p_R} , \quad \rho^* = \frac{\rho}{\rho_R} , \quad A = \frac{a}{a_R} , \quad T^* = \frac{T}{T_R} , \quad U = \frac{u}{a_R} ,$$

$$V^* = \frac{v}{v_R} , \quad F^* = \frac{F}{v_R/L} , \quad X = \frac{x}{L} , \quad Z = \frac{a_R t}{L} .$$

The reference state is the air at 14.7 psia and 70° F, L is the length of the exhaust pipe and V_R is the cylinder displacement.

After the governing equations and the corresponding boundary conditions are rewritten in finite difference forms, a numerical solution technique can be applied in order to obtain the transient solution. The procedure adapted in this study is described in four steps as follows:

a) Construction of the grid

b) Computation of the pipe interior points

c) Computation of the cylinder and cylinder-end points

d) Computation of the surge tank and surge tank-end points

a) Construction of the grid: In order to apply the finite difference equations to the numerical solution technique, the grid size must be determined on the X-Z plane. The only theoretical restriction on the selection of the grid size is given by the Courant-Friedrichs-Lewy stability criterion which states

$$\frac{\Delta X}{\Delta Z} \geq |U| + A \ . \qquad (4.36)$$

Within the criterion described by Equation (4.36), the numerical solution is stable. The length of a reach ΔX is predetermined and remains constant throughout the computation. The time increment ΔZ, however, is adjusted according to Equation (4.35) at each instant of computation in order to minimize the computational error caused by the linear interpolation. The maximum value of $|U| + A$ at each time of computation is chosen to adjust ΔZ at that particular instant of computation.

b) Computation of the pipe interior points: Figure 27 shows the X-Z diagram to illustrate the computational procedure. With known conditions at time $Z = Z_o$, the objective is to compute the properties at point P at time $Z = Z_o + \Delta Z$. The unknown properties at point P are the pressure, velocity, and density. The available equations are three compatibility relations along the C^+ , C^- , and C^P characteristics. The slopes of these characteristics within the unit grid, bounded by ΔX and ΔZ, are assumed to be constant. By using the properties at point A as a first approximation, the C^+ and C^-

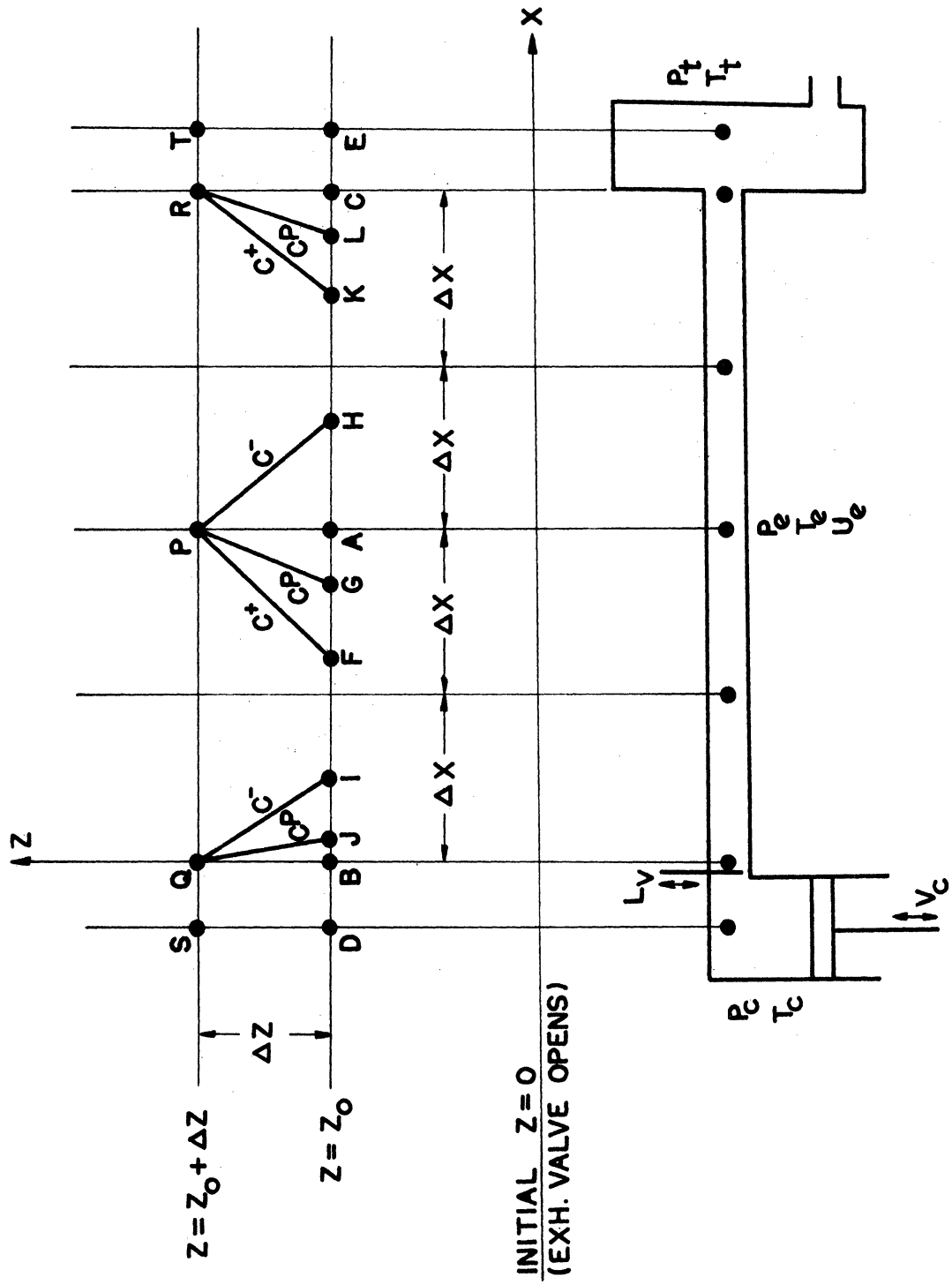

Figure 27. X-Z Diagram for the Illustration of Computational Procedure

characteristics may be drawn passing through point P. The properties at points F and H are computed by interpolating linearly between the adjacent grid points. Equations (4.30) and (4.32) are applied between points P and F and between points P and H, respectively. The resulting equations are then solved simultaneously for the pressure and the velocity at point P. Next, the density at point P is computed by applying Equation (4.34). The temperature and the speed of sound at point P are computed from the equation of state at that point. The whole procedure is then repeated once with the new slopes of the three characteristics by taking the average values of velocity and speed of sound between points P and A.

c) Computation of the cylinder and cylinder-end points:

The procedure for the computation of the cylinder and cylinder-end points is somewhat complicated since the equations governing points S and Q must be solved simultaneously. In addition, the flow conditions at the valve throat must be determined in order to select a proper valve flow equation. The cylinder mass at point S is computed from Equation (4.16). The cylinder pressure at point S is computed from either Equation (4.17) or (4.19) depending upon the flow direction at the valve. The second-order Runge-Kutta method is used to solve the differential equations in the above computations. With the new cylinder volume computed from the piston motion, the speed of sound and the temperature in the cylinder at point S are then computed. By applying Equation (4.32) and a proper valve equation, the pressure and the velocity at point Q are computed. Newton's iteration procedure is used to solve the valve equation. The density at point Q is obtained from Equation (4.34),

and the equation of state at point Q may be used to compute the temperature and the speed of sound at point Q. The whole procedure is repeated once with the new slopes of the characteristics. In the case of reverse flow, C^p characteristics fall beyond the physical boundary. In this case the cylinder properties at point D may be substituted for the solution of Equation (4.34).

Convergence in Newton's method for solutions to the valve equations was quite rapid and the number of iterations required was in most cases usually less than 5 with the convergence limit of 0.001. Figure 28 shows a typical valve equations plot for $k = 1.4$ and $\phi = 0.25$.

d) Computation of the surge tank and surge tank-end points: The general procedure adapted in this case is similar to the procedure just described for computation of the cylinder and cylinder-end points. The properties at point T in Figure 27 are computed from Equation (4.28) by applying the second-order Runge-Kutta method. The properties at the known points C and E are used as a first approximation. Either Equation (4.29a) or (4.29b) and Equation (4.30) are used to compute the pressure and the velocity at point R. Equation (4.34) is then used to compute the density at point R. Other properties at point R are computed from the equation of state at that point. The whole procedure is repeated once with the new values of velocity and speed of sound at point R. For the reverse flow at point R, the properties at point E are used to solve Equation (4.34).

4.5 Initial Conditions and Other Input Variables for the Simulation Program

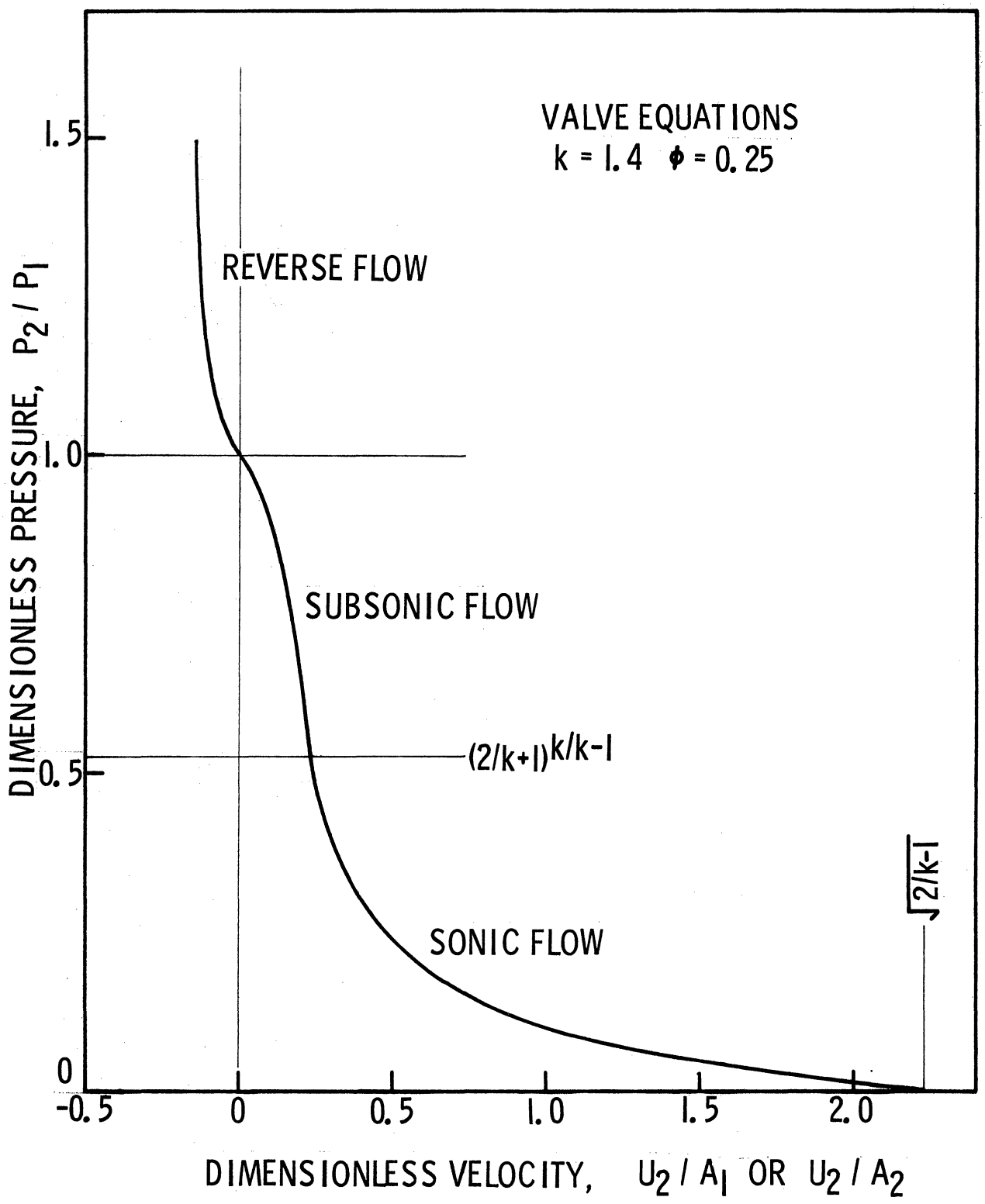

Figure 28. A Typical Valve Equations Plot

In order to start the sequence of the numerical computation, the initial conditions must be specified. Since the computer simulation is performed during the exhaust period, the exhaust valve opening is chosen as the initial timing with respect to the engine cycle. The initial conditions along the pipe are assumed uniform. The initial exhaust pressure is assumed equal to the average surge tank pressure, and the initial exhaust gas temperature is assumed equal to the average gas temperature in the exhaust pipe. The initial exhaust velocity is assumed zero. The initial surge tank pressure is assumed equal to the average surge tank pressure and its temperature is assumed constant as mentioned in Section 4.3.3.

The initial cylinder pressure is measured at the exhaust valve opening from the pressure-time trace. The initial cylinder gas temperature, however, cannot be readily measured due to its highly transient nature. A simple thermodynamic analysis is developed in order to compute the initial gas temperature. From the equation of state for the gas in the cylinder,

$$T_{EO} = \frac{P_{EO} V_{EO}}{m_{EO} R_{EO}} \quad , \tag{4.37}$$

where the subscript EO denotes the cylinder conditions at the exhaust valve opening. Assuming no leakage in the cylinder, m_{EO} must be equal to the fresh charge plus the mass of the residual gas.

$$m_{EO} = (1 + FA)m_a + m_r \tag{4.38}$$

where m_a is the mass of air per cycle and m_r the mass of the residual

gas, and FA the fuel-air ratio. The mass of the residual gas is computed by assuming that the combustion products remaining in the cylinder undergo an isentropic process during the exhaust period. Therefore,

$$m_r = m_{EO}(v_{EC}/v_{EO})(p_{EC}/p_{EO})^{1/k} \qquad (4.39)$$

Substituting Equations (4.39) and (4.38) into Equation (4.37), and after the mass of air per cycle m_a is replaced by the average air mass flow rate $\dot{m}_a$ into the engine intake system, Equation (4.37) reduces to

$$T_{EO} = \frac{p_{EO}v_{EO}[1 - (v_{EC}/v_{EO})(p_{EC}/p_{EO})^{1/k}](RPM)}{2R(1 + FA)\dot{m}_a} \quad , \qquad (4.40)$$

where RPM is the engine speed.

Table II lists the engine data required to run the simulation program. The table does not include the control parameters which were necessary to perform various numerical computation procedures.

TABLE II

ENGINE DATA REQUIRED FOR THE SIMULATION PROGRAM

Input Parameter	Symbol	Unit	Value
Engine:			
a. Cylinder Geometry	-	-	Described in Chapter III
b. Engine Speed	RPM	rpm	Variable
c. Air Mass Flow Rate	m_a	lbm/min	Variable
d. Fuel Mass Flow Rate	m_f	lbm/min	Variable
e. Cylinder Pressures (at EVO and EVC)	P_c	psia	Variable
f. Exhaust Valve Timing	-	ATDC	Opens at 146° Closes at 10°
g. Instantaneous Exhaust Valve Lift	L_v	in.	Function of Crank Angle

TABLE II (CONTINUED)

Input Parameter	Symbol	Unit	Value
Exhaust System:			
a. Exhaust Pipe Diameter	D	in.	1 5/8
b. Exhaust Pipe Length	L	in.	39
c. Surge Tank Volume	V_t	$in.^3$	4070
d. Average Exhaust Gas Temperature	T_e	deg. R	Variable
e. Average Surge Tank Pressure	P_t	psia	Variable
f. Average Surge Tank Temperature	T_t	deg. R	Variable
g. Exhaust Pipe Wall Temperatures	T_w	deg. R	Variable
h. Specific Heat Ratio of Exhaust Gas	k	-	1.35
i. Specific Heat Ratio of Air	k	-	1.4
j. Gas Constant of Exhaust Gas	R	lbf-ft/lbm-R	51

V. COMPARISON AND DISCUSSION OF THE SIMULATION AND EXPERIMENTAL RESULTS

Comparisons between the experimental data and the theoretical results were made in order to examine the validity of the mathematical model developed in Chapter IV. The test runs were also aimed at investigating performances of the schlieren-streak system at several different engine conditions. The data comparisons are presented in terms of cylinder pressure, exhaust pressure, and exhaust gas velocity, all of which were plotted as functions of engine crank angle.

5.1 Engine Test Conditions

Seven test runs were made with different combinations of engine test conditions. The test conditions for each run are listed in Table III. The engine parameters chosen for these test runs are the engine speed, the load, and the ignition timing. Among these parameters, the speed and the load were considered to be most influential on exhaust velocity profiles. Test runs 1 to 3 were made with a motored engine at engine speeds of 600, 800, and 1000 RPM. Test runs 4 to 7 were performed under firing conditions at two different settings of each engine parameters.

5.2 Motored Engine Data

In figure 29 through 34, the simulation results are compared with the experimental data for test runs 1 to 3. Although slight discrepancies in amplitude of pressure waves are observed, general agreement between the simulation and the experimental results are

TABLE III

ENGINE CONDITIONS FOR TEST RUNS[1]

Run No.	Speed	Load	Ignition Timing (Deg., ATDC)
Engine Motored:			
1	600	-	-
2	800	-	-
3	1000	-	-
Engine Fired:			
4	600	Full	13
5	1000	Full	13
6	1000	Part[2]	13
7	1000	Part[2]	30

[1]Relative fuel-air ratio for all test runs = 1.3
[2]Approximately three quarters of full load.

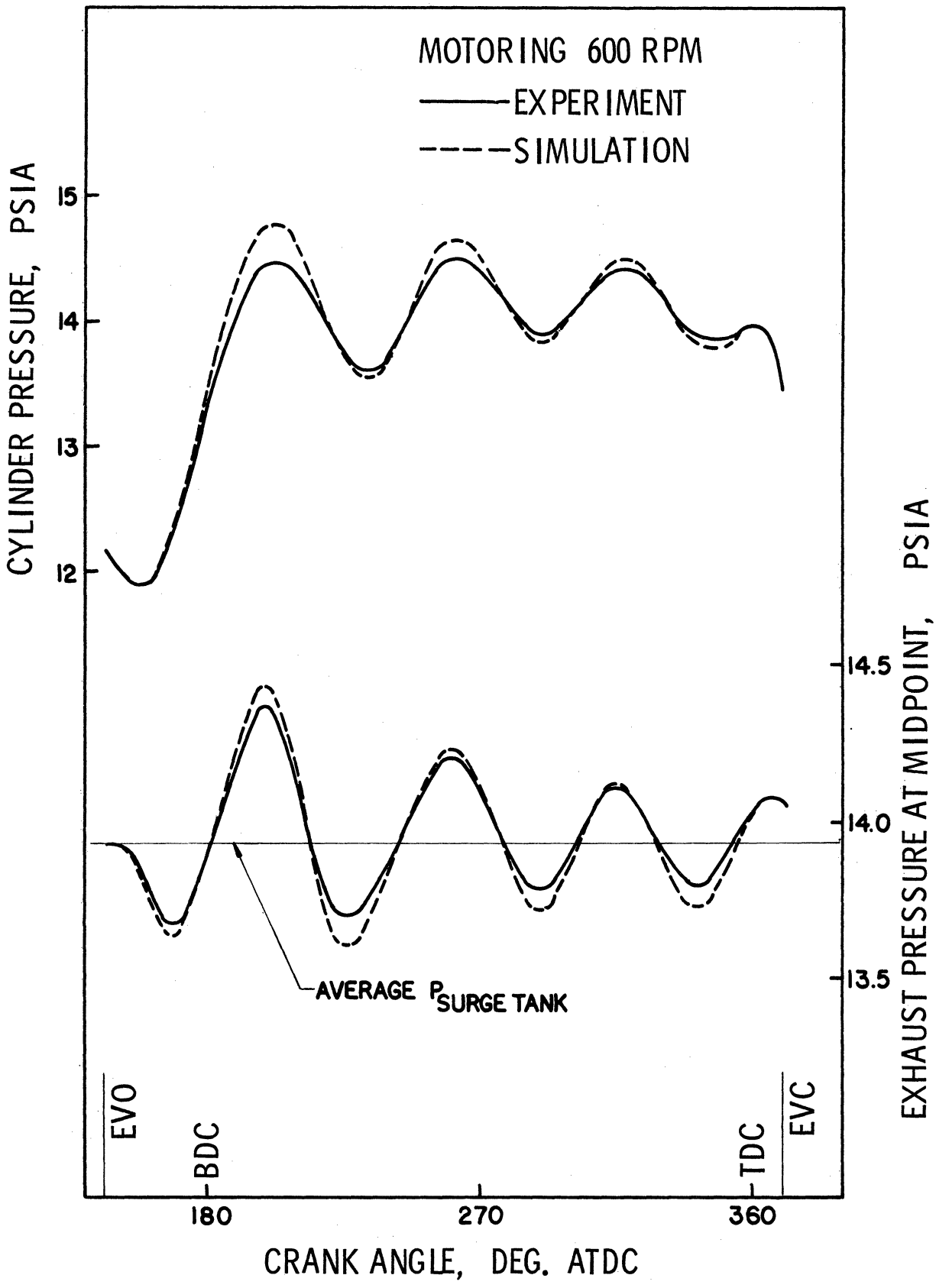

Figure 29. Comparisons of Cylinder and Exhaust Pressure - Experimental and Theoretical Results for Test Run No. 1

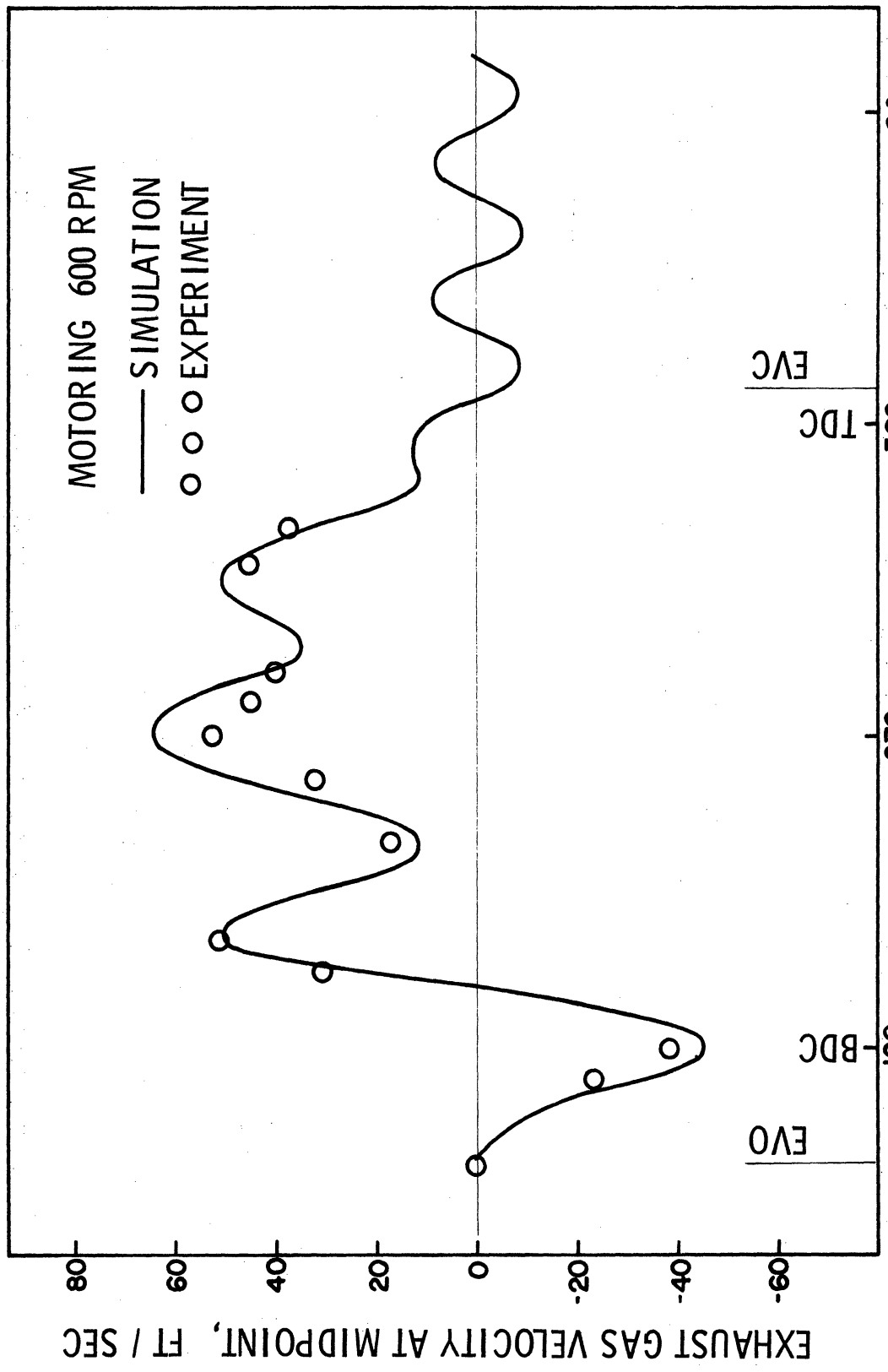

Figure 30. Comparison of Exhaust Gas Velocity - Experimental and Theoretical Results for Test Run No. 1

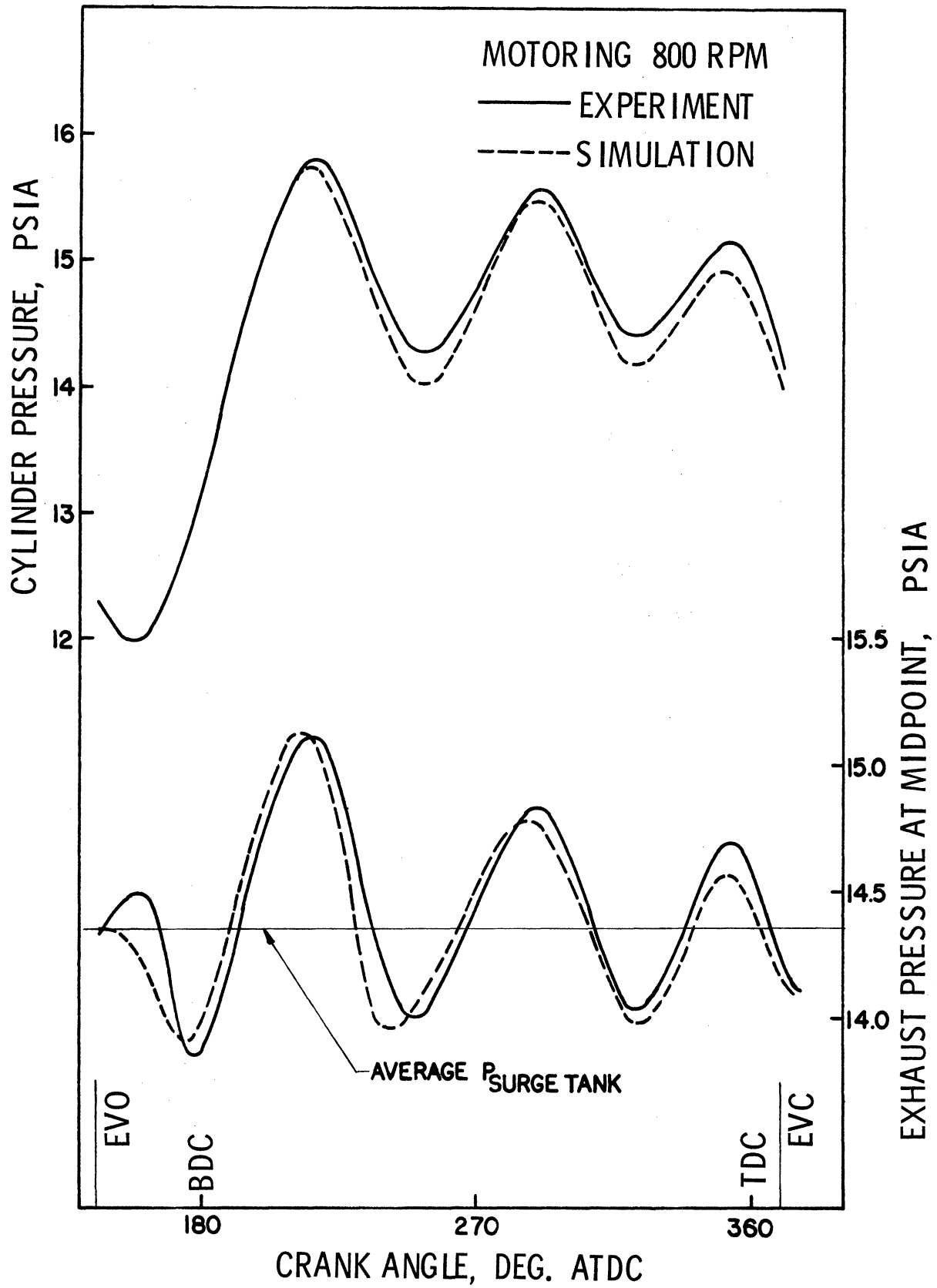

Figure 31. Comparisons of Cylinder and Exhaust Pressures - Experimental and Theoretical Results for Test Run No. 2

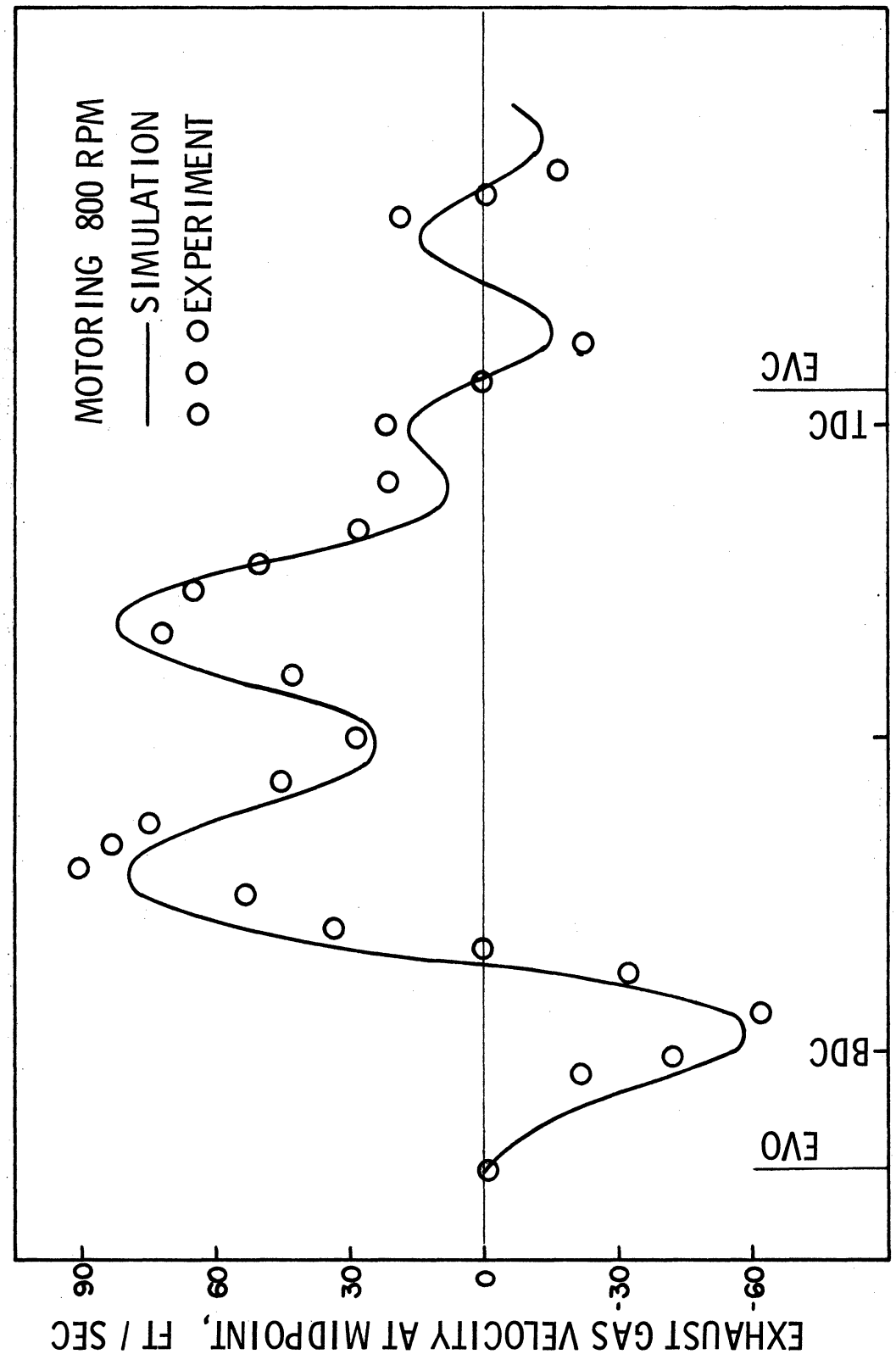

Figure 32. Comparison of Exhaust Gas Velocity - Experimental and Theoretical Results for Test Run No. 2

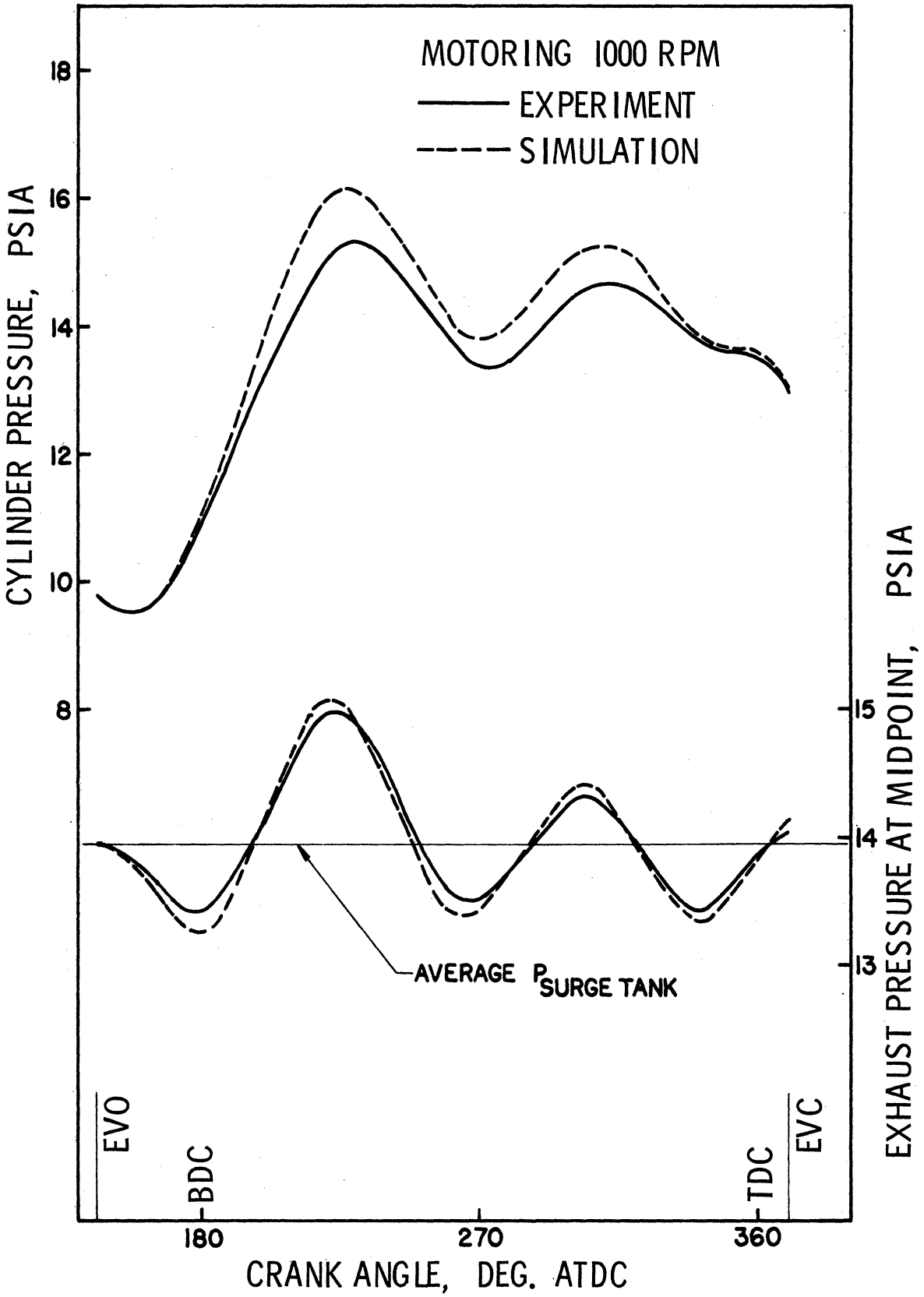

Figure 33. Comparisons of Cylinder and Exhaust Pressures - Experimental and Theoretical Results for Test Run No. 3

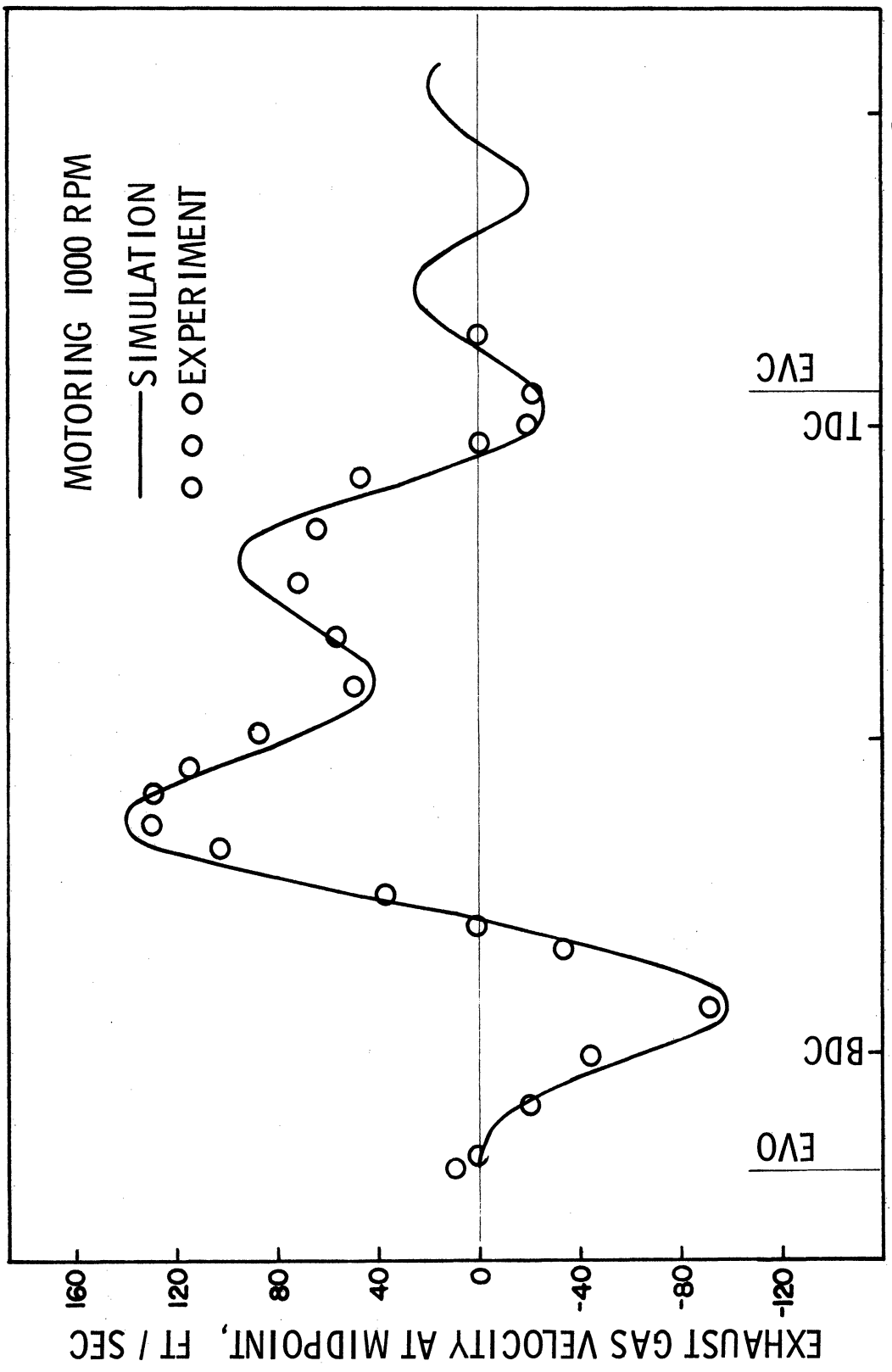

Figure 34. Comparison of Exhaust Gas Velocity - Experimental and Theoretical Results for Test Run No. 3

good. In particular, the timing of flow reversals predicted by the simulation agree very well with the experimental results obtained from schlieren-streak pictures.

Figures 35 through 38 show the effect of engine speed on wave actions in the cylinder and the exhaust pipe. Fluctuation amplitudes in both pressure and velocity data increase as the engine speed increases. This is due to the fact that the pressure difference across the exhaust valve is initially greater at high engine speed, generating a strong initial pressure pulse in the exhaust system. The number of flow fluctuations per engine cycle is obviously smaller at high engine speed, since the engine cycle period is shorter.

Instantaneous distributions of exhaust pressure and velocity along the pipe are shown in Figure 39 and 40. These data were obtained from the simulation results for test run 3. The largest pressure fluctuations occur at the valve end while the largest velocity fluctuations are observed near the surge tank end.

5.3 Firing Engine Data

In Figures 41 through 48, the simulation results are presented and compared with the experimental data for test runs 4 to 7. At the beginning of an exhaust stroke, the exhaust gas velocity reaches up to 500 ft/sec due to large blowdown pulses. Several flow reversals are observed following the velocity peak. These flow reversals are primarily caused by the pressure waves reflecting back and forth within the exhaust system. The attenuation of pressure amplitudes is relatively slow during an exhaust period. This indicates that there are little

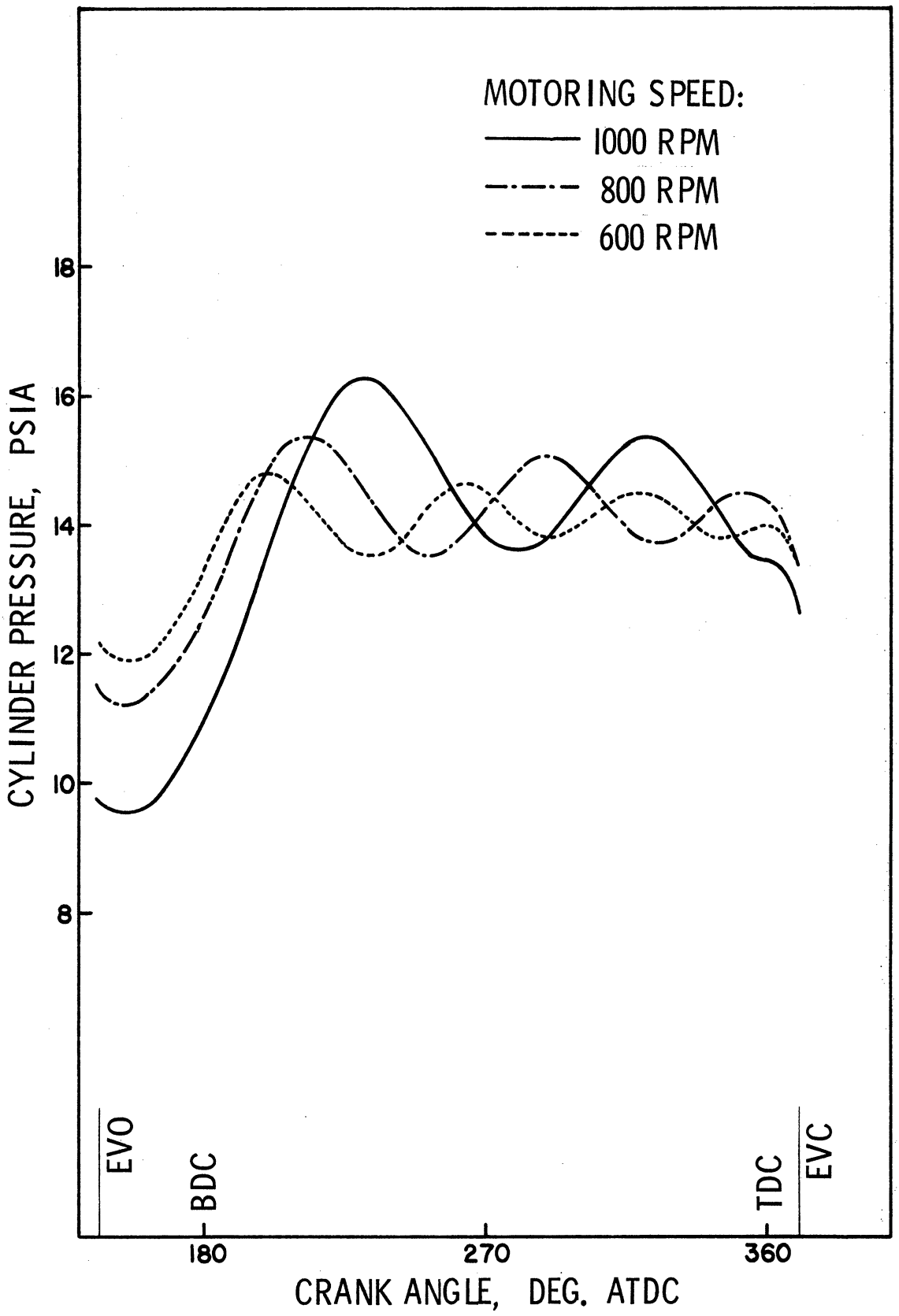

Figure 35. Effect of Engine Speed on Cylinder Pressure - Theoretical Results

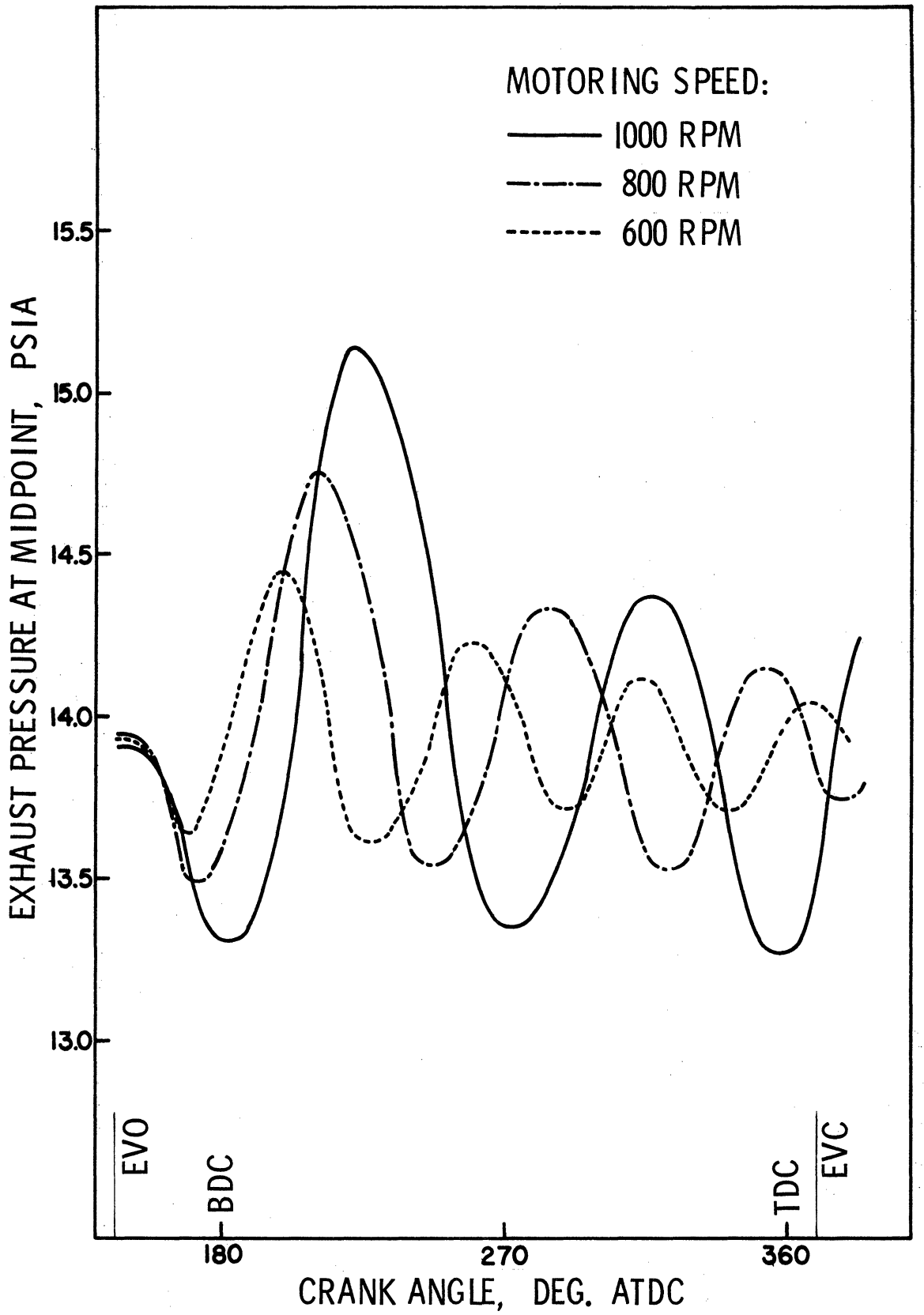

Figure 36. Effect of Engine Speed on Exhaust Pressure - Theoretical Results

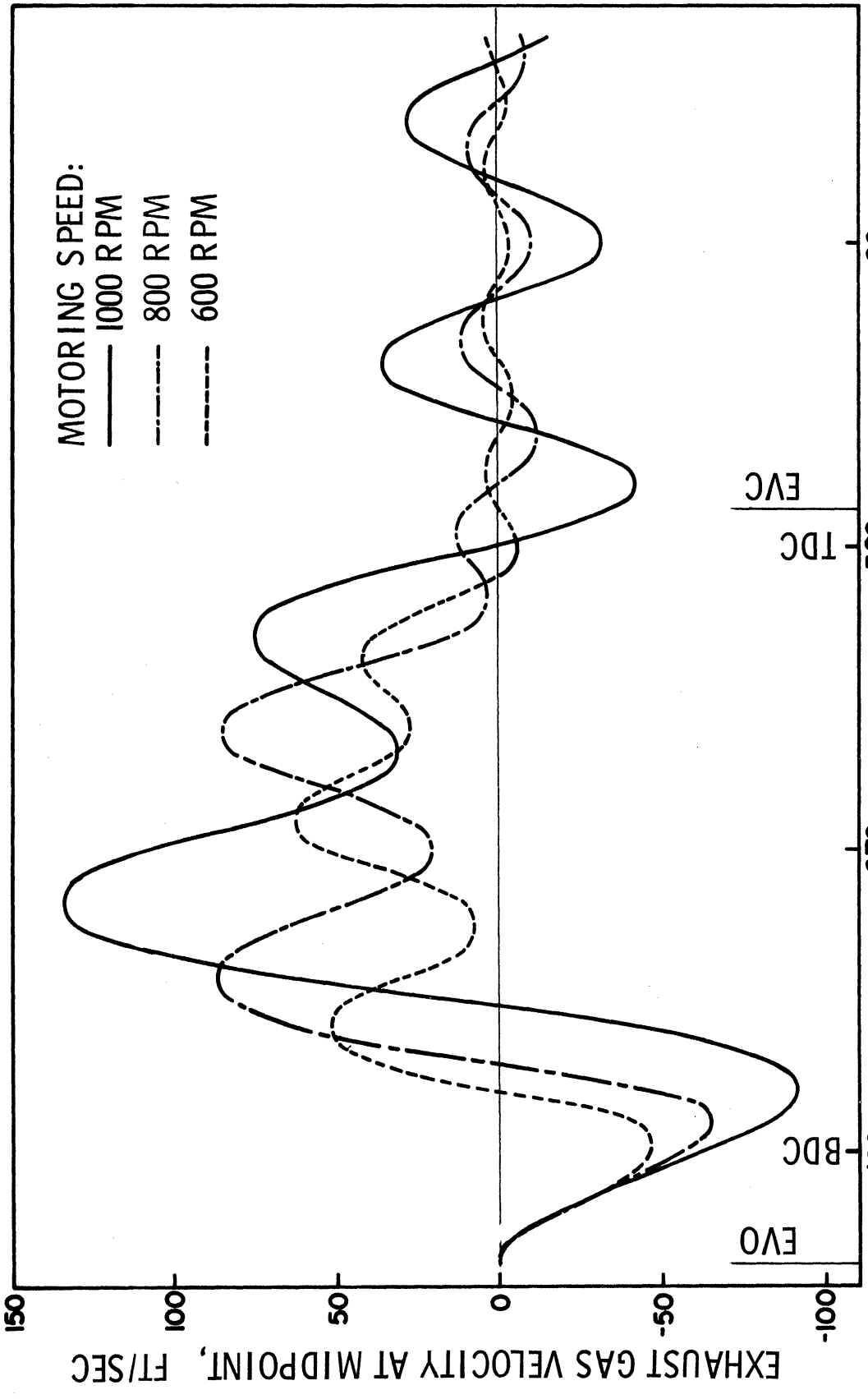

Figure 37. Effect of Engine Speed on Exhaust Velocity - Theoretical Results

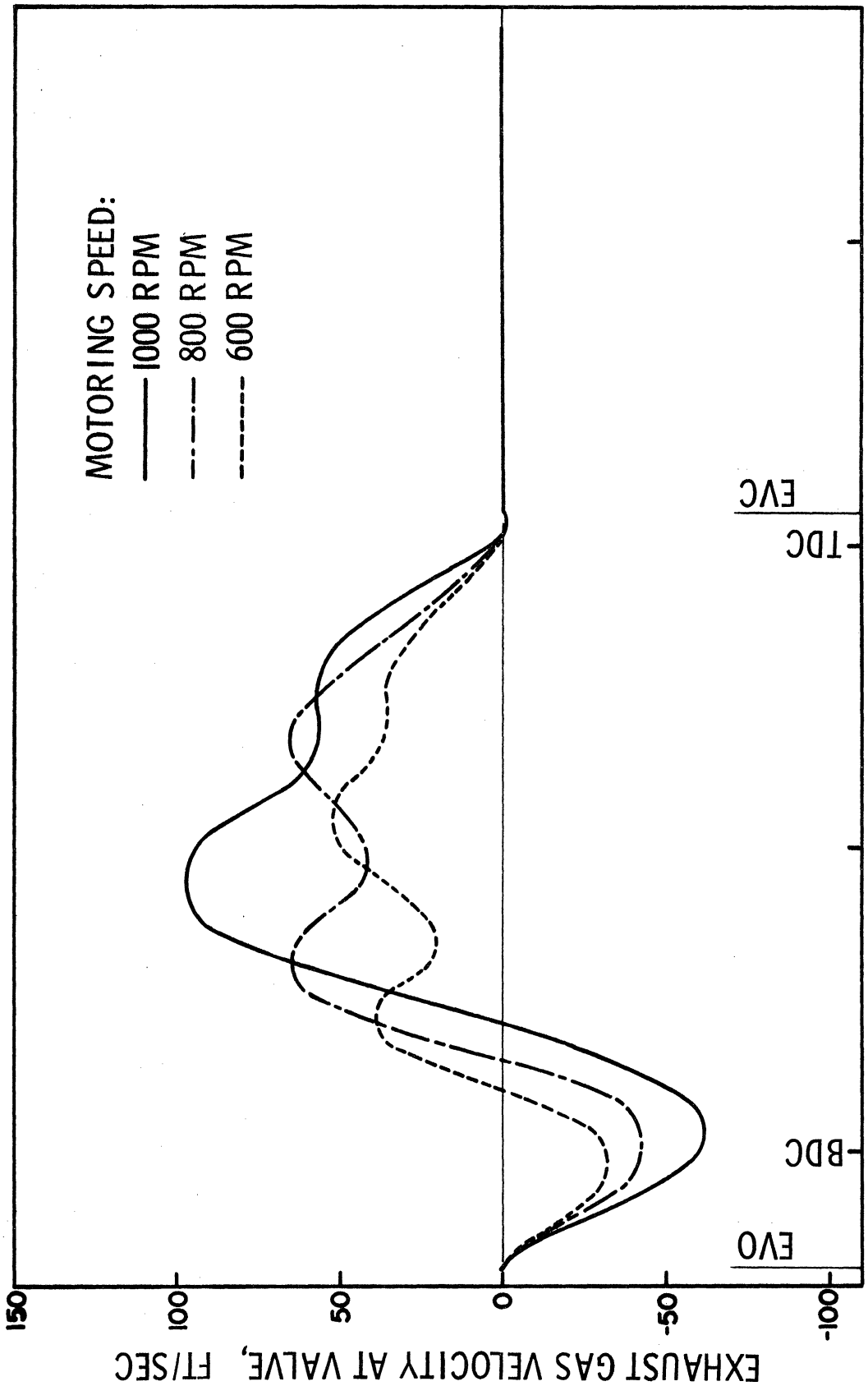

Figure 38. Effect of Engine Speed on Exhaust Velocity at Valve End - Theoretical Results

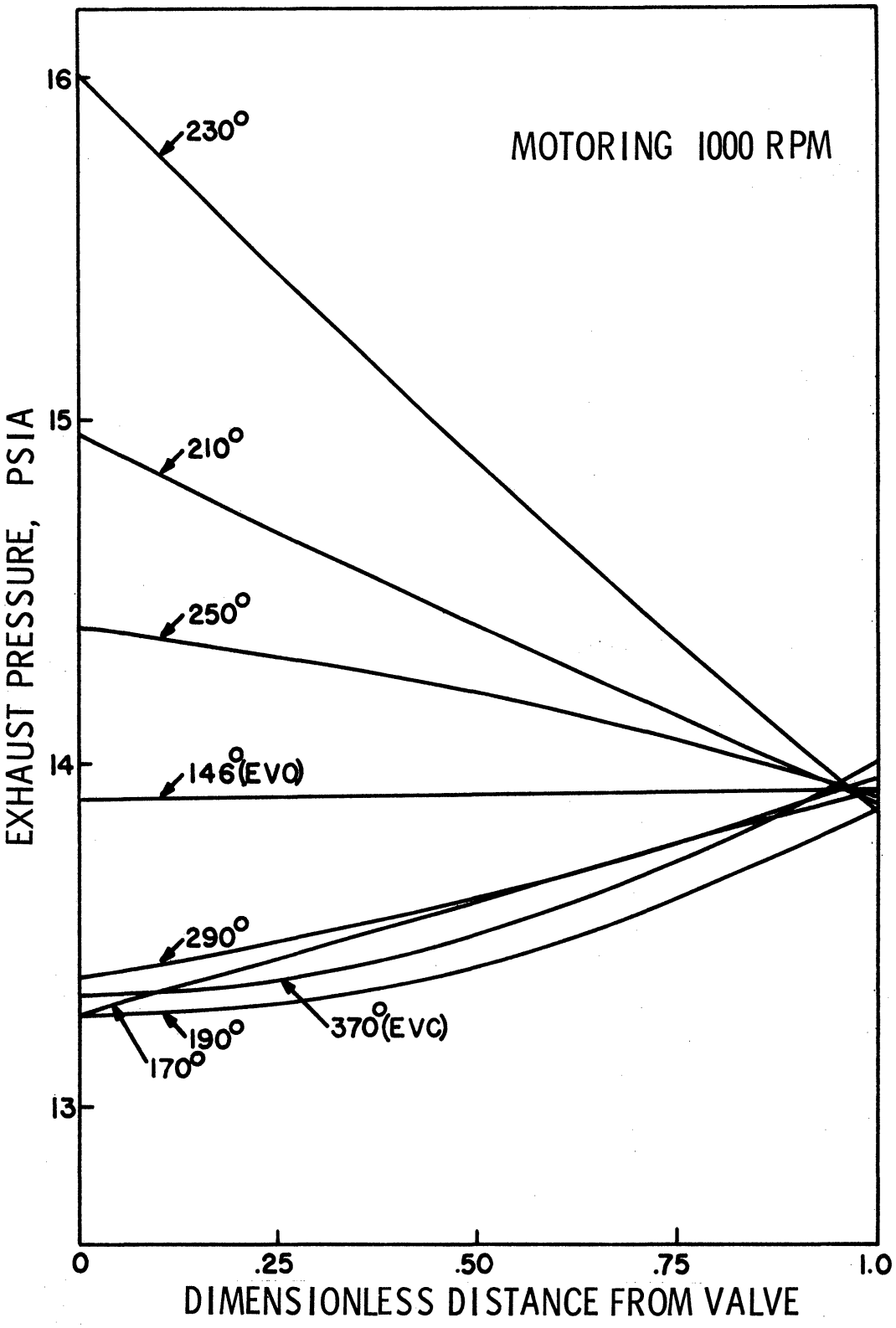

Figure 39. Instantaneous Pressure Distribution along the Exhaust Pipe - Theoretical Results

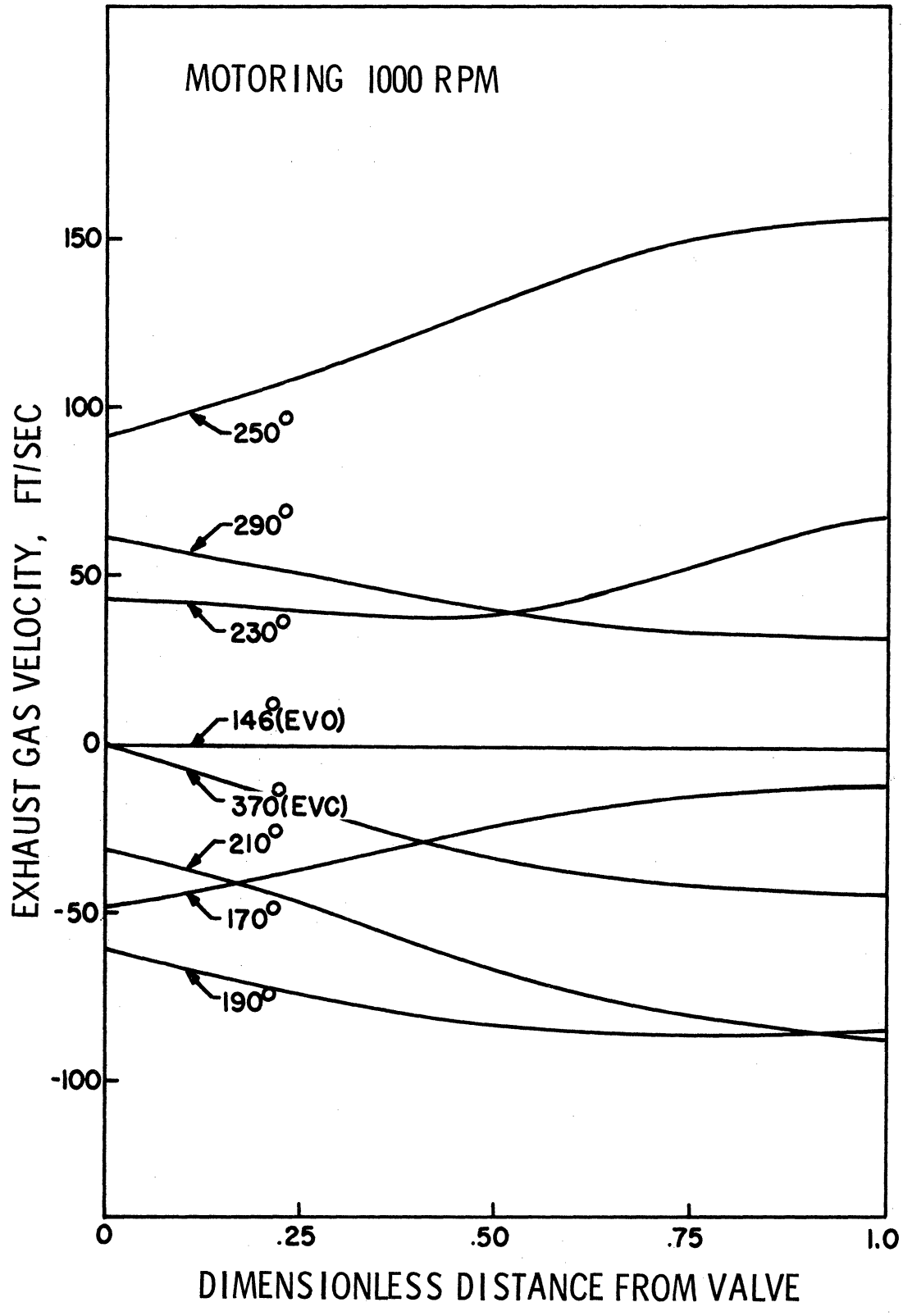

Figure 40. Instantaneous Velocity Distribution along the Exhaust Pipe - Theoretical Results

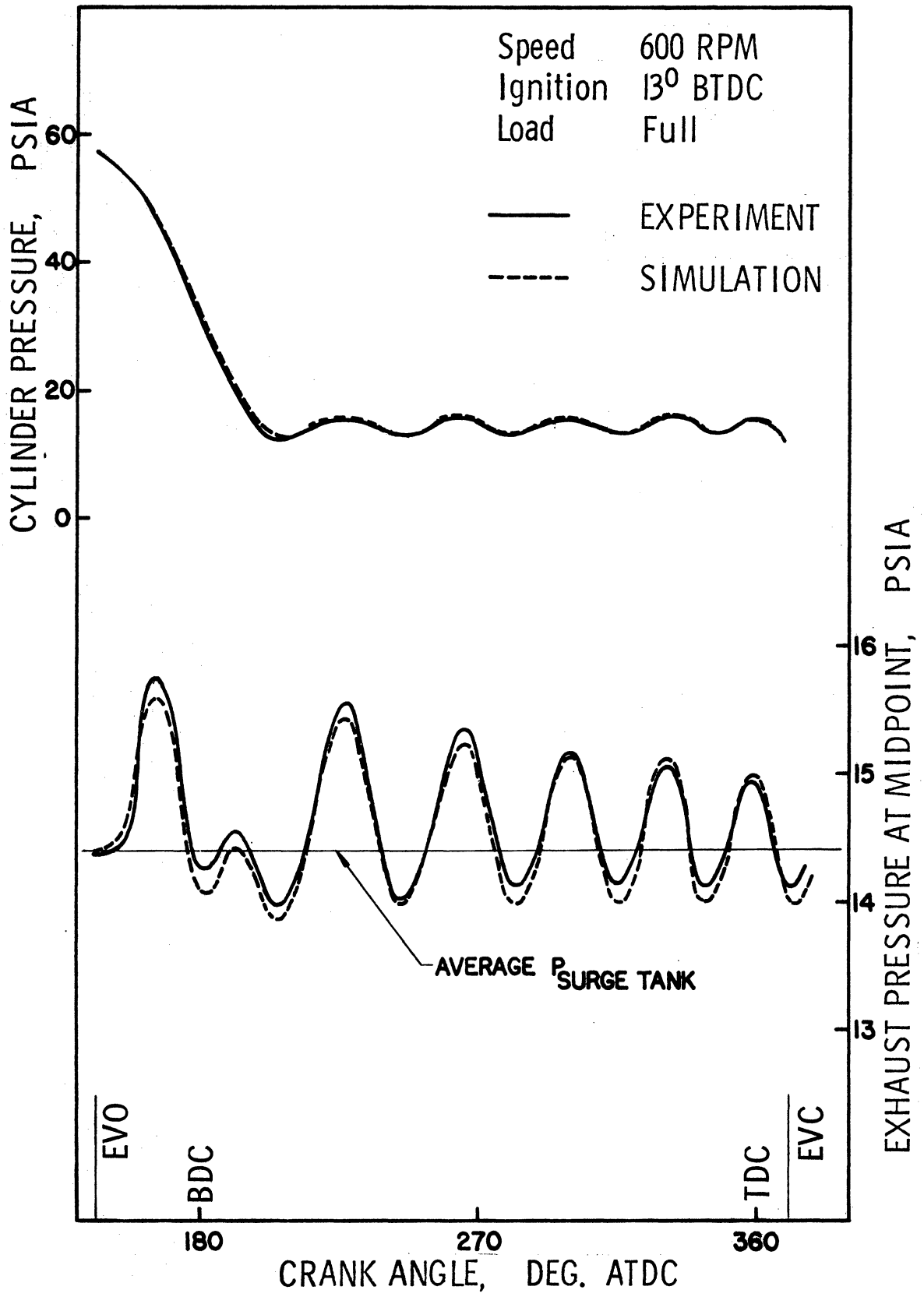

Figure 41. Comparisons of Cylinder and Exhaust Pressures - Experimental and Theoretical Results for Test Run No. 4

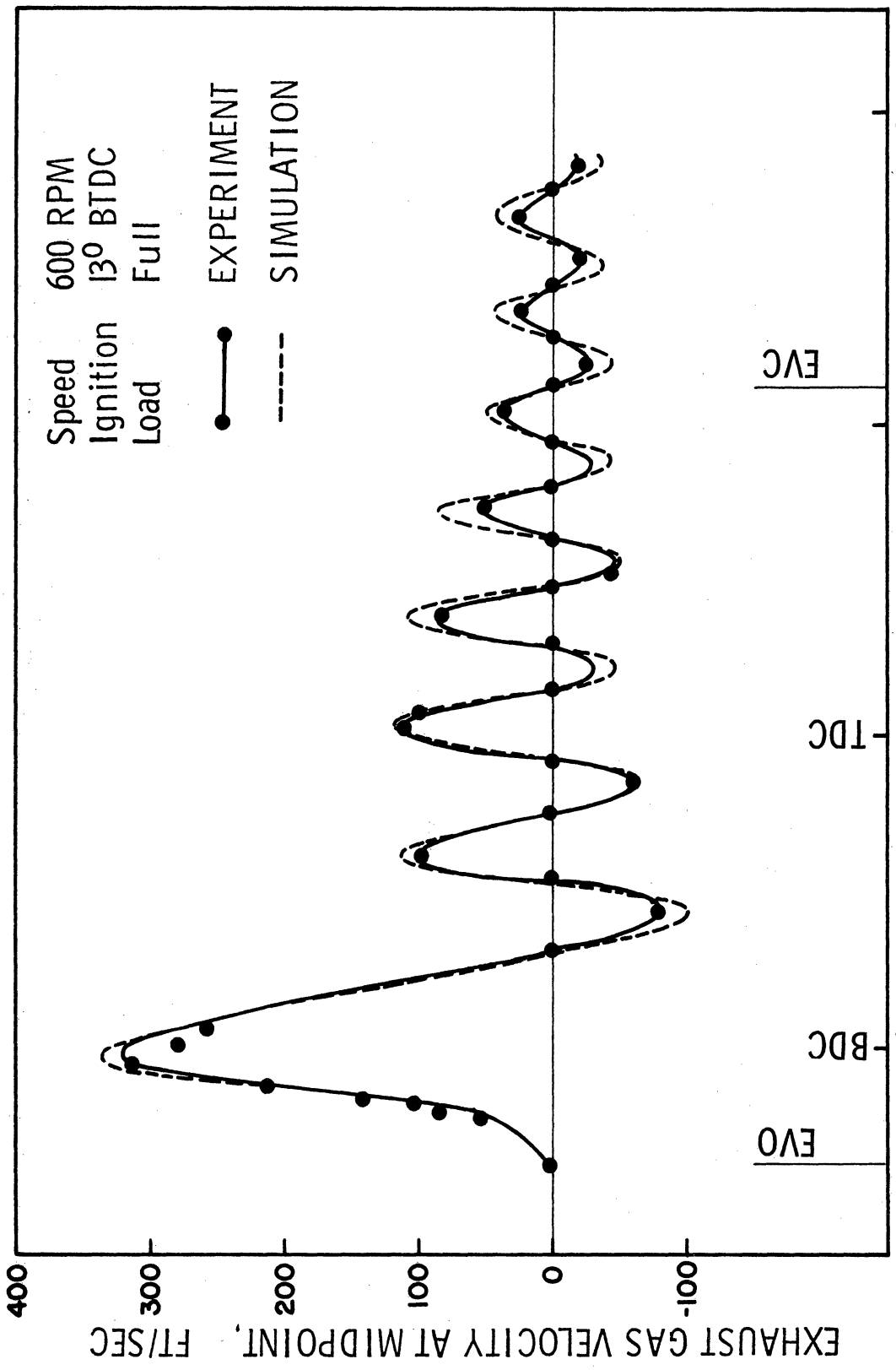

Figure 42. Comparison of Exhaust Gas Velocity - Experimental and Theoretical Results for Test Run No. 4

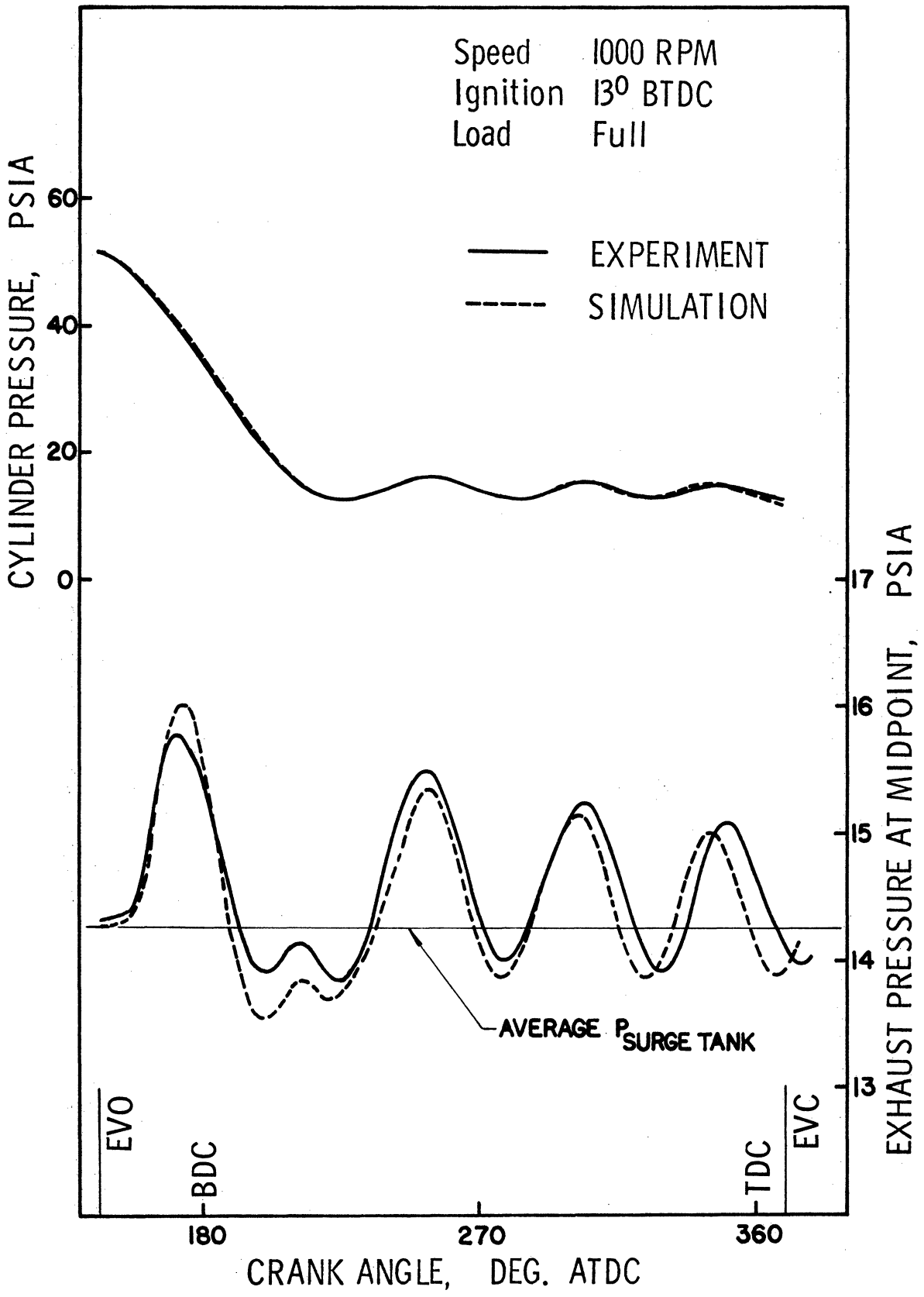

Figure 43. Comparisons of Cylinder and Exhaust Pressures - Experimental and Theoretical Results for Test Run No. 5

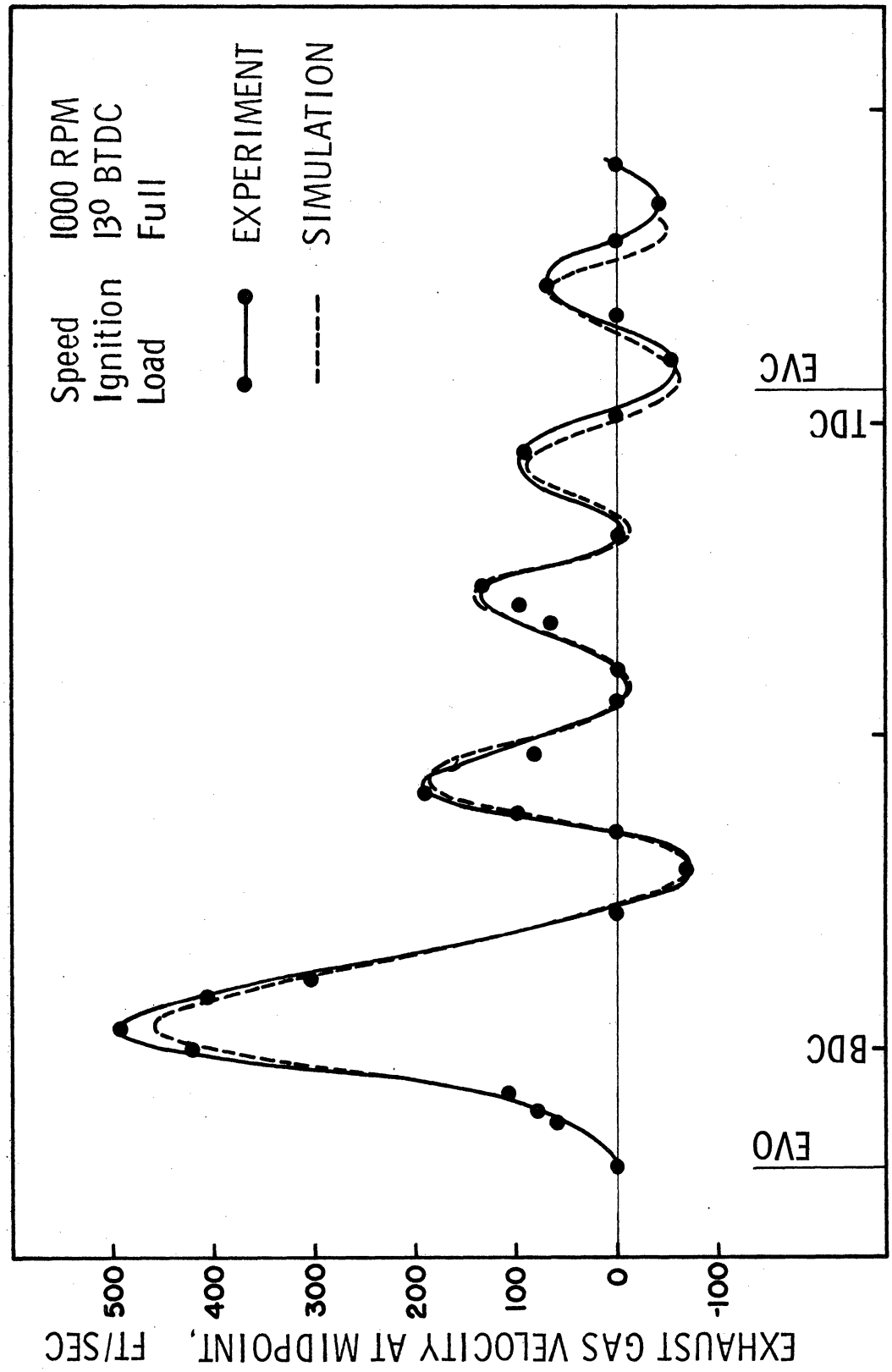

Figure 44. Comparison of Exhaust Gas Velocity - Experimental and Theoretical Results for Test Run No. 5

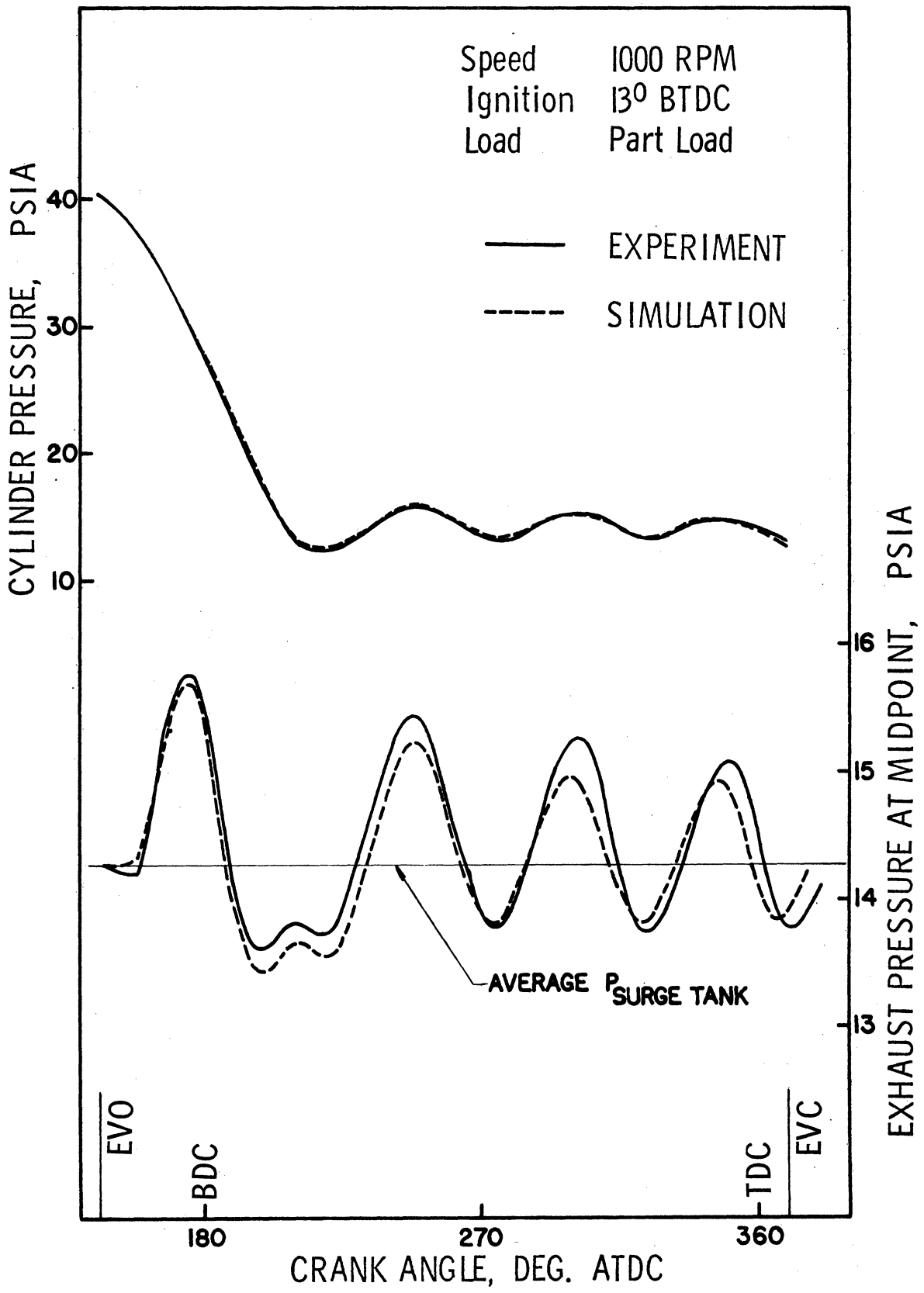

Figure 45. Comparisons of Cylinder and Exhaust Pressures - Experimental and Theoretical Results for Test Run No. 6

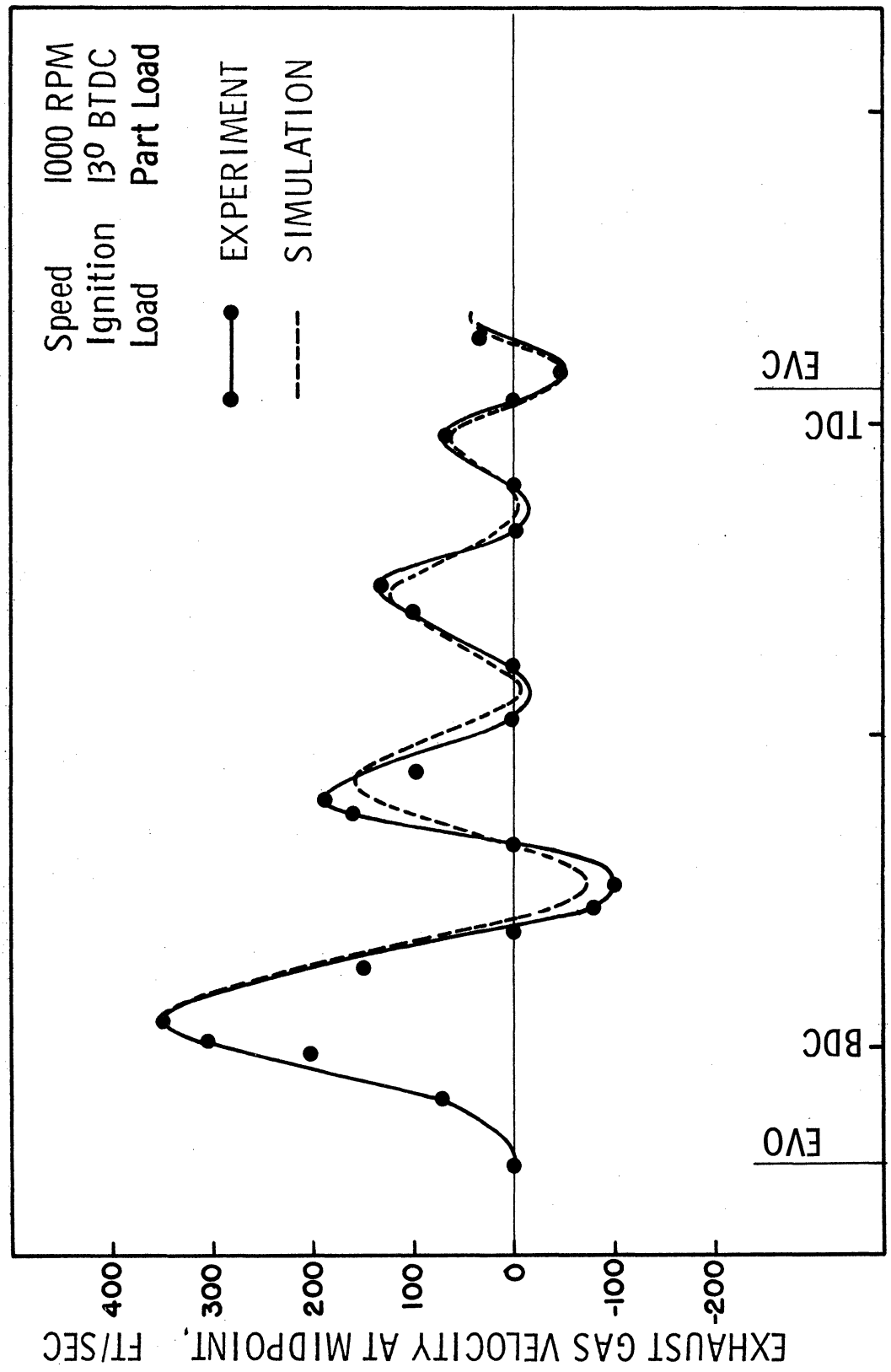

Figure 46. Comparison of Exhaust Gas Velocity - Experimental and Theoretical Results for Test Run No. 6

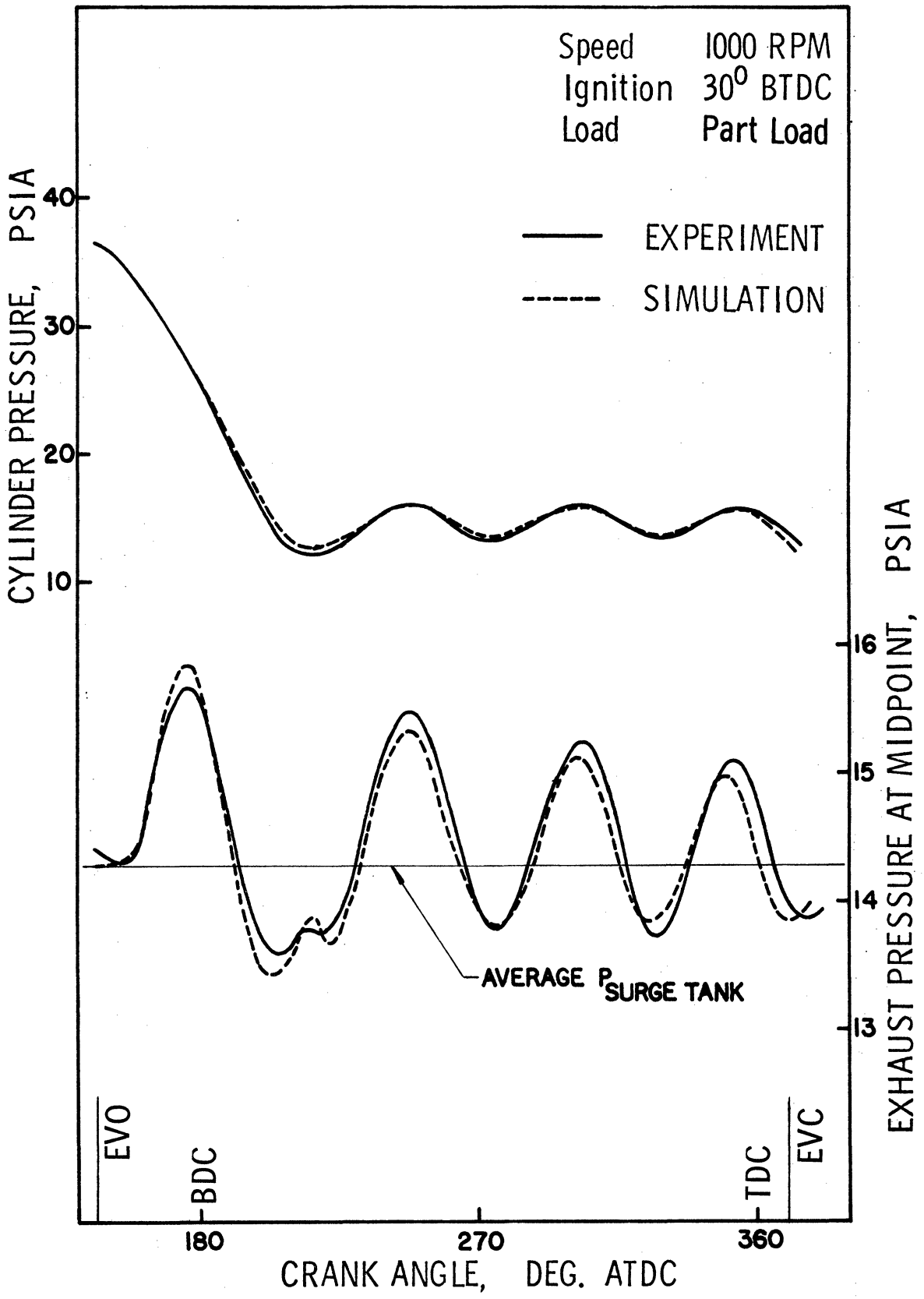

Figure 47. Comparisons for Cylinder and Exhaust Pressures - Experimental and Theoretical Results for Test Run No. 7

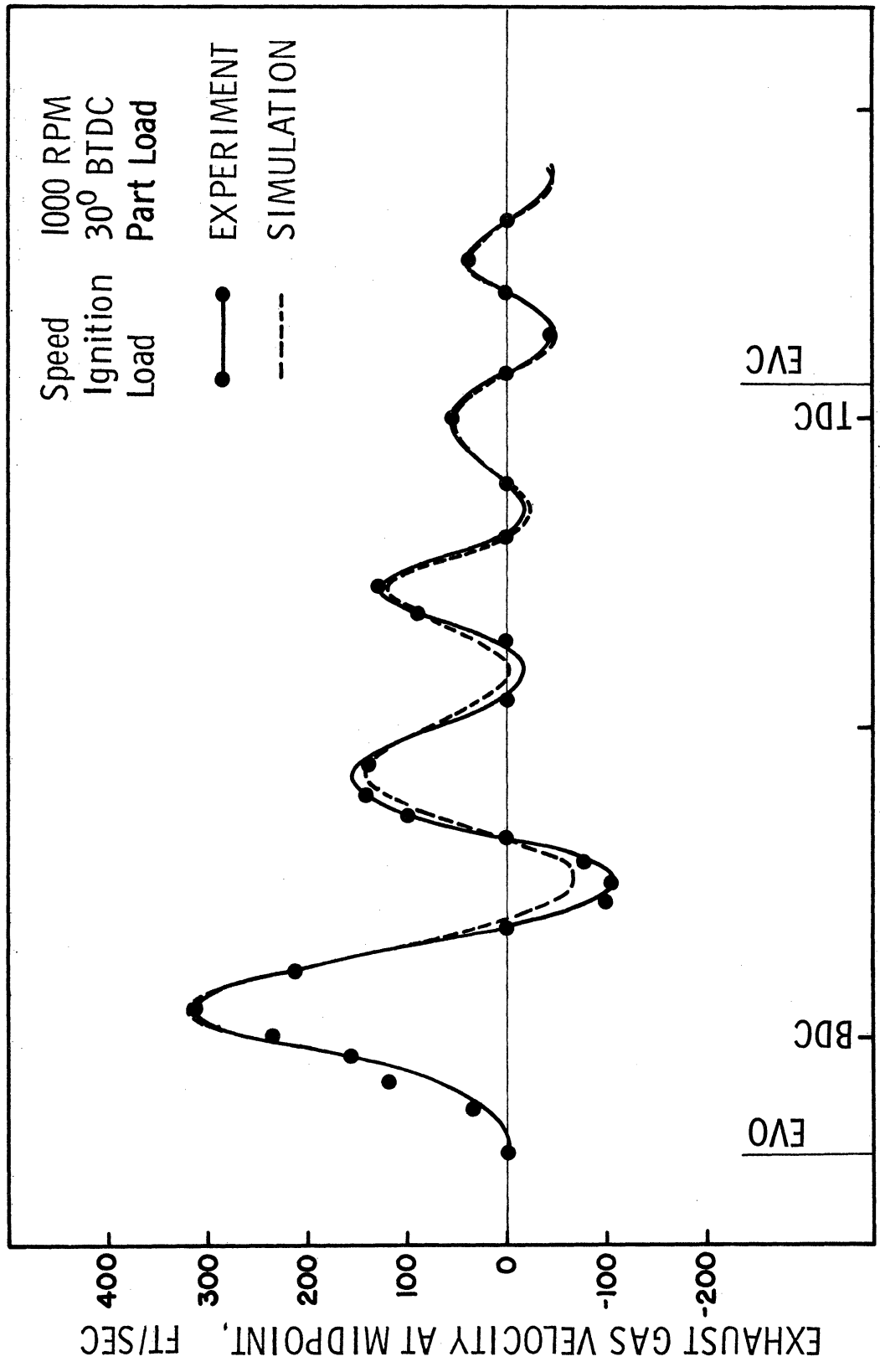

Figure 48. Comparison of Exhaust Gas Velocity - Experimental and Theoretical Results for Test Run No. 7

energy losses by wave reflections at both ends of the pipe. Friction also contributes to a certain degree to the pressure attenuation. In a short pipe, however, the effect of friction is considered to be minor. The exhaust gas temperature determines the speed of the pressure waves. In a firing engine, the gas temperature is nearly four times as high as that in a motored engine. Consequently, the wave speed in a firing engine is twice the speed in a motored engine. This can be easily verified by comparing pressure data for both firing and motored conditions at a constant engine speed. Overall agreement between the theoretical results and the experiment data is within ±10%. This supports the validity of the underlying physical assumptions and numerical techniques employed in the development of the mathematical model.

Effects of the various engine parameters on the pressure and velocity data are shown in Figure 49 through 54. The effect of engine speed is similar to that in a motored engine. Higher speeds cause larger fluctuations in both pressure and velocity data. An interesting observation can be made by comparing the piston speed and the exhaust gas velocity during an exhaust stroke, excluding the blowdown period. During the blowdown period the gas in the cylinder expands through the exhaust valve causing a rapid pressure drop in the cylinder. During this period the piston remains near bottom dead center and does not have any appreciable effect on the cylinder pressure. After this blowdown period, however, pressures in the cylinder and the exhaust pipe are equalized and the exhaust gas flows through the valve as if it were an incompressible fluid. By neglecting the wave action for a moment, the exhaust gas velocity in the pipe can be approximated by the piston speed multiplied by the area ratio between the piston area and

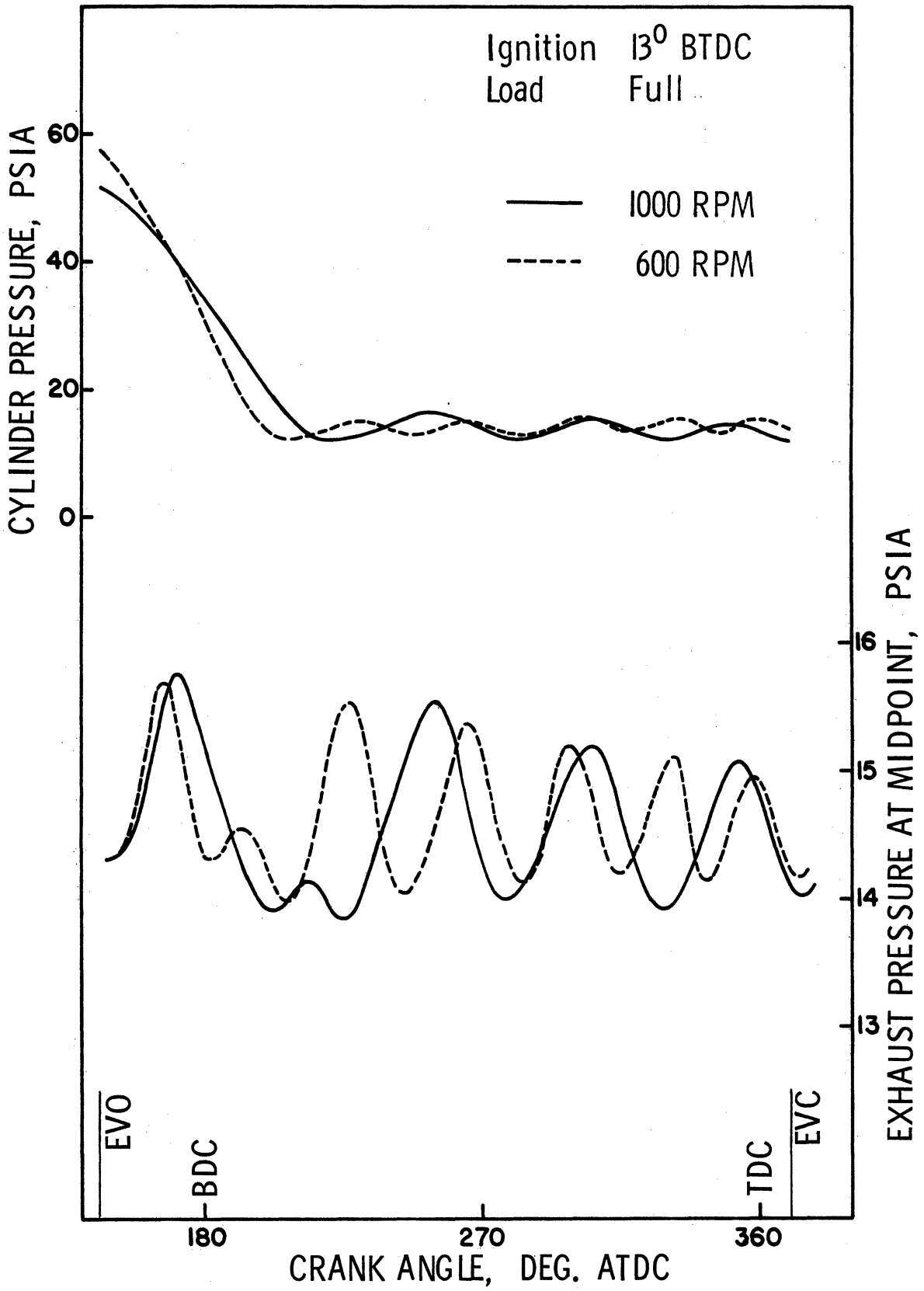

Figure 49. Effects of Engine Speed on Cylinder and Exhaust Pressures - Theoretical Results

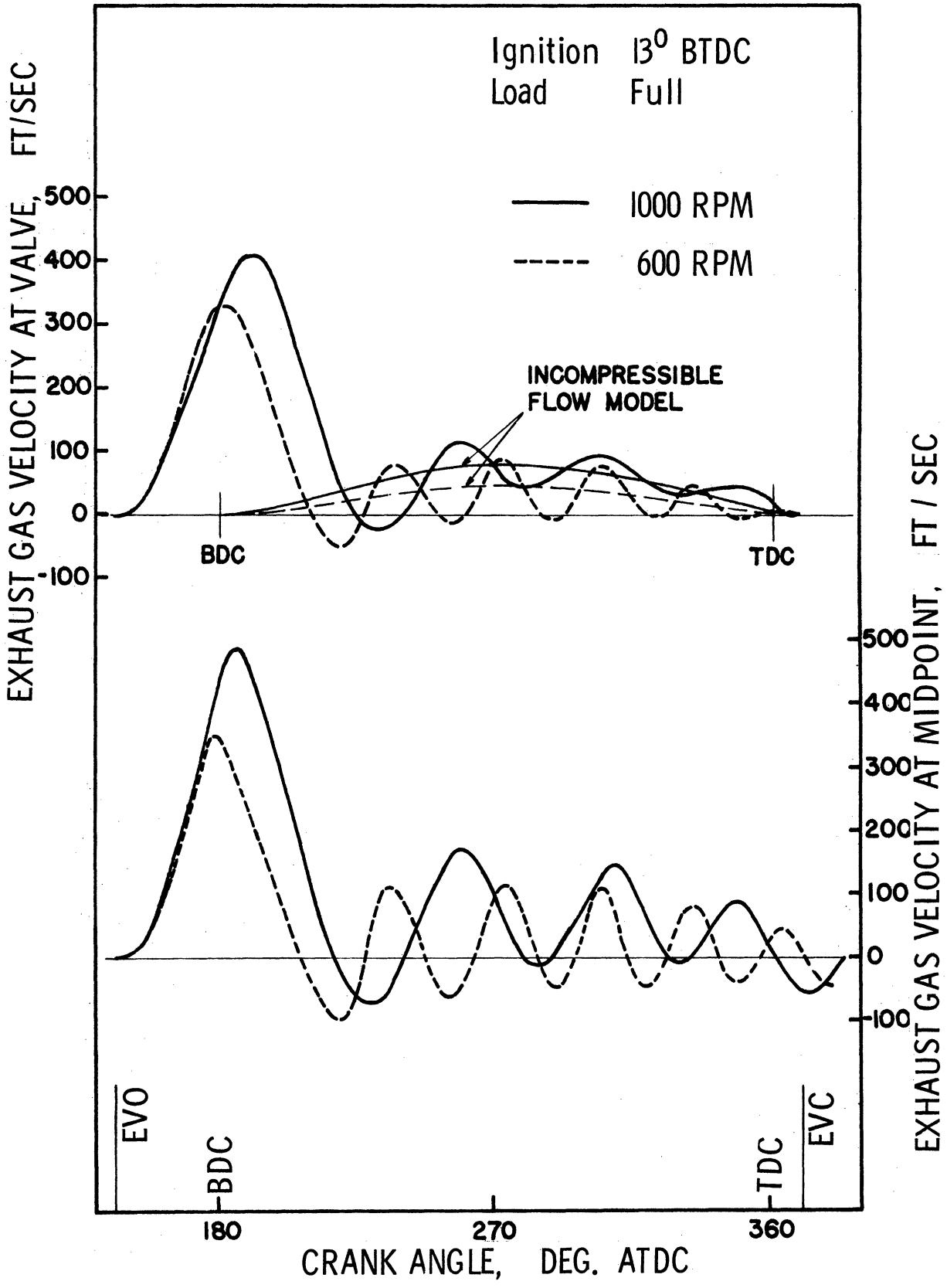

Figure 50. Effects of Engine Speed on Exhaust Gas Velocities - Theoretical Results

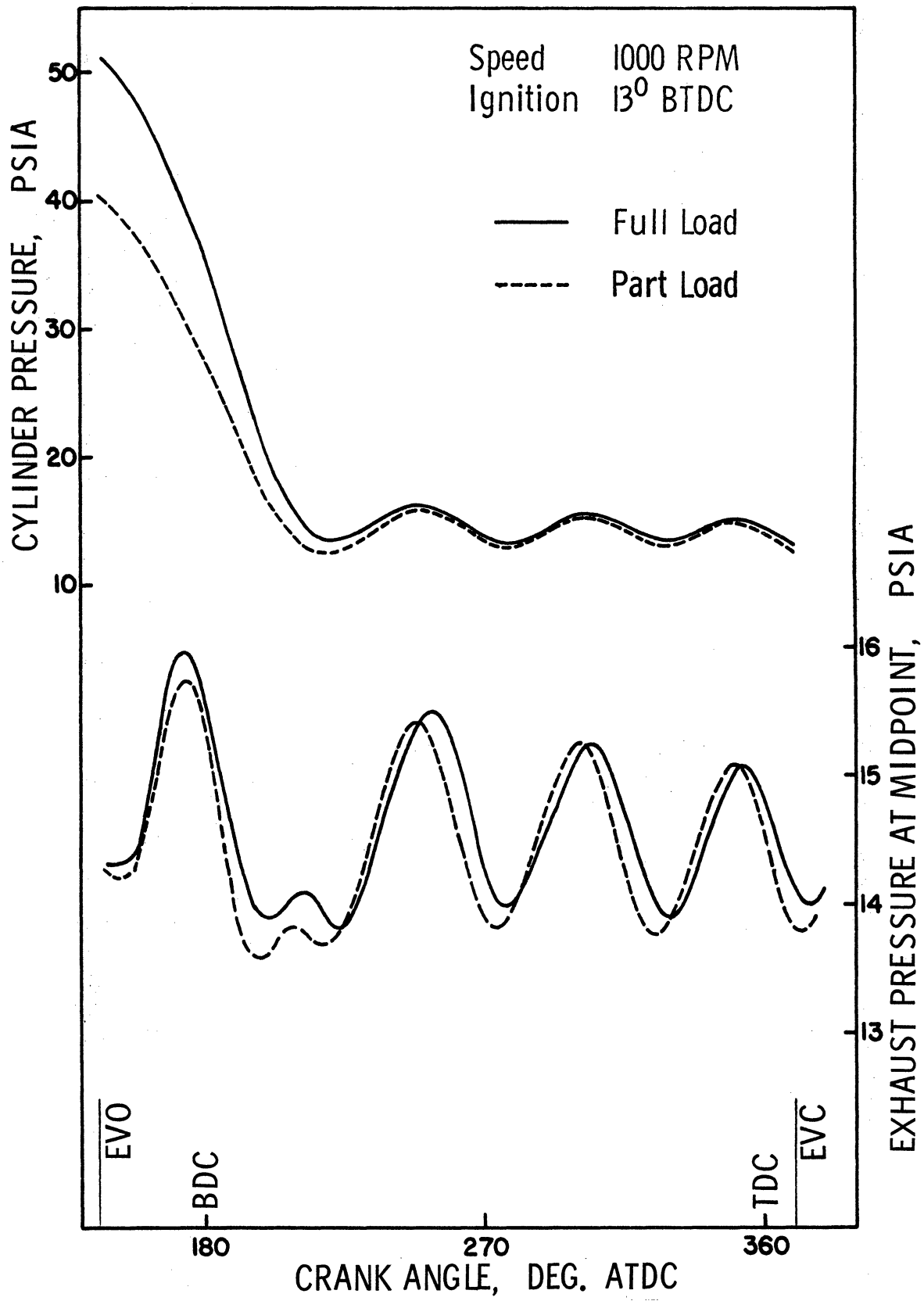

Figure 51. Effects of Engine Load on Cylinder and Exhaust Pressures - Theoretical Results

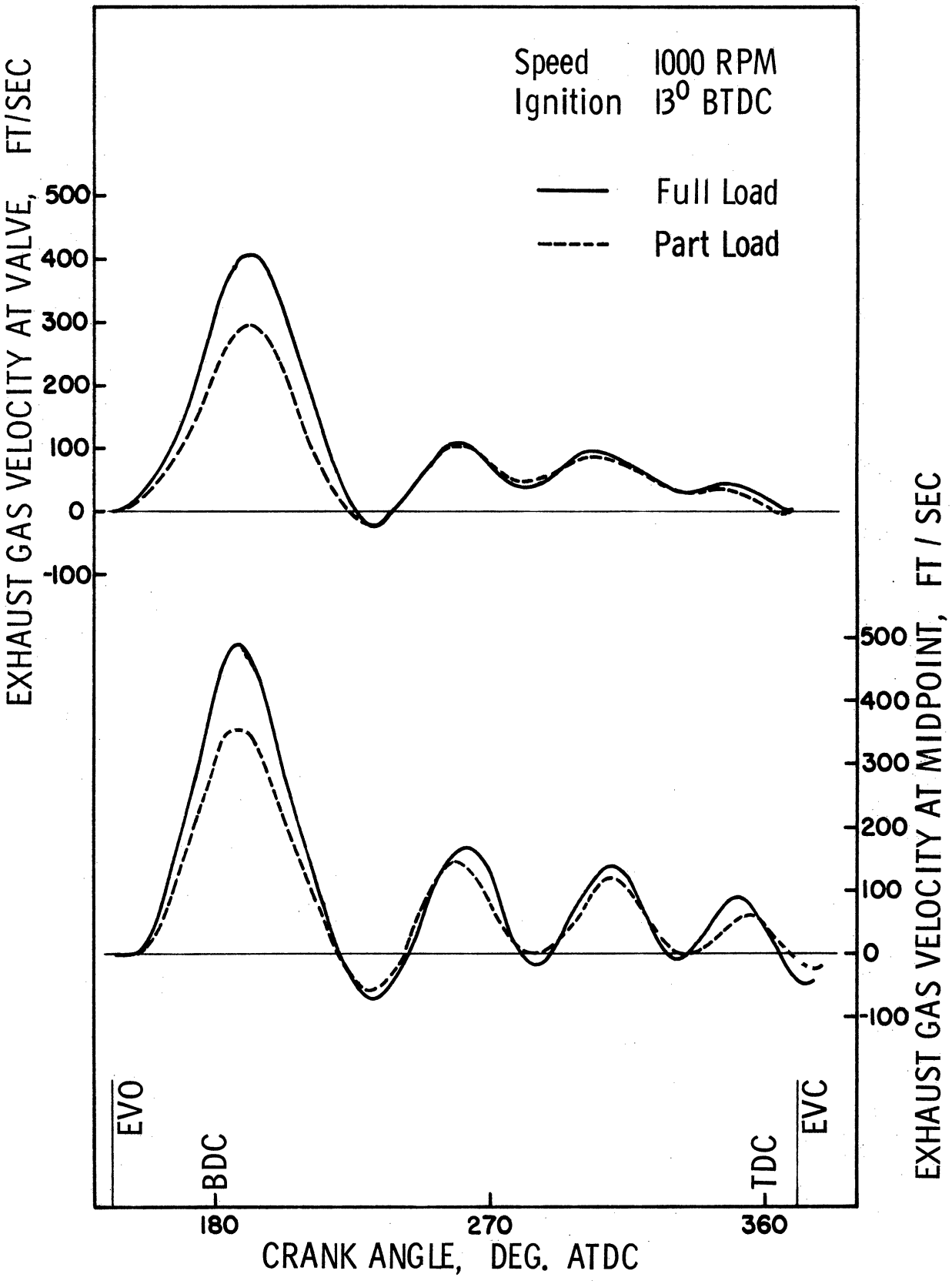

Figure 52. Effects of Engine Load on Exhaust Gas Velocities - Theoretical Results

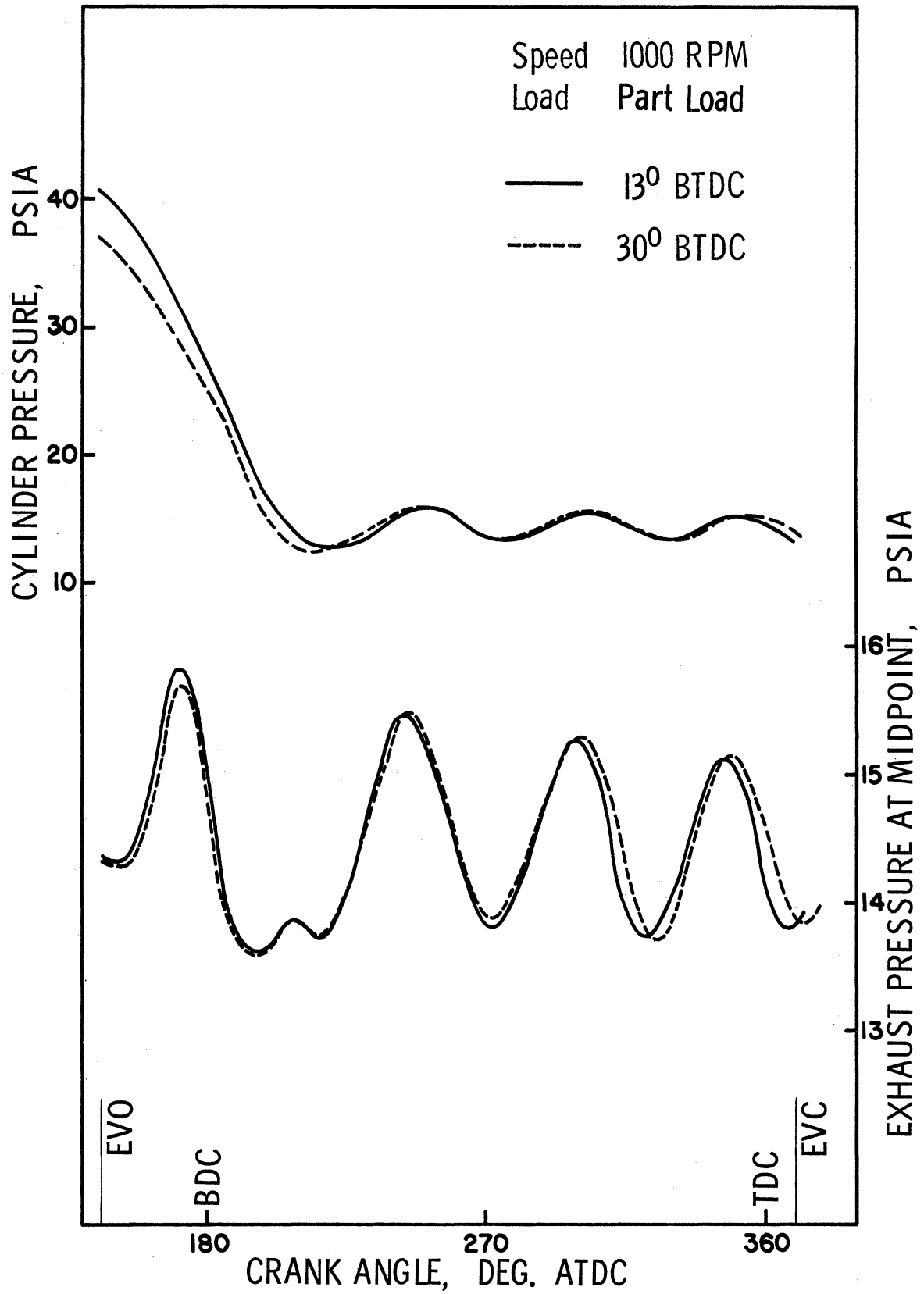

Figure 53. Effects of Ignition Timing on Cylinder and Exhaust Pressures - Theoretical Results

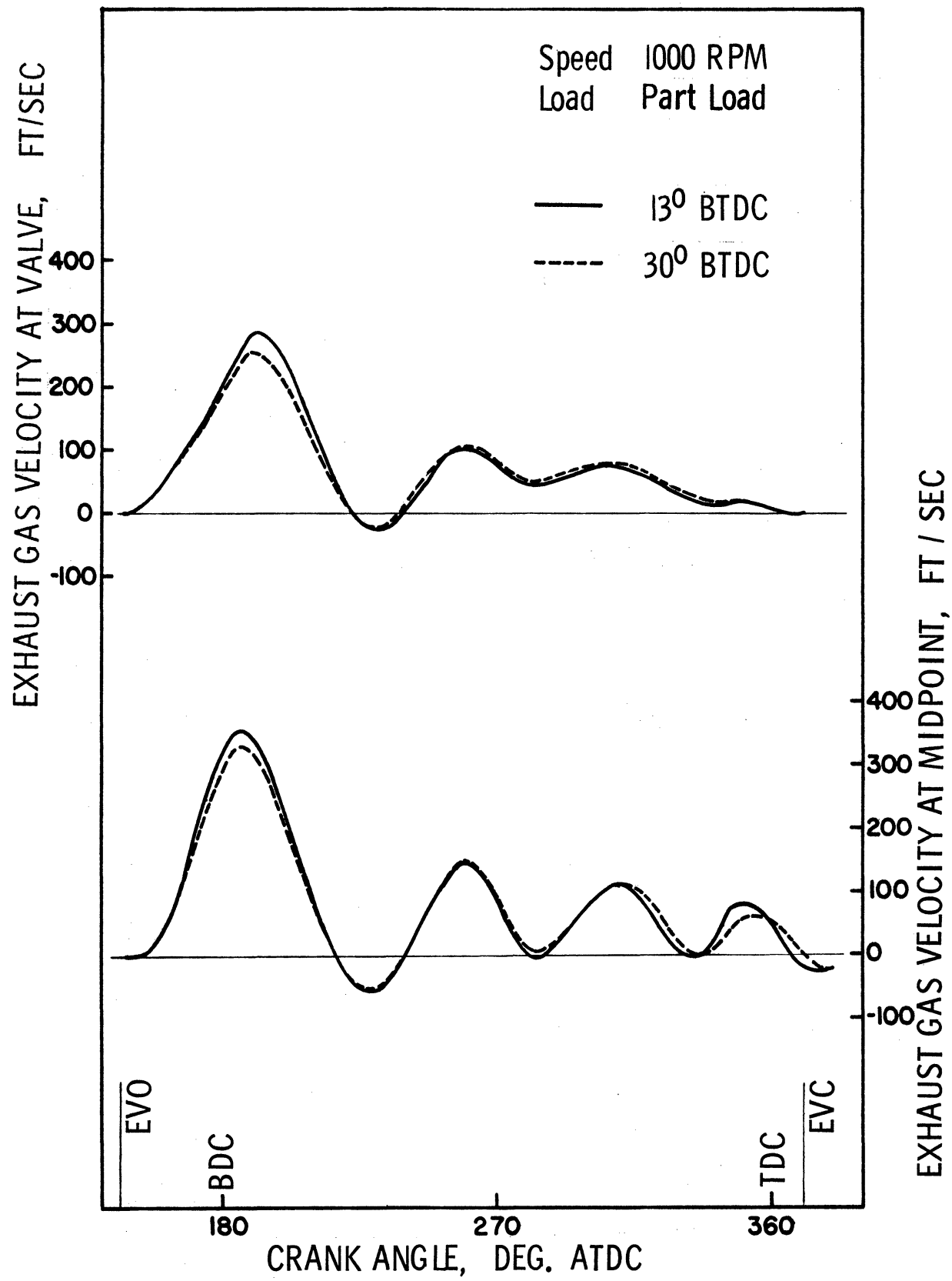

Figure 54. Effects of Ignition Timing on Exhaust Gas Velocity - Theoretical Results

the pipe cross-sectional area. Figure 50 shows such a velocity profile superimposed on the corresponding theoretical exhaust velocity profile. It is seen to be nearly equal to the average exhaust gas velocity obtained by connecting medium points in the fluctuating velocity profile.

The effect of engine load on the exhaust flow is appreciable only during blowdown, at least within the rage of load variation in this study, as can be seen in Figure 51 and 52. No significant effects due to ignition timing was detected, as shown in Figures 53 and 54.

Instantaneous distributions of exhaust pressures and velocities along the pipe for test run 5 are shown in Figures 55 and 56. The results are similar to those shown in Figure 39 and 40 for a motored engine. Figure 57 shows instantaneous distributions of exhaust gas temperatures along the pipe for the same test run. The temperature distributions are generally much steeper than those of pressures and velocities. During the early portion of the exhaust stroke, the exhaust gas near the valve is always hotter then the downstream gas, as the hot gas in the cylinder expands through the valve. However, during the later part of the exhaust stroke, the peak temperature appears at the middle of the exhaust pipe. This is probably due to several flow reversals occurring within the pipe.

5.4 Discussion of the Simulation Results

5.4.1 Overall Continuity Check

The overall mass continuity provides a reasonably good check on whether or not simulation results are physically meaningful in a gross sense. This continuity check is particularly important in a

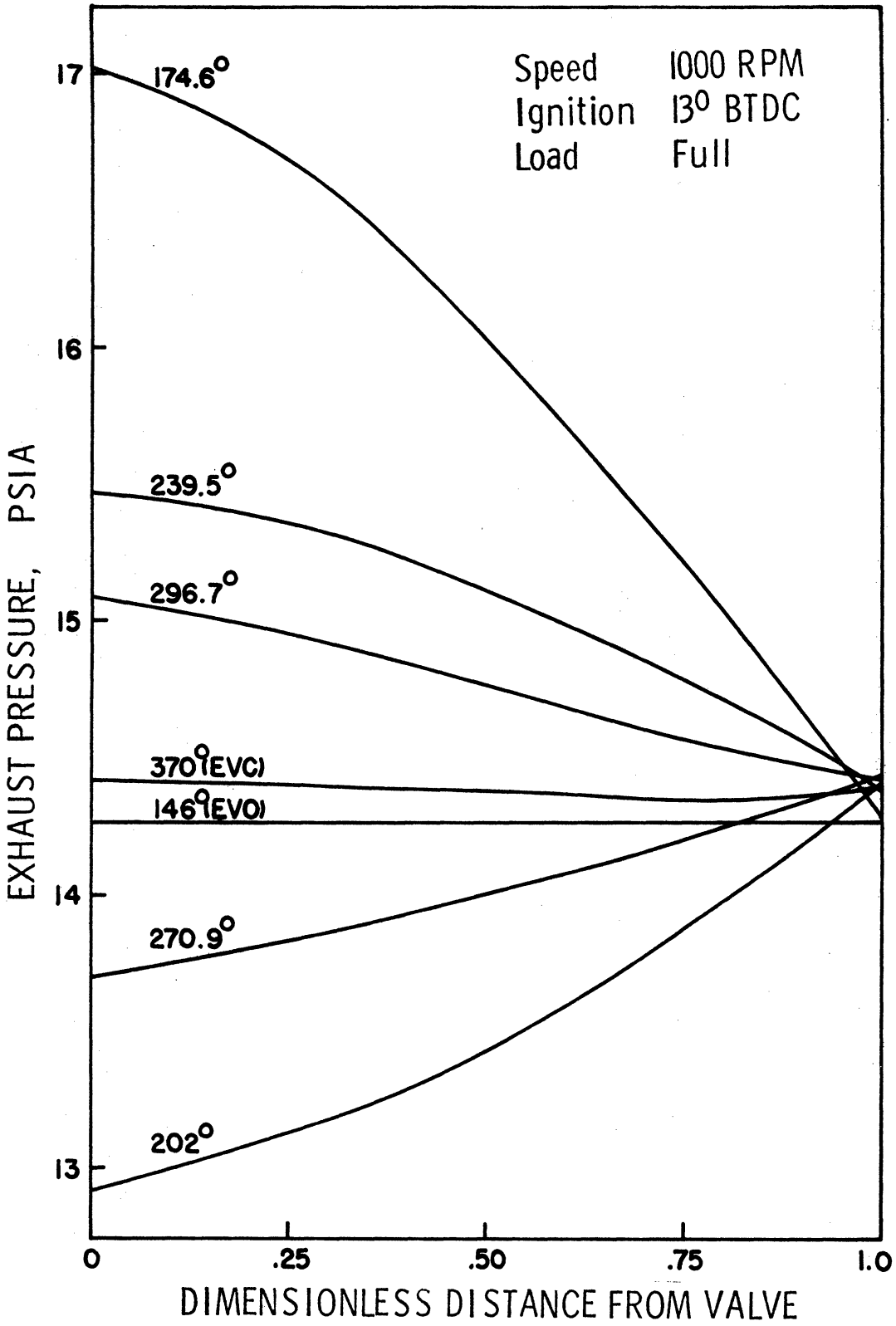

Figure 55. Instantaneous Pressure Distribution along the Exhaust Pipe - Theoretical Results

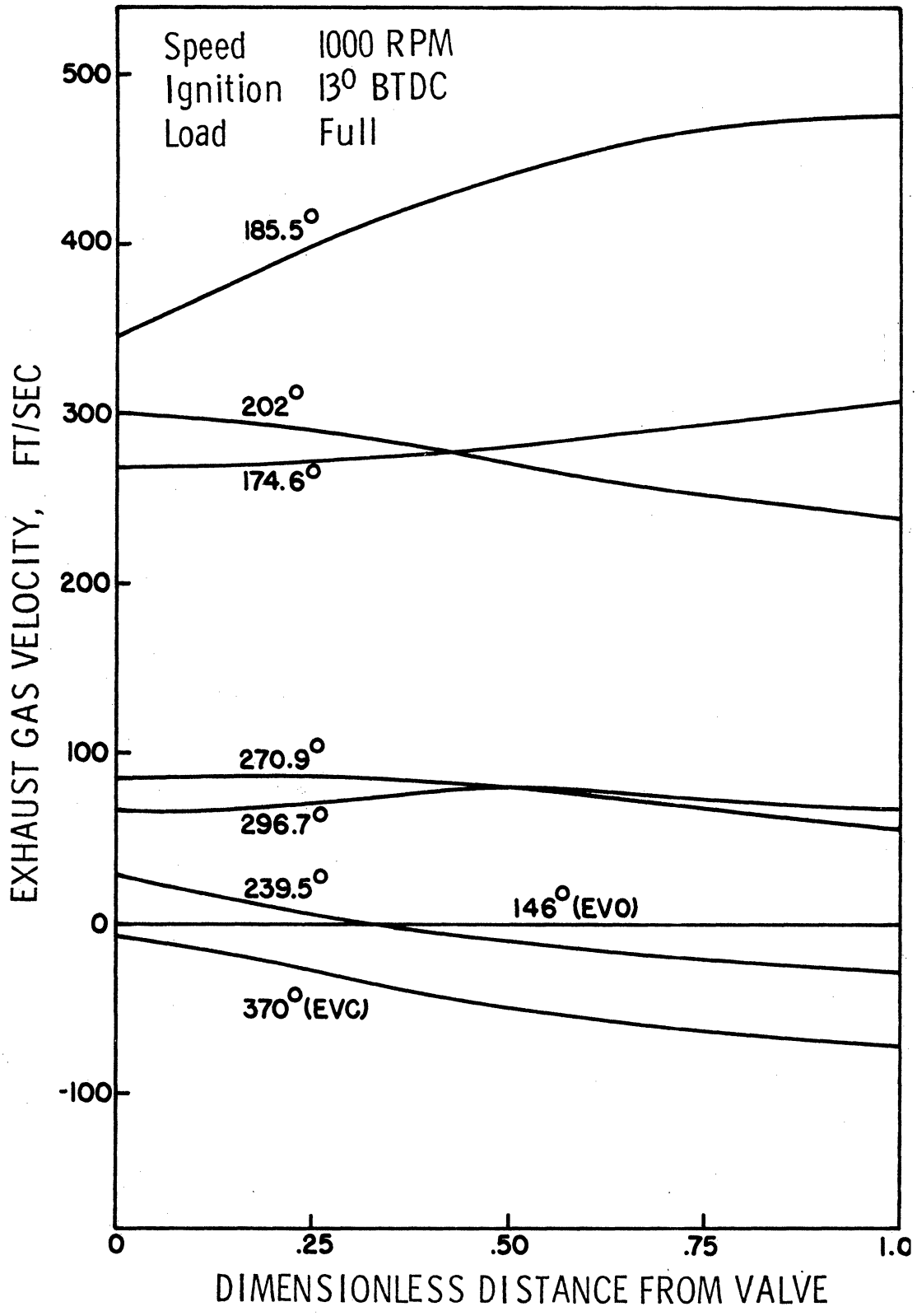

Figure 56. Instantaneous Velocity Distribution along the Exhaust Pipe - Theoretical Results

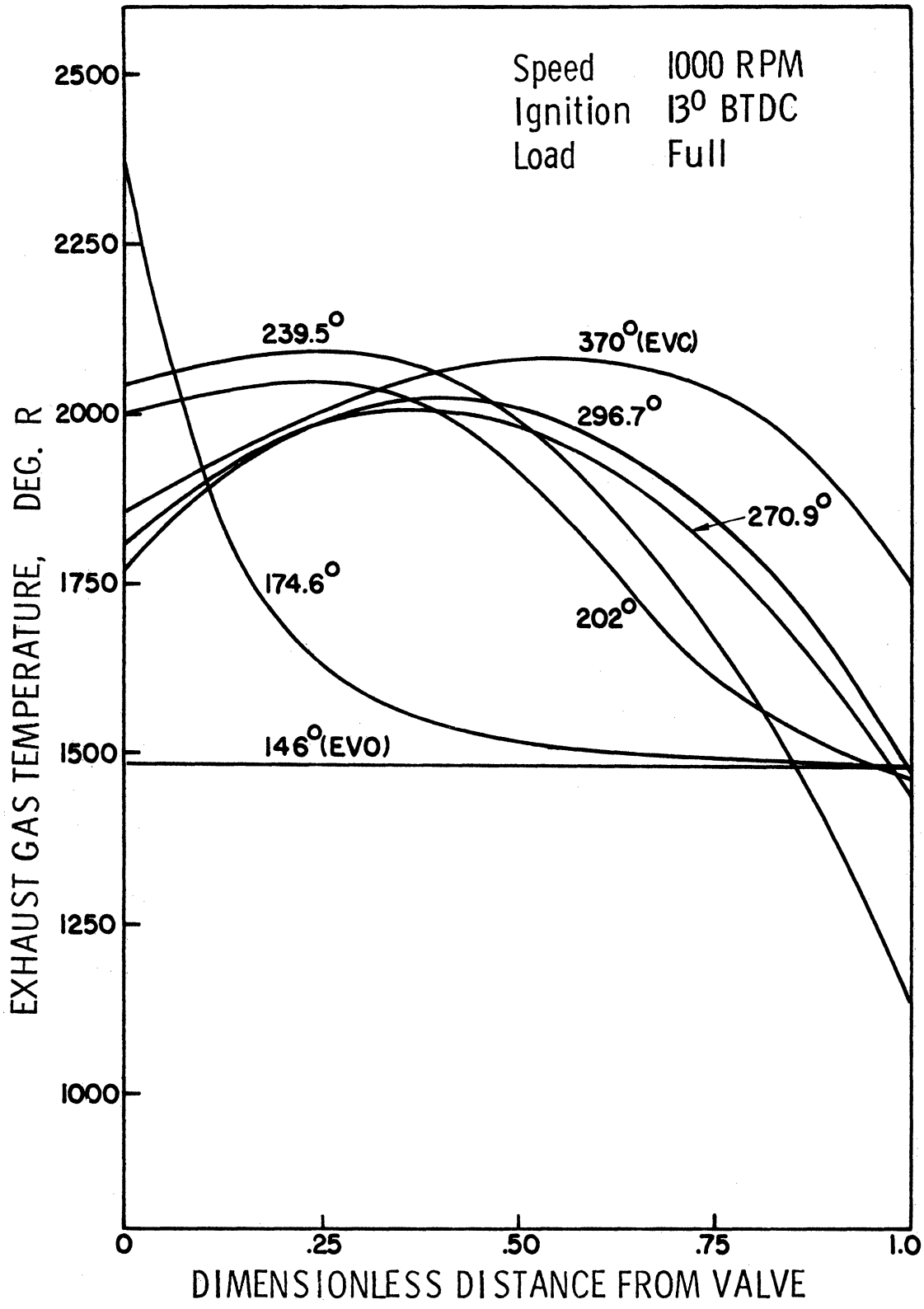

Figure 57. Instantaneous Gas Temperature Distribution along the Exhaust Pipe - Theoretical Results

complex numerical computation procedure. Table IV shows such a continuity check for all test runs performed in this study. The experimental values for average mass flow rates were measured at the intake system. The mass flow rates included both air and fuel. The theoretical values were computed at the cylinder end of the exhaust pipe by integrating instantaneous mass flow rates over the entire exhaust stroke. If there were no leakage in the engine system, these two values would have to be equal in order to satisfy the law of mass conservation. As shown in the table, the theoretical results are consistently larger than the experimental values. These discrepancies are considered to be due to engine blow-by leakages, since the simulation program assumed no leakage in the engine system. With the engine conditions similar to that of test run 5, the blow-by leakage was measured at approximately 4.3 % of the total mass flow rate. If this leakage is used to compensate the discrepancies between the experimental and theoretical results, the resulting average percentage errors are 0.5 % for motored engines and 4.5 % for firing engines. Larger discrepancies in firing engines are probably caused by the temperature fluctuations occuring in a firing engine. Although it may not be known how well the computer program simulated actual exhaust gas temperatures, adding another severe variation of a dependent variable may cause more computation errors in the overall mass continuity.

5.4.2 Comparison of Exhaust Gas Temperatures and the Effect of Heat Transfer

Although good agreement was obtained in the pressure and velocity data, it was always questionable whether or not the computed

TABLE IV

COMPARISON OF AVERAGE MASS FLOW RATE - THEORETICAL AND EXPERIMENTAL RESULTS

Run No.	Average Mass Flow Rate, lbm/min		% Error
	Experimental (Air Fuel)	Theoretical (Exhaust Gas)	
1	.375	.392	4.5
2	.444	.465	4.7
3	.487	.513	5.3
4	.449	.502	11.0
5	.539	.596	10.5
6	.457	.490	7.2
7	.452	.482	6.6

gas temperature agreed well with actual temperatures in an engine as indicated by Daneshyar in his discussion of a paper by Benson[4]. Since no attempt was made in this study to measure instantaneous exhaust gas temperatures, a direct answer to this question could not be made. As an alternative,a comparison was made with the experimental data published in an existing literature. Tabaczynski et al.[30] measured instantaneous exhaust temperatures near the exhaust valve with an optical technique. Radiation emissions from the 4.4μ CO_2 band in the emission spectrum of the exhaust gas were measured by a monochromater, and the gas temperature was computed from the emission data. The engine conditions at which Tabaczynski's data were obtained were similar to those of test run 5 in this study. The engine they used was identical to that of this study. Nonleaded gasoline was used with wide open throttle. The comparison is shown in Figure 58. Other relevant engine test conditions are also listed in the figure for comparison purposes. Reasonably good agreement between the two results is shown.

Heat transfer was expected to have certain effects on the temperature profile. Figure 59 shows the effect of cylinder heat transfer on the exhaust temperature and pressure. By neglecting the cylinder heat transfer, the average exhaust temperature was increased by approximately 7%. The effect of heat transfer on the pressure was less pronounced. The pressure amplitude remained virtually unchanged, but the wave speed was affected slightly. This change in wave speed is obvious because the wave speed is directly determined by the temperature field of the exhaust gas.

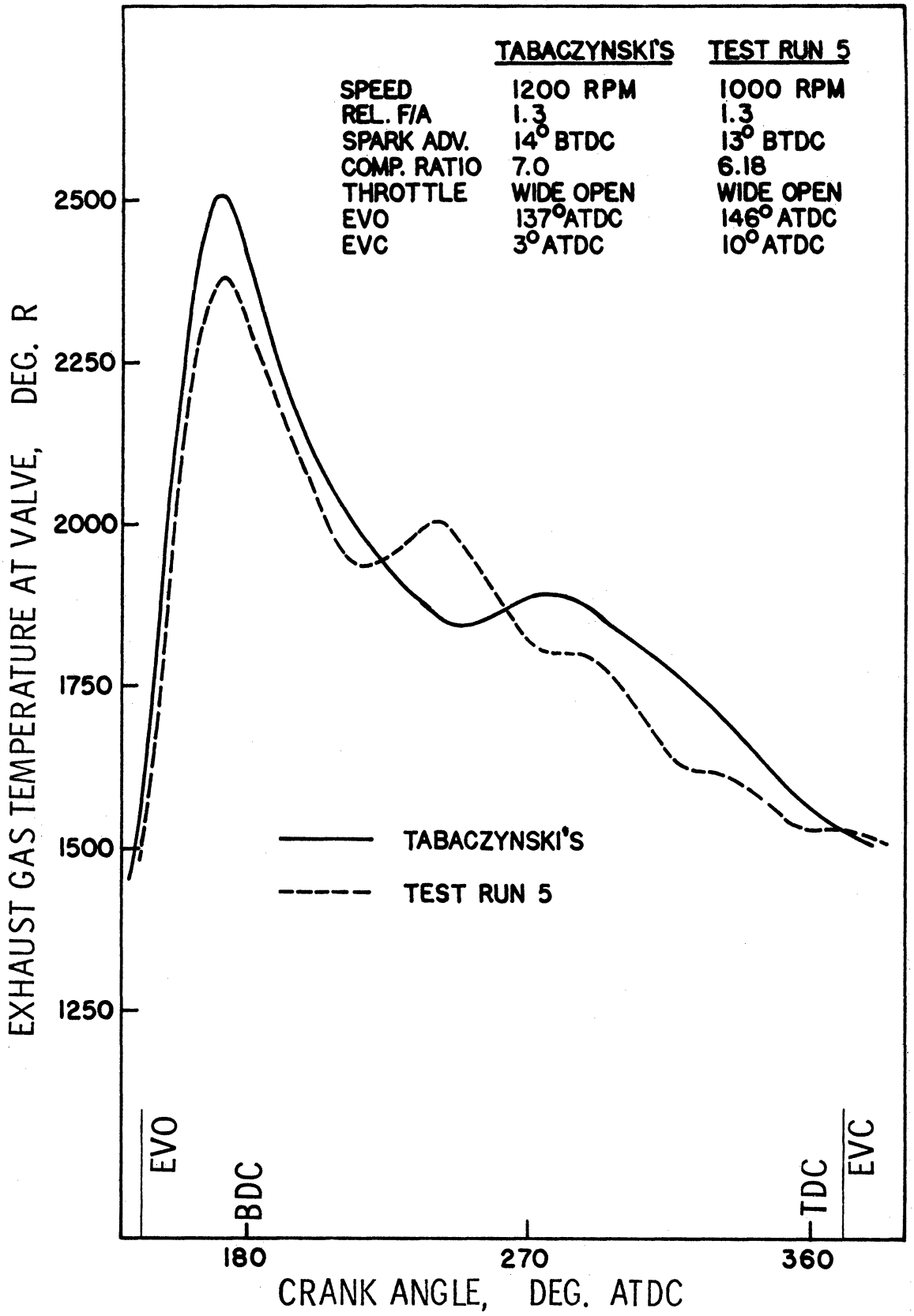

Figure 58. Comparison of Exhaust Gas Temperatures

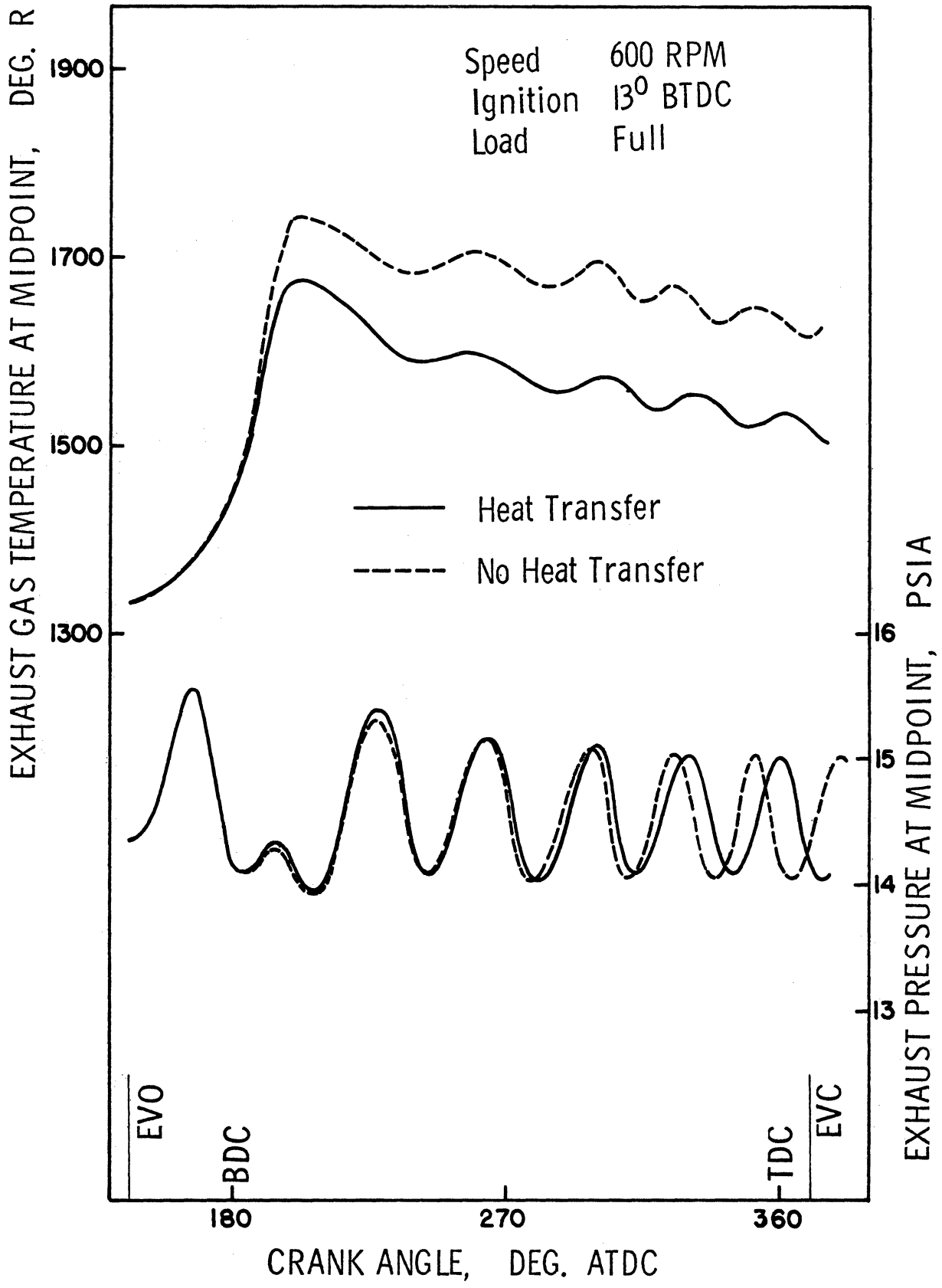

Figure 59. Effect of Cylinder Heat Transfer

5.4.3 The effect of Interpolation

Due to temperature fluctuations in the exhaust gas flow, the wave speed of a pressure pulse in the exhaust pipe varied considerably during an exhaust stroke. This variation was particularly severe in a firing engine. The variation of wave speed necessitate a linear interpolation procedure in applying the finite difference equations between two grid points in the x-t plane. For example, in order to apply the characteristic equations to compute the properties at point P in Figure 27, the properties at points F, H, and G must be known. However, these points usually do not coincide with the grid points at which the flow properties are known. Consequently, an interpolation procedure must be adapted to compute the flow properties at these points. A maximum error of interpolation results when these points lie halfway between the two adjacent grid points. The effect of the interpolation on pressure pulsations is shown in Figure 60 for a motored engine. The exhaust pressure profiles are shown in this figure as a function of the reach number which determines the grid size along the distance axis in the X-Z diagram. The computation error due to the interpolation undoubtedly dominated the decaying of pressure pulsations. Although a small grid size may be used to minimize the degree of interpolation, this is somewhat limited by the cost of computing time. An optimum grid size had to be sought to satisfy these two contradicting requirements. As mentioned in Chapter IV, a variable time increment was used in all firing engine cases in order to minimize the interpolation. In this study, most of the computer runs were made with the reach number from 10 to 16 with reasonable computing costs.

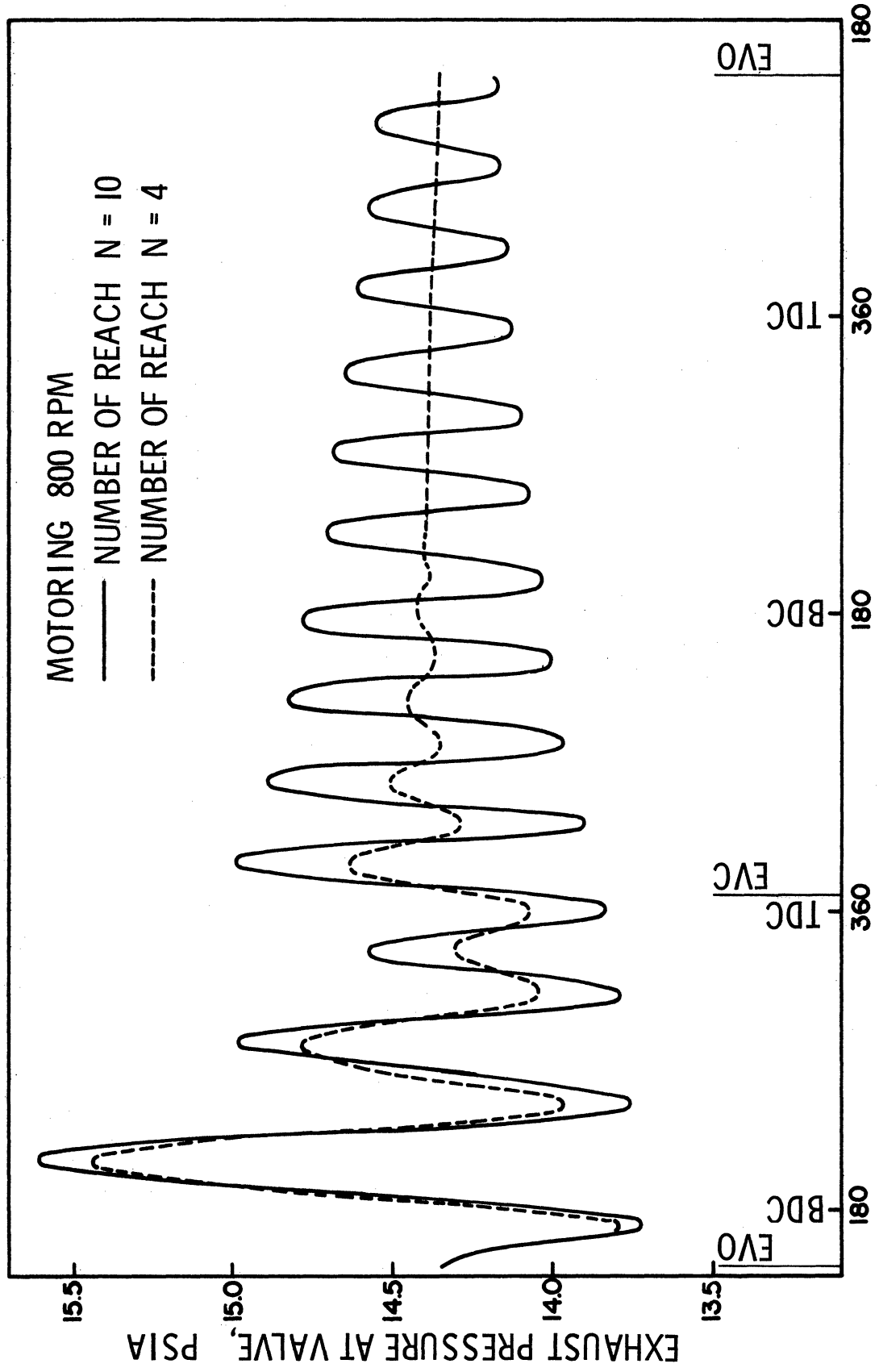

Figure 60. Effect of Interpolation on Pressure Pulsations

5.4.4 The Effect of Exhaust Gas Composition

Variations of the specific heat ratio k and the gas constant R as functions of gas composition and temperature are well known. The effect of these variations on the exhaust pressure, temperature, and velocity was investigated by using several different values of k and R for a fired engine. The result, as shown in Table V, indicated minor effects of these variations. The results also agrees with Benson et al.[4]

TABLE V

EFFECT OF GAS COMPOSITION ON EXHAUST FLOW IN A FIRED ENGINE

	% Deviation from the Result Computed with k = 1.35 and R = 51.0		
k or R	Temperature	Pressure	Velocity
k = 1.3	+3	+1	+1
k = 1.4	-3	-1	-1
R = 55	-2	-1	-1

VI. SUMMARY AND CONCLUSIONS

In this study, a schlieren-streak optical system was successfully applied to measure exhaust gas velocities in an internal combustion engine. The local density variations within the exhaust gas stream were used as the velocity tracer. The velocity data obtained by the new method was compared with those measured by a hot-wire anemometer. Good agreement between the two results demonstrated that the schlieren-streak system could be used effectively as a flow velocity meter, particularly in pulsating flow measurements. The major advantage of using this technique is that it requires a relatively simple experimental set-up compared with other optical techniques and it gives the flow velocity directly without any complex calibration procedures or data reduction processes.

Applications of the schlieren-streak method to other flow systems are quite possible, provided that the flow under investigation contains enough detectable local density variations. Studies on the creation and behavior of local density variations will undoubtedly be helpful in determining the applicability of the schlieren-streak method. Investigations on the effect of artificial tracer particles on the schlieren streak images are of prime interest for further development of this technique.

To gain fundamental understanding of the pulsating exhaust flow, a computer simulation program was developed from the theory of gas dynamics. The method of characteristics was used to solve the governing equations. Appropriate boundary conditions were specified at both ends

of the exhaust pipe. The cylinder conditions were computed instantaneously by a thermodynamic analysis. The simulation results were compared with the experimental data measured at several engine test conditions. Excellent agreement was obtained in both pressure and velocity data. It was also shown that the computed exhaust temperature agreed reasonably well with the experimental data obtained in another investigation under similar engine conditions.

The exhaust gas flow, as confirmed both theoretically and experimentally, exhibited severe flow pulsations. Several flow reversals were observed during an exhaust stroke. The effect of pressure wave actions on flow pulsations was important during the second half of an exhaust stroke, while the effects of other engine parameters, such as speed and load, were predominant in determining the blowdown pulses. The quasi-steady heat transfer model appears to give reasonable results in representing unsteady heat transfer, despite the discrepancies shown by some early investigations. Measurements of instantaneous gas temperature are definitely needed for further studies of this area.

APPENDIX I

DERIVATION OF CHARACTERISTIC EQUATIONS BY THE METHOD OF CHARACTERISTICS

Rewriting Equations (4.1), (4.2), and (4.6),

$$\frac{\partial \rho}{\partial t} + \frac{\partial}{\partial x}(\rho u) = 0 \qquad \text{(A1.1)}$$

$$\frac{\partial u}{\partial t} + u\frac{\partial u}{\partial x} + \frac{1}{\rho}\frac{\partial p}{\partial x} + \frac{1}{\rho}\frac{4}{D}\tau_w = 0 \qquad \text{(A1.2)}$$

$$\frac{\partial p}{\partial t} + u\frac{\partial p}{\partial x} - a^2\left(\frac{\partial \rho}{\partial t} + u\frac{\partial \rho}{\partial x}\right) - (k-1)\frac{4}{D}(\tau_w + q_w) = 0 \qquad \text{(A1.3)}$$

Then Equations (A1.3) + $a^2\times$(A1.1) + $\rho a\times$(A1.2) give

$$\left[\frac{\partial p}{\partial t} + (u+a)\frac{\partial p}{\partial x}\right] + \rho a\left[\frac{\partial u}{\partial t} + (u+a)\frac{\partial u}{\partial x}\right] - (k-1)\frac{4}{D}(\tau_w + q_w)$$

$$+ \frac{4a}{D}\tau_w = 0 \ , \qquad \text{(A1.4)}$$

while Equations (A1.3) + $a^2\times$(A1.1) - $\rho a\times$(A1,2) give

$$\left[\frac{\partial p}{\partial t} + (u+a)\frac{\partial p}{\partial x}\right] - \rho a\left[\frac{\partial u}{\partial t} + (u+a)\frac{\partial u}{\partial x}\right] - (k-1)\frac{4}{D}(\tau_w + q_w)$$

$$+ \frac{4a}{D}\tau_w = 0 \ . \qquad \text{(A1.5)}$$

The differential of any dependent variable y along a curve of slope c in the x-t plane is given by

$$\left(\frac{dy}{dt}\right)_c = \frac{\partial y}{\partial t} + c\frac{\partial y}{\partial x} \ .$$

Applying Equations (A1.4) and (A1.5) along such curves, one obtain

$$\frac{dp}{dt} \pm \rho a \frac{du}{dt} - (k-1)\frac{4}{D}(\tau_w u + q_w) \pm \frac{4a}{D}\tau_w = 0 \qquad \text{(A1.6)}$$

along curves of slopes

$$\frac{dx}{dt} = u \pm a \ . \qquad \text{(A1.7)}$$

Equation (A1.3) becomes

$$\frac{dp}{dt} - a^2\frac{d\rho}{dt} - (k-1)\frac{4}{D}(\tau_w u + q_w) = 0 \qquad \text{(A1.8)}$$

along a curve of slope

$$\frac{dx}{dt} = u \ . \qquad \text{(A1.9)}$$

Equations (A1.7) and (A1.9) represent the slopes of wave characteristics with Equations (A1.6) and (A1.8) the compatibility conditions required along these curves, respectively.

APPENDIX II

ANALYSIS OF THE PISTON MOTION

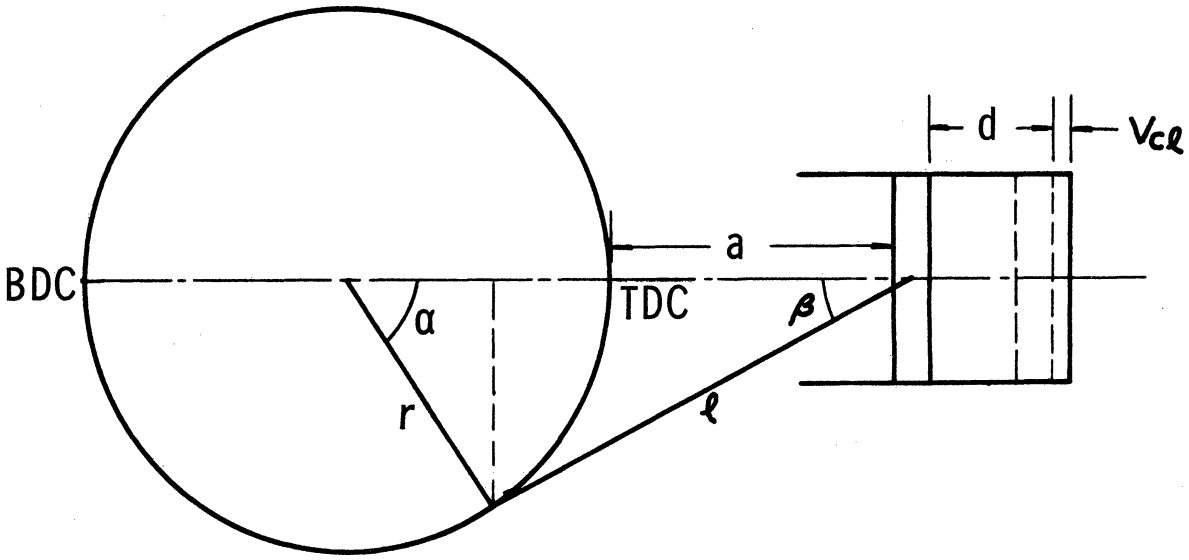

Figure A2.1 Cylinder Piston Motion

The instantaneous cylinder volume as a function of either the crank angle or time can be derived exactly from the engine geometry and engine speed. From Figure A2.1 the instantaneous cylinder volume can be expressed as follows:

$$v_c = v_{c\ell} + \pi B^2 d/4 \ , \qquad \text{(A2.1)}$$

where

v_c = Instantaneous cylinder volume

$v_{c\ell}$ = Cylinder clearance volume

B = Cylinder bore

d = Instantaneous linear cylinder displacement.

From the trgonometric relations,

$$d = \ell(1 - \sqrt{1 - (r^2/\ell^2)\sin\alpha}\ ) + r(1 - \cos\alpha), \qquad (A2.2)$$

where ℓ is the length of the connecting rod and r the length of the crank arm. However, d can be approximated, within a maximum error of less than .04% in this study, by

$$d \simeq r(1 - \cos\alpha + (r/2\ell)\ \sin^2\alpha)\ . \qquad (A2.3)$$

The cylinder clearance volume can be expressed in terms of the compression ratio by

$$v_{c\ell} = \pi B^2 s/4r_c\ , \qquad (A2.4)$$

where

s = Stroke

r_c = Compression ratio.

Substituting Equations (A2.3) and (A2.4) into Equation (A2.1) yields

$$v_c = (\pi B^2/4)[s/r_c + (s/2)\{1-\cos\alpha+(s/4\ell)\sin^2\alpha\}]. \qquad (A2.5)$$

The rate of cylinder volume change as a function of either the crank angle or time is

$$\frac{dv_c}{d\alpha} = (\pi B^2 s/8)[\sin\alpha + (s/4\ell)\sin 2\alpha] \qquad (A2.6)$$

and

$$\frac{dv_c}{dt} = (\pi^2 B^2 s/240)(RPM)[\sin\alpha + (s/4\ell)\sin 2\alpha], \qquad (A2.7)$$

where $dv_c/d\alpha$ is expressed in $in.^3/rad.$ and dv_c/dt in $in.^3/sec.$

APPENDIX III

DERIVATION OF VALVE EQUATIONS BASED ON THE CONSTANT-PRESSURE MODEL FOR THE EXHAUST VALVE FLOW

Based on the assumptions introduced in Section 4.4.1, the conservation laws of energy and mass and the equation of state for the exhaust valve flow can be written as follows:

Energy: $$h_e^\circ = h_t^\circ = h_c \qquad \text{(A3.1)}$$

Mass: $$\phi u_t \rho_t = u_e \rho_e \qquad \text{(A3.2)}$$

State: $$a_c^2 = k p_c / \rho_c \qquad \text{(A3.3a)}$$

$$a_t^2 = k p_t / \rho_t \qquad \text{(A3.3b)}$$

$$a_e^2 = k p_e / \rho_e \qquad \text{(A3.3c)}$$

where the subscript c denotes the cylinder, e the exhaust pipe, and t the valve throat. Expressing the enthalpy in terms of local speed of sound and flow velocity, Equation (A3.1) becomes

$$a_e^2 + \frac{k-1}{2} u_e^2 = a_t^2 + \frac{k-1}{2} u_t^2 = a_c^2 \qquad \text{(A3.4)}$$

Another equation required to solve for the unknowns comes from the flow conditions at the valve throat, which are determined by the pressure ratio across the valve. Four different flow conditions are possible:

a) Sonic flow: $$p_e/p_c < [2/(k+1)]^{k/(k-1)}$$

b) Subsonic flow: $[2/(k+1)]^{k/(k-1)} < p_e/p_c < 1$

c) Reverse flow: $p_e/p_c > 1$

d) Closed valve

a) Sonic flow from cylinder to exhaust pipe

When the flow at the valve throat is sonic, the constant-pressure model assumes an isentropic flow from the cylinder to the valve throat, and the sonic condition at the valve throat. The resulting equations are

$$p_t/p_c = (\rho_t/\rho_c)^k = (a_t/a_c)^{2k/(k-1)} \tag{A3.5}$$

$$a_t = u_t \ . \tag{A3.6}$$

The above set of equations is manipulated such that the flow variables at the valve throat do not appear in the final form of the valve equation. From Equation (A3.4),

$$(u_e/a_c)^2 = 2/(k-1)\ [1 - (a_e/a_c)^2]. \tag{A3.7}$$

By combining Equations (A3.2), (A3.3), (A3.5), and (A3.6),

$$(a_e/a_c)^2 = [1/\phi](u_e/a_c)(p_e/p_c)[(k+1)/2]^{(k+1)/[2(k-1)]}. \tag{A3.8}$$

Substituting Equation (A3.8) into Equation (A3.7) gives

$$(u_e/a_c)^2 + 2W_1(u_e/a_c) - 2/(k-1) = 0 \tag{A3.9}$$

where

$$W_1 = [1/(k-1)][(k+1)/2]^{(k+1)/[2(k-1)]}\ (1/\phi)(p_e/p_c).$$

Solving Equation (A3.9) for u_e/a_c,

$$u_e/a_c = -W_1 + \sqrt{W_1^2 + 2/(k-1)} \quad . \tag{A3.10}$$

b) Subsonic flow from cylinder to exhaust pipe

A similar procedure is applied to the subsonic flow case except that the sonic condition at the valve throat is now replaced by a constant pressure between the throat and the valve.

$$p_t = p_e \tag{A3.11}$$

The final result is

$$u_e/a_c = -W_2 + \sqrt{W_2^2 + 2/(k-1)} \quad , \tag{A3.12}$$

where

$$W_2 = \frac{[1/(k-1)](1/\phi)(p_e/p_c)^{(k-1)/k}}{\sqrt{[2/(k-1)][1 - p_e/p_c)^{(k-1)/k}}} \quad .$$

c) Subsonic flow from the exhaust pipe to cylinder (reverse flow)

In the reverse flow case, the constant-pressure model assumes an isentropic flow from the exhaust pipe to the valve throat and a constant pressure between the valve throat and the cylinder. Thus,

$$p_e/p_t = (\rho_e/\rho_t)^k = (a_e/a_t)^{2k/(k-1)} \tag{A3.13}$$

$$p_c = p_t \tag{A3.14}$$

are used along with Equations (A3.2) through (A3.4) to derive the valve equation. From Equation (A3.4),

$$(u_e/a_e)^2 = [2/(k-1)][(a_c/a_e)^2 - 1]. \qquad (A3.15)$$

By combining Equations (A3.2), (A3.3), (A3.13), and (A3.14),

$$(a_c/a_e)^2 = [(k-1)/2](1/\phi^2)(u_e/a_e)^2(p_c/p_e)^{-2/k} + (p_c/p_e)^{(k-1)/k}. \qquad (A3.16)$$

Substituting Equation (A3.16) into Equation (A3.15) yields

$$(u_e/a_e)^2 = \frac{[2/(k-1)][1 - (p_c/p_e)^{(k-1)/k}]}{[(1/\phi^2)(p_c/p_e)^{-2/k} - 1]}$$

Taking the negative value of u_e/a_e,

$$u_e/a_e = - \left[\frac{[2/(k-1)][1 - (p_c/p_e)^{(k-1)/k}}{[(1/\phi^2)(p_c/p_e)^{-2/k} - 1]} \right]^{1/2}. \qquad (A3.17)$$

d) Closed valve

The obvious physical flow condition in this case is

$$u_e = 0. \qquad (A3.18)$$

REFERENCES

1. Bayley, F. J., Edwards, P. A. and Singh, P. P., "The Effect of Flow Pulsations on Heat Transfer by Forced Convection from a Flat Plate," International Developments in Heat Transfer, Pt. II, Section B, Proc. 1961-62 Heat Transfer Conference, ASME, 1961-1962, pp. 499-509.

2. Benson, R. S. and Woods, W. A., "Wave Action in the Exhaust System of a Supercharged Two-Stroke-Engine Model," Int. J. Mech. Sci., Vol. 1, 1960, pp. 253-281.

3. Benson, R. S., Garg, R. D. and Woollatt, D., "A Numerical Solution of Unsteady Problems," Int. J. Mech. Sci., Vol. 6, 1964, pp. 117-144.

4. Benson, R. S., "A Computer Program for Calculating the Performance of an Internal Combustion Engine Exhaust System," Proc. Instn. Mech. Engrs., Vol. 182, Pt. 3L, 1967-68, pp. 91-108.

5. Benson, R. S., Wild, A. and Woollatt, D., "Effects of Variable Specific Heats and Gas Composition on Unsteady Flow Calculations," Proc. Instn. Mech. Engrs., Vol. 184, Pt. 3G(i), 1969-70, pp. 101-107.

6. Bowman, J. E., "A Streak Camera Method for the Measurement of Flow Velocity in a Hypersonic Gun Tunnel," RARDE Memorundum(B), 28/63, May, 1963.

7. Chapman, A. J., Heat Transfer, Second Edition, Macmillan Co., New York, 1967.

8. Cole, B. N. and Mills, B., "The Theory of Sudden Enlargements Applied to the Poppet Exhaust-Valve, with Special Reference to Exhaust-Pulse Scavenging," Proc. Instn. Mech. Engr., Vol. IB, No. 8, 1952-53, pp. 364-377.

9. Daneshyar, H., "Numerical Solution of Gas Flow Through an Engine Cylinder," Int. J. Mech. Sci., Vol. 10, 1968, pp. 711-722.

10. Danial, W. A. and Wentworth, J. T., "Exhaust Gas Hydrocarbons - Genesis and Exodus," SAE Paper, 486B, March, 1962.

11. Eichelberg, G., "Some New Investigation on Old Combustion-Engine Problems," Engineering, London, Vol. 148, 1939, pp. 463-466 and 547-550.

12. Foreman, J. W., Jr., George, E. W. and Lewis, R. D., "Measurement of Localized Flow Velocity in Gases With a Laser Doppler Flowmeter," Appl. Phys. Letters, Vol. 7, No. 4, 1965, pp. 77-78.

13. Goyal, M., Scharpf, G. and Borman, G., "The Simulation of Single Cylinder Intake and Exhaust Systems," SAE Paper, 670478, 1967.

14. Hatta, K., Kotake, S. and Aoki, I., "Heat Transfer in Unsteady Flows," Heat Transfer - Japanese Research, Vol. 1, No. 1, 1972, pp. 1-10.

15. Holder, D. W. and North, R. J., "Schlieren Methods," AGARDograph, No. 23, Pt. 1, 1956.

16. Horlock, J. H. and Woods, W. A., "The Thermodynamics of Charging and Discharging Processes," Proc. Instn. Mech. Engrs., Vol. 180, Pt. 3F, 1965-66, pp. 16-24.

17. Huffaker, R. M., "Laser Doppler Detection Systems for Gas Velocity Measurement," Appl. Optics, Vol. 9, No. 5, May, 1970, pp. 1026-1039.

18. Ishigaki, Hiroshi, "The Effect of Oscillation on Flat Plate Heat Transfer," J. Fluid Mech., Vol. 47, Pt. 3, 1971, pp. 537-546.

19. Jenny, E., "Unidimensional Transient Flow with Consideration of Friction, Heat Transfer, and Change of Section," The Brown Boveri Review, Vol. 57, 1950, pp. 447-461.

20. Kaneko, Y., Kuroda, H. and Tanaka, K., "Small Engines - Concept Emission Vehicles," SAE Paper, 710296, January, 1971.

21. Kastner, L. J., Williams, T. J. and White, J. B., "Poppet Inlet Valve Characteristics and Their Influence on the Induction Process," Proc. Instn. Mech. Engr., Vol. 178, Pt. 1, No. 36, 1963-64, pp. 955-974.

22. Lanz, O., Johnson, C. C. and Morikawa, S., "High-Resolution Laser Doppler Velocity Measurement of Bidirectional Pulsating Flow," Appl. Phys. Letters, Vol. 17, No. 12, 1970, pp. 523-525.

23. Ohigashi, S. Hamamoto, Y. and Tanabe, S., "A New Digital Method for Measuring Gas Flow Velocity by Electric Discharge," SAE Paper, 690180, January, 1969.

24. Oppenheim, A. K. and Chilton, E. G., "Pulsating-Flow Measurement - A Literature Survey," ASME Transaction, February, 1955, pp. 231-248.

25. Overbye, V. D., Bennethum, J. E., Uyehara, O. A. and Myers, P. S., "Unsteady Heat Transfer in Engines," SAE Transaction, Vol. 69, 1969, pp. 461-494.

26. Owczarek, J. E., Fundamentals of Gas Dynamics, International Textbook Co., 1964.

27. Rann, C. S., "Measurement of Gas Velocity in a Flame," J. Sci. Instrum., Vol. 44, 1967, pp. 227-228.

28. Schwar, M. J. R. and Weinberg, F. J., "Velocity Measurement by Combining the Doppler Principle with the Schlieren Method," Nature, Vol. 221, No. 5178, January, 1969, pp. 357.

29. Streeter, V. L. and Wylie, E. B., Hydraulic Transients, McGraw-Hill Book Co., 1967.

30. Tabaczynski, R. J., Heywood, J. B. and Keck, J. C., "Time-Resolved Measurements of Hydrocarbon Mass Flowrate in the Exhaust of a Spark-Ignition Engine," SAE Paper, 720112, January, 1972.

31. Taylor, C. F. and Taylor, E. S., The Internal Combustion Engine, Second Edition, International Textbook Co., Scranton, 1961.

32. Thompson, D. H., "A Tracer-Particle Fluid Velocity Meter Incorporating a Laser," J. Sci. Instrum., Vol. 45, 1968, pp. 929-932.

33. Weinberg, F. J., Optics of Flames, Butterworths & Co., 1963.

34. Winsor, R. E., "Relationship of Cyclic Combustion Variations and Mixture Motion in a Spark-Ignition Engine," Ph.D. Thesis, The University of Michigan, 1972

35. Woods, W. A. and Kahn, S. R., "An Experimental Study of Flow through Poppet Valves," Proc. Instn. Mech. Engr., Vol. 180, Pt. 3N, 1965-66, pp. 32-41.

36. Wright, E. H. and Gill, K. F., "Theoretical Analysis of the Unsteady Gas Flow in the Exhaust System of an Engine," J. Mech. Engng. Sci., Vol. 8, No. 1, 1966, pp. 70-90.